



# A static and dynamic theory for photo-flexoelectric liquid crystal elastomers and the coupling of light, deformation and electricity

Amir Hossein Rahmati <sup>a</sup>, Kosar Mozaffari <sup>a</sup>, Liping Liu <sup>b,c,\*</sup>, Pradeep Sharma <sup>a,d,\*</sup>

<sup>a</sup> Department of Mechanical Engineering, University of Houston, TX 77204, USA

<sup>b</sup> Department of Mechanical Aerospace Engineering, Rutgers University, NJ 08854, USA

<sup>c</sup> Department of Mathematics, Rutgers University, NJ 08854, USA

<sup>d</sup> Department of Physics, University of Houston, TX 77204, USA

## ARTICLE INFO

### Keywords:

Liquid crystal elastomers  
Light  
Deformation  
Electricity  
Flexoelectricity

## ABSTRACT

Photoactive nematic liquid crystal elastomers permit generation of large mechanical deformation through impingement by suitably polarized light. The light-induced deformation in this class of soft matter allows for devices such as transducers and robots that may be triggered wirelessly. While there is no ostensible direct coupling between light and electricity in nematic liquid crystal elastomers, in this work, we take cognizance of the fact that the phenomenon of flexoelectricity is universal and present in all dielectrics. Flexoelectricity involves generation of electrical fields due to strain gradients or conversely, the production of mechanical deformation through electrical fields. Barring some specific contexts, the flexoelectric effect is in general rather weak in *hard* materials. However, due to the facile realization of strain gradients (e.g. flexure) in soft materials, we expect flexoelectricity to be highly relevant for liquid crystal elastomers thus, *prima facie*, furnishing a deformation-mediated mechanism to couple light and electricity. In this work, we develop nonlinear equilibrium and dynamical models for photo-flexoelectric nematic liquid crystal elastomers and analyze the precise conditions underpinning an appreciable coupling between light and electricity. A careful scaling analysis reveals that there is an optimal size-scale at which the flexoelectricity-mediated photo-electric effect is maximized. We find that with conservative estimates of the flexoelectric coefficients of these materials, the electrical power generation is rather modest for typical optical load. However, our proposed coupling is an appropriate modality for optical sensing. Furthermore, design of next-generation liquid crystal elastomers with high flexoelectricity as well as exploitation of size-effects could ameliorate extraction of electrical power from light illumination.

## 1. Introduction

The prospects of producing electricity through radiation and specifically, light, needs little motivation. The mechanism is wireless and thus can be remotely administered and proceeds at maximal speed allowed by the known physical laws (Fig. 1). The intense and storied research in the broadly defined field of photovoltaics is a testament to this. In this work, we attempt to understand the mechanics underpinning the coupling between light and electricity in an entirely different class of materials: photoactive nematic liquid crystal elastomers.

Crudely, a liquid crystal elastomer (LCE) is a marriage between conventional rubbery polymers and liquid crystals. The result is a rubber-like, very soft solid but one that appears to inherit several idiosyncrasies of the liquid crystal structure (Warner and

\* Corresponding authors.

E-mail addresses: [liu.liping@rutgers.edu](mailto:liu.liping@rutgers.edu) (L. Liu), [psharma@central.uh.edu](mailto:psharma@central.uh.edu) (P. Sharma).

<https://doi.org/10.1016/j.jmps.2024.105949>

Received 5 August 2024; Received in revised form 27 October 2024; Accepted 8 November 2024

Available online 19 November 2024

0022-5096/© 2024 Elsevier Ltd. All rights are reserved, including those for text and data mining, AI training, and similar technologies.

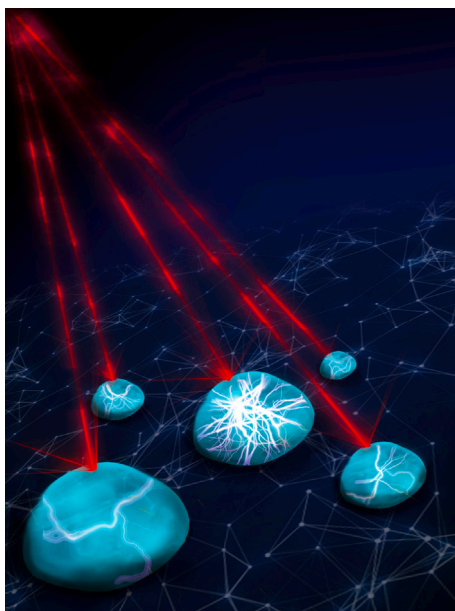


**Fig. 1.** The wireless generation of electricity through radiation is a prized energy inter-conversion mechanism motivating photovoltaics and other such devices. The light-electricity coupling is uncommon at the material level and photo-active liquid crystal elastomers, with the mediation of flexoelectricity, may provide a route to engineer such an effect.

Terentjev, 2007). LCEs can exhibit large deformation (up to 400%) (Herbert et al., 2021) in response to a wide range of stimuli including heat (Thomsen et al., 2001), electric field (Fowler et al., 2021), magnetic field (Kaiser et al., 2009) and light (Finkelmann et al., 2001). The explored applications for these materials include soft robotics and actuation (He et al., 2019; Annapooranan et al., 2023; Wang et al., 2023, 2019a; Yuan et al., 2017), optics (Brannum et al., 2019), biomedicine (Ferrantini et al., 2019; Turiv et al., 2020; Roach et al., 2019) and consumer devices (Iseki, 2019). In addition, recent developments in synthesis methods for LCEs have simplified the fabrication processes which has stimulated considerable interest in these materials (Ula et al., 2018; Wang et al., 2022; Chen et al., 2023).

The LCEs are cross-linked polymer networks containing mesogens (Ohm et al., 2010)—rigid rod-like molecules that have a strong tendency toward self-organization (Herbert et al., 2021). The mesogens are covalently linked to the polymer chain backbone where flexibility of polymer network permits rotation and motion of mesogens retaining liquid crystalline property of the material (Ula et al., 2018; Chanda and Roy, 2006). The LCEs can exhibit different phases and the phase transitions can lead to large macroscopic strains. Fig. 2 shows an LCE initially in the so-called nematic phase (where mesogens are aligned in one direction). Application of an external stimulus such as heat can trigger phase transition from this nematic to an isotropic state in which nematic mesogens are randomly oriented. This causes a contraction along the direction of nematic mesogens. The LCEs can be found in different phases distinguished by the positional and orientation order of the mesogens: e.g. nematic, smectic and cholesteric. We avoid further discussion on the molecular structure of LCEs and simply refer the reader to an expansive literature for an overview on this topic (Cf. Warner and Terentjev, 2007). The focus of our work is on the more common embodiment of LCEs based on the nematic phase.

Central to this paper is the very unique property of the LCEs pertaining to photo-induced actuation (Kumar et al., 2016; Li et al., 2012; Yu and Ikeda, 2011; Van Oosten et al., 2007; Camacho-Lopez et al., 2004). Essentially, light can induce rapid, large and reversible strain in these materials. The strain generated in the LCEs in response to light irradiation can be due to either photothermal or photochemical reasons (Pang et al., 2019). The photothermal effect is due to conversion of light to heat inside the material which can raise the temperature and trigger phase transition (thus leading to a large deformation—see reviews Dong and Zhao, 2018; Shang et al., 2019; Bisoyi et al., 2019). On the other hand, the photochemical effect may be observed in the LCEs if liquid crystal molecules contain photoisomerizable groups such as azobenzene (Dunn, 2007). The irradiation of light to azobenzene molecules can lead to trans→cis and cis→trans isomerizations generating a macroscopic deformation. The trans→cis isomerization occurs when azobenzene molecules are exposed to UV light. This isomerization changes the shape of the molecules from rod-like to strongly kinked rods which act as impurities and dilute the nematic ordering and lead to nematic to isotropic phase transition (Dunn, 2007). This phase transition can be reversed by exposing the material to visible light (Ube and Ikeda, 2019). In addition to this effect, the exposure of nematic LCE to a polarized light can induce reorientation of the nematic mesogens (Pang et al., 2019). The light induced reorientation effect, also known as the Weigert effect (Weigert, 1919), is a result of repeated trans–cis–trans isomerization cycles in response to polarized light irradiation (Ube and Ikeda, 2014). Several experimental studies have highlighted photo-induced reorientation in nematic liquid crystal polymers (Hrozhyk et al., 2009; White et al., 2009; Luo et al., 2021).

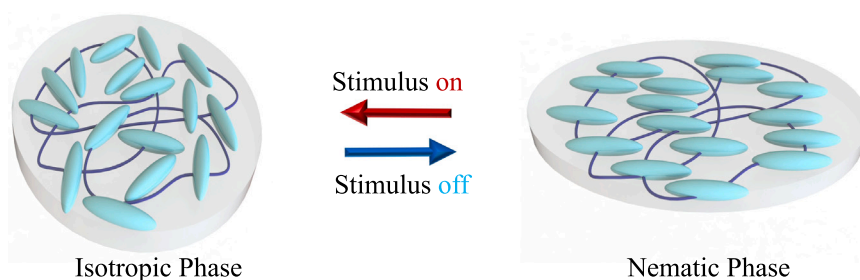


Fig. 2. Schematic illustration of strain induced as a result of phase transition in LCE in response to stimulus.

From the viewpoint of the development of mathematical theories to describe LCEs, three broad topics are relevant to the present study<sup>1</sup>: mechanical behavior, electromechanical coupling, photoactivity. We briefly summarize some representative literature on each of these in the following paragraphs.

In an early work, a phenomenological strain energy function for ideal nematic solids was proposed by [Bladon et al. \(1993\)](#)—the so-called BTW model. This neo-classical strain–energy function, which is a simple extension of the classical theory of rubber based on Gaussian polymer chains, emerged from statistical mechanics considerations of LCE microstructure ([Biggins et al., 2012](#)). Several others followed. For instance, a continuum theory for nematic elastomers was presented by [Anderson et al. \(1999\)](#) where they considered the directional effect of nematic mesogens by introducing orientational forces that expend power over the time-rate of the orientation field and comply with an orientational momentum balance. This approach was motivated by the seminal works of [Ericksen \(1961\)](#) and [Leslie \(1968\)](#), originally developed to study liquid crystals. [Chen and Fried \(2006\)](#) emphasized the need to correctly incorporate kinematic constraints while [DeSimone and Teresi \(2009\)](#) refined the anisotropic part of the BTW model and presented two new nonlinear extensions. In contrast to the BTW model, the approach of DeSimone and Teresi was able to capture the semi-soft behavior of LCEs. <sup>2</sup> [Agostiniani and DeSimone \(2012\)](#) presented an Ogden-type extension of free energy of nematic elastomer. In addition to monodomain LCEs, extension of the previously-discussed theoretical approaches to polydomain LCEs are also available in the literature ([Zhou and Bhattacharya, 2021](#); [Biggins et al., 2012](#)).

The behavior of LCEs under the action of electrical fields has also received attention in the literature ([Zentel, 1986](#); [Yusuf et al., 2005](#); [Fowler et al., 2021](#)). LCEs are not piezoelectric so the key electromechanical coupling mechanism (at least the one explored most widely in the literature) is that due to the electrostatic Maxwell stress or alternatively electrostriction. A conventional dielectric elastomer film, when subjected to a potential difference across its thickness, tends to contract along the direction of an applied electric field ([Rahmati et al., 2019](#); [Yang et al., 2017](#); [Zhao and Suo, 2010](#); [Cohen et al., 2016](#); [Kim et al., 2012](#)). However, LCEs may contract ([Fowler et al., 2021](#); [Davidson et al., 2019](#); [Guin et al., 2020](#)) or expand ([Urayama et al., 2006](#); [Urayama, 2007](#)) along the direction of applied electric field. This distinction is due to the markedly different microstructure of LCEs compared to conventional elastomers. The LCEs have an anisotropic dielectric tensor ([Warner and Terentjev, 2007](#)) and the material properties along the direction of the nematic mesogens are different from those in the perpendicular direction. The electrical Maxwell stress generates a force that depends on the alignment direction of the nematic mesogens ([Guin et al., 2020](#)). Also, the electrical field may trigger reorientation of nematic mesogens which tend to align themselves with electric field ([Corbett and Warner, 2009a](#)). This behavior that leads to an expansion along the direction of the electric field is also due to the anisotropic nature of the LCEs ([Fukunaga et al., 2008](#)). Therefore, there is a competition between the Maxwell stress and director reorientation effects in these materials ([Corbett and Warner, 2009b](#)) and the response is significantly more nuanced as compared to conventional elastomers and highly variable based on the boundary condition of the problem and material properties including viscoelasticity ([Corbett and Warner, 2009b](#)). Modeling the complex electro-mechanical response of LCEs has motivated several theoretical studies ([Eringen, 2000](#); [Fukunaga et al., 2008](#); [Menzel et al., 2009](#); [Terentjev et al., 1999](#); [Diaz-Calleja et al., 2013](#); [Díaz-Calleja and Díaz-Boils, 2014](#); [Calleja et al., 2014](#); [Menzel and Brand, 2008](#); [Müller and Brand, 2005](#); [Terentjev et al., 1994](#); [Xu and Huo, 2021](#); [Corbett and Warner, 2009a,b](#)). Although it has been shown that the effect of the Maxwell stress could be considerable ([Fowler et al., 2021](#); [Davidson et al., 2019](#); [Guin et al., 2020](#)), it is sometimes omitted ([Xu and Huo, 2021](#); [Corbett and Warner, 2009a,b](#); [Xu et al., 2022](#)).

Light-induced actuation in photoactive LCEs has been modeled by several groups ([Jin et al., 2010](#); [Warner and Mahadevan, 2004](#); [Zhang and Huo, 2018](#); [Warner et al., 2010](#); [Lin et al., 2012](#); [Corbett and Warner, 2007](#); [You et al., 2012](#)). Many studies have primarily focused on one specific class of deformation such as bending ([Warner and Mahadevan, 2004](#); [Corbett and Warner, 2007](#)) or they do not consider the effect of light polarization ([Hogan et al., 2002](#); [Liu and Onck, 2017](#); [Lin et al., 2012](#)). Recently, [Bai](#)

<sup>1</sup> Of course, we focus only on aspects germane to the topic of our paper and there are many aspects pertaining to models for LCEs that are beyond the scope of our paper e.g. statistical mechanics of LCEs at the microscale ([Brighenti et al., 2021](#)), atomistic considerations ([Illytskyi et al., 2012](#)), defects ([Acharya and Dayal, 2014](#)), polydomain engineering ([Biggins et al., 2012](#)), instabilities ([Pampolini and Triantafyllidis, 2018](#); [Mihai and Goriely, 2021](#)), low-dimensional modeling ([Babaei et al., 2021](#); [LoGrande et al., 2023](#)), design of devices among others.

<sup>2</sup> The semi-soft behavior means that stress–strain diagram is composed of three different parts. Initially, the material shows a hard response under small strains and then a soft response is observed accompanied by the reorientation of the nematic directors and, finally, once nematic directors are all aligned along the direction of maximum stretch, a stiffer response is observed.

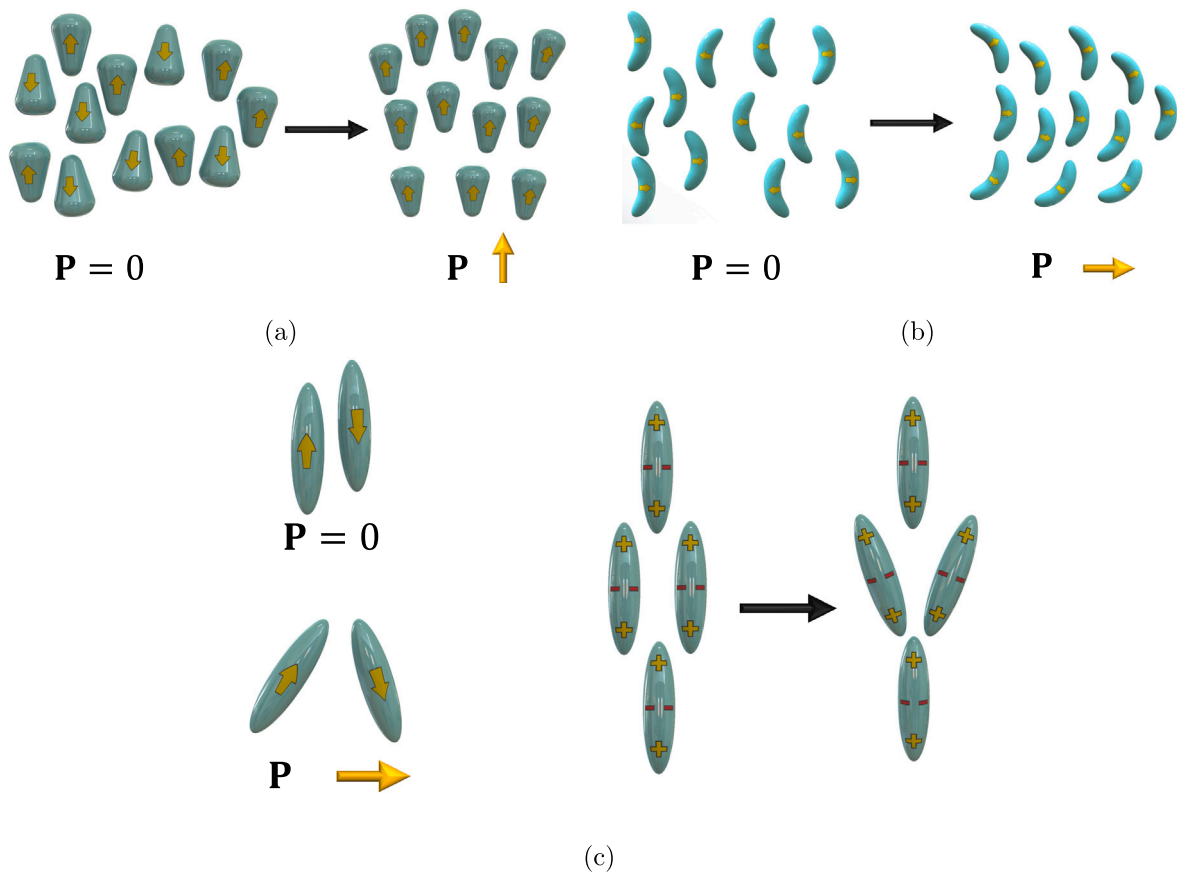


Fig. 3. The mechanism of the flexoelectricity for LCs with (a) wedge (pear) shaped molecules, (b) banana shaped molecules and (c) rod shaped molecules.

and Bhattacharya (2020) used a free-energy developed by Corbett and Warner (2006) to study photomechanical coupling in a photoactive LCE under both light illumination and mechanical stress. They explored the effect of light polarization direction on the reorientation of nematic directors and showed that nematic mesogens tend to align themselves in the direction perpendicular to light polarization direction. In another work, Babaei et al. (2021) explored the generation of torques in slender structures for potential application in soft robotics.

The conventional electromechanical coupling – piezoelectricity – admits a direct relation between mechanical deformation and electrical fields. However, piezoelectricity is restricted to only a subset of typically hard crystalline materials that lack centrosymmetry e.g. ceramics such as PZT, BaTiO<sub>3</sub> among others. There are some examples of piezoelectric polymers (e.g. PVDF) although the effect is rather weak and these polymers are relatively hard compared to soft elastomers. In contrast, flexoelectricity refers to the coupling between gradients of mechanical deformation and electrical polarization (and conversely, electrical field gradients and deformation). Unlike piezoelectricity, flexoelectricity is universal and present in all dielectrics including soft materials such as rubbers, 2D materials such as graphene ribbons or manifestly non-piezoelectric materials like Silicon. There has been a significant surge of interest in flexoelectricity and in particular, noting that flexoelectricity leads to the size-dependency of electromechanical coupling, researchers have advocated several tantalizing applications that can result from its exploitation especially by manipulating length-scale features. Some examples of this are: (1) creating piezoelectric materials without using piezoelectric materials (Sharma et al., 2007; Greco et al., 2024), (2) energy harvesting (Deng et al., 2014a; Jiang et al., 2023) including from rather exotic sources such as crumpling of paper (Wang et al., 2019b), (3) implications in biology (Torbaty et al., 2022) that range from mechanical behavior (Liu and Sharma, 2013), to mammalian hearing mechanism (Breneman et al., 2009; Deng et al., 2019) and even musical perception (Mozaffari et al., 2023), (4) fracture and defects (Mao and Purohit, 2015; Abdollahi et al., 2015; Giannakopoulos and Rosakis, 2020), (5) ferroelectricity in nanostructures (Catalan et al., 2011), (6) sensors and actuators (Bhaskar et al., 2016; Yan et al., 2023; Mathew and Kulkarni, 2023). We refer the reader to the following overviews that are good resources for further information on this phenomenon (Krichen and Sharma, 2016; Nguyen et al., 2013; Ahmadpoor and Sharma, 2015; Yudin and Tagantsev, 2013; Zubko et al., 2013; Deng et al., 2017).

We find it somewhat ironic that although the phenomenon of flexoelectricity was first noted in liquid crystals (Meyer, 1969), a theory for flexoelectricity for LCEs is conspicuously absent. While flexoelectricity in conventional elastomers (to various degrees of sophistication) has been addressed (Grasinger et al., 2021; Deng et al., 2014b; Codony et al., 2021) there is little literature on

this effect in LCEs (with just a few exceptions which we will highlight below). In liquid crystals, flexoelectricity refers to electrical polarization caused by a gradient of the mesogens orientation pattern (Meyer, 1969; Helfrich, 1974; Buka and Éber, 2013). The mechanism of flexoelectricity in liquid crystals depends on the molecule shape of the mesogens (see Fig. 3) (Nguyen et al., 2013). As shown, for wedge (pear) shaped molecule (Fig. 3(a)) a splay arrangement of the molecules leads to generation of a non-zero polarization and for banana shaped molecules (Fig. 3(b)) polarization is produced in response to bending arrangement of the molecules (Jiang et al., 2013). For rod shaped molecules shown in Fig. 3(c), both bending and splay rotation of molecules can break the anti-parallel polarization symmetry of the polarization and create a net polarization (Prost and Marcerou, 1977; Cheung et al., 2004). The formation of a quadrupoles can also contribute to exhibition of flexoelectric effect (Fig. 3(c)) (Cheung et al., 2004). It has been observed experimentally that liquid crystals with rod shaped molecule have flexoelectric coefficient in the order of 1 pC/m while the flexoelectric coefficient of the banana shaped molecules is three orders of magnitude larger (Kumar et al., 2009; Harden et al., 2006; Xiang et al., 2017; Takezoe and Takanishi, 2006). As already hinted earlier, we are aware of just a few works on flexoelectricity in LCEs. Harden et al. (2010) experimentally showed side-bent bent-core LCEs can exhibit a ‘‘giant’’ flexoelectric coefficient ( $\sim 30$  nC/m). Chambers et al. (2009) reported a large flexoelectric coupling in a calamitic LCE swollen with bent-core liquid crystal ( $\sim 20$  nC/m). Recently, Rajapaksha et al. (2021) also observed a flexoelectric-like response in ionic LCE. The theoretical studies for flexoelectric behavior of LCEs have been rare (Brand and Pleiner, 1994; Menzel, 2008; Menzel and Brand, 2007, 2008) with a nearly non-existent overlap with the present work. Brand and Pleiner (1994) considered flexoelectric effect and presented the hydrodynamic and electrohydrodynamic equations for nematic side-chain elastomers. They generalized (Genies, 1980) work by allowing for couplings to external magnetic and electric fields. They referenced (Genies, 1982) for the form of the flexoelectric tensor. Similarly, flexoelectric terms were considered in a more general energy formulation presented by Menzel (2008), Menzel and Brand (2007) to study cholesteric elastomers under external mechanical and electric fields. They also used a similar energy formulation to study instabilities in nematic elastomers in external electric and magnetic fields (Menzel and Brand, 2008) where they showed flexoelectric terms vanish in their solution. Despite all these efforts, to the best of our knowledge, there is no comprehensive nonlinear theory for flexoelectricity that includes effects of photo-flexoelectricity.

In this work, we develop a comprehensive theory that accounts for the interplay between light, mechanics and electricity in LCEs and represents a first attempt to establish a framework for photo-flexoelectricity. The theory is nonlinear and accordingly, to facilitate analytical solutions for boundary value problems of practical interest, we also present asymptotic forms of the governing equations in various regimes. We also derive, what appear to be, the first dynamical framework for photoflexoelectricity. To enable computational progress in problems that are analytically intractable, we present finite element implementation of the static part of the theory and investigate flexoelectric behavior of LCEs under stretch and bending deformations. Both computationally and through analytical methods, we study several boundary value problems that provide insights into the strain-mediated conversion of light into electricity as well as the role of the size-effect due to flexoelectricity.

## 2. Equilibrium models: a variational formulation

**Notation:** Let  $V_R \subset \mathbb{R}^3$  be the body of the nematic liquid crystal elastomer (LCE) in the reference undeformed configuration. The deformation  $\chi$  maps reference configuration  $V_R$  to the current configuration  $V$ . The material points in the reference configuration are denoted by  $\mathbf{x}$  and the material points in the current configuration are denoted by  $\mathbf{y}$ . The boundary of the body in the current (rep. reference) configuration is denoted by  $\partial V$  (resp.  $\partial V_R$ ). The unit normal to the surface in the current (rep. reference) configuration is denoted by  $\mathbf{v}$  (resp.  $\mathbf{v}_R$ ). The gradient operator in the Lagrangian (resp. Eulerian) coordinates are represented by  $\nabla$  (resp.  $\nabla_y$ ). The gradient of a vector field is denoted by  $\nabla \mathbf{u}$  with components given by  $u_{i,j}$  whereas the divergence of a tensor field is given by  $\text{div} \mathbf{M}$  with components given by  $M_{ij,j}$ , i.e., the divergence operates on row vectors of  $\mathbf{M}$ . For a square matrix  $\mathbf{M}$ ,

$$\text{Sym}(\mathbf{M}) = \frac{1}{2}(\mathbf{M} + \mathbf{M}^\top) \quad \text{and} \quad \text{Skw}(\mathbf{M}) = \frac{1}{2}(\mathbf{M} - \mathbf{M}^\top)$$

denote respectively the symmetric and skew-symmetric part of  $\mathbf{M}$ . For a small scaling parameter  $\epsilon > 0$ , the big  $O(\epsilon)$  means a quantity of the same scale as  $\epsilon$ , i.e.,  $\lim_{\epsilon \rightarrow 0} O(\epsilon)/\epsilon = C_1 > 0$  whereas the small  $o(\epsilon)$  means a quantity that is negligible as compared with  $\epsilon$ , i.e.  $\lim_{\epsilon \rightarrow 0} o(\epsilon)/\epsilon = 0$ .

We start from assuming that the thermodynamic state of the LCE body is described by an order parameter  $Q : V \rightarrow \mathbb{R}$ , director field  $\mathbf{n} : V \rightarrow S^2 := \{\mathbf{e} \in \mathbb{R}^3 : |\mathbf{e}| = 1\}$ , polarization  $\mathbf{p} : V \rightarrow \mathbb{R}^3$  and deformation  $\mathbf{y} : V_R \rightarrow V$ . In terms of state variables  $(Q, \mathbf{y}, \mathbf{n}, \mathbf{p})$ , we identify deformation gradient tensor  $\mathbf{F}$ , Jacobian  $J$ , the Cauchy–Green strain tensors  $\mathbf{C}$  and  $\mathbf{B}$  as

$$\mathbf{F} = \nabla \mathbf{y}, \quad J = \det \mathbf{F}, \quad \mathbf{C} = \mathbf{F}^\top \mathbf{F}, \quad \mathbf{B} = \mathbf{F} \mathbf{F}^\top. \quad (2.1)$$

### 2.1. Energetics

For equilibrium responses of a photo-flexoelectric nematic LCE body under electro-opto-mechanical-nematic loadings, we identify the total free energy  $\mathcal{F}^{\text{tot}}$  of the system as

$$\begin{aligned} \mathcal{F}^{\text{tot}}[Q, \mathbf{y}, \mathbf{n}, \mathbf{p}] &= \mathcal{U}^{\text{tot}}[Q, \mathbf{y}, \mathbf{n}, \mathbf{p}] + \mathcal{P}^{\text{bc}}[\mathbf{y}, \mathbf{n}, \mathbf{p}], \\ \mathcal{U}^{\text{tot}} &= \mathcal{F}^{\text{el-an}} + \mathcal{F}^{\text{Frank}} + \mathcal{F}^{\text{elect}} + \mathcal{F}^{\text{flexo}} + \mathcal{F}^{\text{opt}}, \end{aligned} \quad (2.2)$$

where  $\mathcal{F}^{\text{el-an}}$ ,  $\mathcal{F}^{\text{Frank}}$ ,  $\mathcal{F}^{\text{elect}}$ ,  $\mathcal{F}^{\text{flexo}}$ ,  $\mathcal{F}^{\text{opt}}$ , and  $\mathcal{P}^{\text{bc}}$ , respectively, represents the contribution of the (regular) elasticity, Frank elasticity, electrical energy, flexoelectricity, photo-nematic coupling, and boundary loading devices to the total free energy of the system. Below we define the energy terms in Eq. (2.2) one by one.

**Elasticity.** The regular elasticity  $\mathcal{F}^{\text{el-an}}$  originates from the energetic cost of elastically deform the body and admits two terms (DeSimone and Teresi, 2009):

$$\mathcal{F}^{\text{el-an}}[Q, \mathbf{n}, \mathbf{y}] = \int_{V_R} (W^{\text{elast}} + W^{\text{anis}}). \quad (2.3)$$

Here,  $W^{\text{elast}}$  is the strain elastic energy density of the LCE and  $W^{\text{anis}}$  is the energy contribution due to anisotropy of the nematic mesogens in the load free state. As it was discussed in the introductory section, we use the free energy density proposed by DeSimone and Teresi (2009):

$$W^{\text{elast}}(\mathbf{F}, \mathbf{n}) = \frac{\mu}{2} J^{-2/3} (\mathbf{F}\mathbf{F}^\top) \cdot (\mathbf{F}_\mathbf{n}\mathbf{F}_\mathbf{n}^\top)^{-1} + \frac{1}{2} \kappa (J - 1)^2, \quad (2.4)$$

where  $\mu$  and  $\kappa$  are shear modulus and bulk modulus of the material, and  $\mathbf{F}_\mathbf{n}$  is defined as

$$\mathbf{F}_\mathbf{n} := a^{1/3} \mathbf{n} \otimes \mathbf{n} + a^{-1/6} (\mathbf{I} - \mathbf{n} \otimes \mathbf{n}). \quad (2.5)$$

Here,  $a$  is a material parameter characterizing the amount of spontaneous strain generated along the nematic director direction as a result of the isotropic-to-nematic phase transformation (DeSimone, 2011). It is a combined measure of the degree of order and the strength of the nematic elastic coupling (DeSimone, 2011). We assume the nematic LCE is prolate ( $a > 1$ ), meaning that the isotropic-to-nematic phase transformation leads to an expansion along the nematic direction. Also, we will neglect effect of temperature on all material properties including  $a$ , assuming thus a fixed temperature that is well below the random-to-nematic transition temperature.

Theoretical (Warner et al., 1994; Bladon et al., 1994) and experimental observations (Küpfer and Finkelmann, 1991; Kundler and Finkelmann, 1995) show that *ideal* LCEs can undergo large deformation with minimal or no stress. This behavior is a direct result of the reorientation of nematic directors. The assumption of the isotropic reference state, meaning that all director orientations are equivalent, is indeed the foundation for the ideally soft behavior in liquid crystal elastomers (Biggins et al., 2012; Warner, 1999; Lee and Bhattacharya, 2022). In reality, some anisotropy is induced in LCEs during cross-linking which is often produced using magnetic or stress fields (Warner, 1999; Urayama et al., 2009). Thus, stretching experiments on real nematic elastomers frequently deviate from the ideal response, exhibiting “semi-soft” behavior. In the first stage of the stretch-stress curve, a non-zero shear modulus is observed as the stress increases with strain. In the second stage, a plateau forms at finite stress values, indicating semi-soft behavior. Finally, in the third stage, stress rises again as the material stiffens with further stretching (DeSimone and Teresi, 2009). Semi-soft behavior of LCEs has been the subject of extensive research and is not fully understood yet (Teixeira and Warner, 1999; Mistry et al., 2018). Therefore, it is important to include an anisotropic energy term  $W^{\text{anis}}$  in our energy formulation. DeSimone and Teresi (2009) proposed the following energy term for the anisotropic effect:

$$W^{\text{anis}}(\mathbf{F}) = \frac{\mu_\beta}{2} J^{-2/3} (\mathbf{F}^\top \mathbf{F}) : (\mathbf{F}_\mathbf{N}^\top \mathbf{F}_\mathbf{N})^{-1}, \quad (2.6)$$

where  $\mathbf{N} \in S^2$  is certain direction featured in the parent random phase before nematic phase transition,  $\mathbf{F}_\mathbf{N} = a^{1/3} \mathbf{N} \otimes \mathbf{N} + a^{-1/6} (\mathbf{I} - \mathbf{N} \otimes \mathbf{N})$ , and the modulus  $\mu_\beta$  characterizes how large the anisotropic contribution may be.

The energy functions (2.4) and (2.6) need to be modified for optical effects. In this case, for simplicity we assume incompressibility ( $J \equiv 1$ ) and consider the elastic energy densities are function of variable order parameter  $Q$ . We will use following energy function to incorporate the order parameter  $Q$  (Bai and Bhattacharya, 2020):

$$W^{\text{elast}}(Q, \mathbf{F}, \mathbf{n}) = \frac{\mu}{2} [(\mathbf{F}\mathbf{F}^\top) : \mathbf{L}_\mathbf{n}^{-1} + \log(\det \mathbf{L}_\mathbf{n})], \quad (2.7)$$

where  $\mathbf{L}_\mathbf{n}$  is given as

$$\mathbf{L}_\mathbf{n} = 3Q\mathbf{n} \otimes \mathbf{n} + (1 - Q)\mathbf{I}. \quad (2.8)$$

Similarly, we update the anisotropic energy to incorporate the contribution of the order parameter  $Q$ . To avoid confusion between light-dependent (2.7) and light-independent energy densities (2.4), we introduce two parameters  $a_1$  and  $a_2$  and express the elastic energy density and anisotropic contributions as

$$\begin{aligned} W^{\text{elast}} &= \frac{1}{2} \mu a_1 |\mathbf{F}|^2 + \frac{1}{2} \mu a_2 |\mathbf{F}^\top \mathbf{n}|^2, \\ W^{\text{anis}} &= \frac{1}{2} \mu_\beta a_1 |\mathbf{F}|^2 + \frac{1}{2} \mu_\beta a_2 |\mathbf{F}\mathbf{N}|^2. \end{aligned} \quad (2.9)$$

If the optical effects are included in the analysis,

$$a_1 = \frac{1}{1 - Q}, \quad a_2 = \frac{1}{1 + 2Q} - \frac{1}{1 - Q}, \quad (2.10)$$

and if the optical effects are excluded from the analysis,

$$a_1 = a^{1/3}, \quad a_2 = a^{-2/3}(1 - a). \quad (2.11)$$

We remark that by setting  $a_1 = 1$  and  $a_2 = a - 1$ , the elastic energy density (2.9) is reduced to the BTW energy (Bladon et al., 1993; DeSimone, 2010).

**Frank Elasticity.** The energy term  $\mathcal{F}^{\text{Frank}}$  is referred to as the Frank elasticity which penalize the spatial gradient of the director field  $\mathbf{n}$ . In many conventional formulation of LCEs, the effect of the Frank elasticity is neglected as the Frank elasticity coefficients are often very small (De Gennes and Prost, 1993). As it will be shown here, the Frank elasticity effect is a size-dependent effect and this effect becomes stronger at smaller lengthscale where the flexoelectric effect also becomes important. Also, it will be shown that the formulation becomes thermodynamically unstable if we include the flexoelectric effect and neglect the Frank elasticity. A simple form of free energy function for the Frank elasticity can be written as ( $K_F > 0$ )

$$\mathcal{F}^{\text{Frank}}[\mathbf{y}, \mathbf{n}] = \int_V W^{\text{Frank}}(\nabla_y \mathbf{n}), \quad W^{\text{Frank}}(\nabla_y \mathbf{n}) = \frac{1}{2} K_F |\nabla_y \mathbf{n}|^2. \quad (2.12)$$

In reference configuration, the Frank elastic energy is given by

$$\mathcal{F}^{\text{Frank}}[\mathbf{y}, \mathbf{n}] = \int_{V_R} \frac{1}{2} K_F J |(\nabla \mathbf{n}) \mathbf{F}^{-1}|^2. \quad (2.13)$$

**Remark 1 (General Frank Elasticity).** The energetic cost of different modes of spatial distortion of nematic directors may be different. A more general Frank free energy may be postulated as a quartic form of  $(\mathbf{n}, \nabla_y \mathbf{n})$ :

$$W^{\text{Frank}} = W^{\text{Frank}}(\mathbf{n}, \nabla_y \mathbf{n}) = \mathbb{K}_{ijklmn} n_i n_j n_k n_l n_m n_n,$$

where  $\mathbb{K}$  is a sixth-order tensor. The invariance of Frank energy with respect to an orthogonal transformation of reference configuration (i.e.,  $\mathbf{x} \rightarrow \mathbf{Q}\mathbf{x}$  for any  $\mathbf{Q} \in \text{SO}(3)$ ), together with frame-indifference (i.e.,  $\mathbf{n} \rightarrow \mathbf{Q}'\mathbf{n}$  for any  $\mathbf{Q}' \in \text{SO}(3)$ ), implies that

$$W^{\text{Frank}}(\mathbf{n}, \nabla_y \mathbf{n}) = W^{\text{Frank}}(\mathbf{Q}\mathbf{n}, \mathbf{Q}(\nabla_y \mathbf{n})\mathbf{Q}^T) \quad \forall \mathbf{Q} \in \text{SO}(3). \quad (2.14)$$

We remark that frame-indifference alone does not imply the invariance (2.14). As a consequence, the six-order (isotropic) tensor  $\mathbb{K}_{ijklmn}$  must be such that

$$W^{\text{Frank}}(\mathbf{n}, \nabla_y \mathbf{n}) = \frac{K_1}{2} |\text{div}_y \mathbf{n}|^2 + \frac{K_2}{2} |\mathbf{n} \cdot (\nabla_y \times \mathbf{n})|^2 + \frac{K_3}{2} |\mathbf{n} \times (\nabla_y \times \mathbf{n})|^2 + \frac{K_4}{2} (\text{Tr}(\nabla_y \mathbf{n})^2 - |\text{div}_y \mathbf{n}|^2), \quad (2.15)$$

where the coefficients  $K_{1,2,3,4}$  are called Frank constants. If  $K_1 = K_2 = K_3 = K_4 = K_F$ , the general form (2.15) can be written as (2.12).

**Electrostatics.** Denote by  $\xi : V \rightarrow \mathbb{R}$  the electrical potential and  $\mathbf{e} = -\nabla_y \xi$  the spatial electrical field. The Maxwell equation in the current and reference configurations can be written as

$$\begin{aligned} \mathbf{d} &= -\epsilon_0 \nabla_y \xi + \mathbf{p} & \text{div}(\mathbf{d}) &= 0 & \text{in } V, \\ \tilde{\mathbf{D}} &= -\epsilon_0 J \mathbf{C}^{-1} \nabla \xi + J \mathbf{F}^{-1} \mathbf{p} & \text{div}_y(\tilde{\mathbf{D}}) &= 0 & \text{in } V_R, \end{aligned} \quad (2.16)$$

where  $\mathbf{d}$  (resp.  $\tilde{\mathbf{D}}$ ) is the electrical displacement in the current (resp. reference) configuration, and  $\epsilon_0$  is the electrical permittivity of the vacuum. Suppose that the boundary potential is maintained at  $\xi_b : \partial V_R \rightarrow \mathbb{R}$  by an external circuit:

$$\xi = \xi_b \quad \text{on } \partial V_R. \quad (2.17)$$

Then Eqs. (2.16)–(2.17) uniquely determine the electrical fields for given polarization  $\mathbf{p} : V \rightarrow \mathbb{R}^3$ .

As a nonlocal functional of state variables  $(\mathbf{y}, \mathbf{n}, \mathbf{p})$ , the electrical energy is identified as

$$\mathcal{F}^{\text{elect}}[\mathbf{y}, \mathbf{n}, \mathbf{p}] = \mathcal{E}^{\text{elect}}[\mathbf{y}, \mathbf{p}] + \int_{V_R} W^{\text{pol}}(\nabla_y \mathbf{n}, \mathbf{n}, \mathbf{p}), \quad (2.18)$$

where  $W^{\text{pol}}$  is the polarization energy for recovering appropriate dielectric property of the materials, and

$$\mathcal{E}^{\text{elect}}[\mathbf{y}, \mathbf{p}] = \int_{V_R} \frac{\epsilon_0}{2} J |\mathbf{F}^{-T} \nabla \xi|^2 = \int_V \frac{\epsilon_0}{2} |\nabla_y \xi|^2 \quad (2.19)$$

is the field energy contributed by the local electrical field. Suppose that the LCE is a linear dielectric LCE with dielectric tensor given by

$$\mathbb{D}_{\mathbf{n}} = (\epsilon_c - \epsilon_a) \mathbf{n} \otimes \mathbf{n} + \epsilon_a \mathbf{I}, \quad (2.20)$$

where  $\epsilon_a$  (resp.  $\epsilon_c$ ) is the permittivity along the a-axis (resp. c-axis) of the mesogen and is independent of deformation. To recover the linear dielectric property, we identify (Cf. Liu, 2014)

$$W^{\text{pol}}(\mathbf{F}, \mathbf{n}, \mathbf{p}) = \frac{J}{2} \mathbf{p} \cdot (\mathbb{D}_{\mathbf{n}} - \epsilon_0 \mathbf{I})^{-1} \mathbf{p}, \quad (2.21)$$

where, by (2.20), we find that  $(\mathbb{D}_n - \epsilon_0 \mathbf{I})^{-1} = A_1 \mathbf{n} \otimes \mathbf{n} + A_2 \mathbf{I}$ , and

$$A_1 = -\frac{\epsilon_c - \epsilon_a}{(\epsilon_c - \epsilon_0)(\epsilon_a - \epsilon_0)}, \quad A_2 = \frac{1}{\epsilon_a - \epsilon_0}. \quad (2.22)$$

**Flexoelectricity.** Flexoelectricity refers to the coupling between polarization and strain gradient. In liquid crystals, the coupling is mediated by the director field and modeled by introducing the flexoelectric energy:

$$W^{\text{flexo}} = W^{\text{flexo}}(\mathbf{n}, \nabla_y \mathbf{n}, \mathbf{p}). \quad (2.23)$$

Suppose that the function  $W^{\text{flexo}}(\mathbf{n}, \nabla_y \mathbf{n}, \mathbf{p})$  linearly depends on its arguments (Meyer, 1969; Frank, 1958):

$$W^{\text{flexo}}(\mathbf{n}, \nabla_y \mathbf{n}, \mathbf{p}) = (\mathbf{n} \otimes \mathbf{p}) : \mathbb{F}(\nabla_y \mathbf{n}) = \mathbb{F}_{ijkl} n_i p_j n_k y_l, \quad (2.24)$$

where the fourth-order tensor  $\mathbb{F}_{ijkl}$  is called the flexoelectric tensor. Suppose that the flexoelectric interaction does not have any preferred direction, meaning that

$$W^{\text{flexo}}(\mathbf{Qn}, \mathbf{Q}(\nabla_y \mathbf{n})\mathbf{Q}^T, \mathbf{Qp}) = W^{\text{flexo}}(\mathbf{n}, \nabla_y \mathbf{n}, \mathbf{p}) \quad \forall \mathbf{Q} \in \text{SO}(3).$$

The reader is again cautioned that the principle of frame-indifference alone does not imply the above requirement. As is well-known (Gurtin et al., 2010), isotropic fourth-order tensor can in general be written as  $\mathbb{F}_{ijkl} = -f'_b \delta_{ik} \delta_{jl} - f_b \delta_{il} \delta_{jk} - f_s \delta_{ij} \delta_{kl}$ . Therefore,

$$\begin{aligned} W^{\text{flexo}}(\mathbf{n}, \nabla_y \mathbf{n}, \mathbf{p}) &= -f_s (\nabla_y \cdot \mathbf{n})(\mathbf{p} \cdot \mathbf{n}) - f'_b \mathbf{n} \cdot (\nabla_y \mathbf{n})\mathbf{p} - f_b \mathbf{p} \cdot (\nabla \mathbf{n})\mathbf{n} \\ &= -f_s (\nabla_y \cdot \mathbf{n})(\mathbf{p} \cdot \mathbf{n}) + f_b (\mathbf{n} \times (\nabla_y \times \mathbf{n})) \cdot \mathbf{p}, \end{aligned} \quad (2.25)$$

where we have used  $\mathbf{n} \cdot (\nabla_y \mathbf{n})\mathbf{p} = 0$  since  $|\mathbf{n}| = 1$  and  $(\mathbf{n} \times (\nabla_y \times \mathbf{n})) \cdot \mathbf{p} = \mathbf{n} \cdot (\nabla_y \mathbf{n})\mathbf{p} - \mathbf{p} \cdot (\nabla_y \mathbf{n})\mathbf{n}$ . Also, the two independent flexoelectric coefficients  $f_s, f_b \in \mathbb{R}$  characterize the coupling of polarization with the splay and bending of the director field, respectively. In conclusion, the free energy contributed by flexoelectricity can be expressed as ( $\mathbb{F}_{ijkl} = -f_b \delta_{il} \delta_{jk} - f_s \delta_{ij} \delta_{kl}$ )

$$\mathcal{F}^{\text{flexo}}[\mathbf{n}, \mathbf{y}, \mathbf{p}] = \int_V W^{\text{flexo}}(\mathbf{n}, \nabla_y \mathbf{n}, \mathbf{p}) = \int_{V_R} \mathbf{J}(\mathbf{n} \otimes \mathbf{p}) : \mathbb{F}((\nabla \mathbf{n})\mathbf{F}^{-1}). \quad (2.26)$$

We note that a common practice in formulation of flexoelectricity for liquid crystals is to use electrical field as the independent thermodynamic variable and postulate the flexoelectric energy as (Adler et al., 2015):

$$\mathcal{F}^{\text{flexo}} = \int_V [e_s (\nabla_y \cdot \mathbf{n})(\nabla_y \xi \cdot \mathbf{n}) - e_b (\mathbf{n} \times \nabla_y \times \mathbf{n}) \cdot \nabla_y \xi], \quad (2.27)$$

where  $e_b$  and  $e_s$  are flexoelectric coefficients. However, we use polarization as the independent variable for applying the principle of minimum free energy to the system and, thus, employ the energy (2.26) instead of (2.27). Finally, the sign convention for two different terms given in (2.27) are different among different authors (Adler et al., 2015; Elston, 2008; De Gennes and Prost, 1993; Meyer, 1969).

**Photo-nematic Coupling.** The coupling between nematic director and light is included in the formulation through  $\mathcal{F}^{\text{opt}}[Q, \mathbf{n}]$  which is proposed as (Bai and Bhattacharya, 2020) :

$$\begin{aligned} \mathcal{F}^{\text{opt}}[Q, \mathbf{n}] &= \int_{V_R} W^{\text{opt}}(Q, \mathbf{n}), \\ W^{\text{opt}} &= \mu_n (1 - c(Q, \mathbf{n})) [g^{-1}(Q)Q - \log Z(Q) - \frac{1}{2}(1 - c(Q, \mathbf{n}))\bar{J}_n Q^2], \\ g(x) &= -\frac{1}{2} - \frac{1}{2x} + \frac{1}{2x} \sqrt{\frac{3x}{2}} \frac{\exp(\frac{3}{2}x)}{\int_0^{\sqrt{\frac{3x}{2}}} \exp(y^2) dy}, \\ Z(Q) &= \frac{\exp[g^{-1}(Q)]}{1 + g^{-1}(Q)(1 + 2Q)}, \quad c(Q, \mathbf{n}) = f \frac{I [1 + Q(3(\mathbf{n} \cdot \mathbf{n}_0)^2 - 1)]}{3 + I [1 + Q(3(\mathbf{n} \cdot \mathbf{n}_0)^2 - 1)]}, \end{aligned} \quad (2.28)$$

where  $\mathbf{n}_0 \in S^2$  represents the direction of the polarization of the applied light to the material. Also,  $I, f, \bar{J}_n$  and  $\mu_n$ , respectively, represent light intensity, fraction of photoactive mesogens, interaction between mesogens and photoactivation modulus.

**Boundary conditions.** The LCE body  $V_R$  or  $V$  interacts with the environment through boundary loading devices. Recall that  $\mathbf{v}_R \in S^2$  (resp.  $\mathbf{v} = \mathbf{J}\mathbf{F}^{-T} \mathbf{v}_R / |\mathbf{J}\mathbf{F}^{-T} \mathbf{v}_R| \in S^2$ ) represents the unit outward normal on  $\partial V_R$  (resp.  $\partial V$ ). The electro-mechanical-nematic loading conditions are prescribed as follows.

1. Mechanically, the traction on the reference configuration is denoted by  $\tilde{\mathbf{t}}_b : \partial V_R \rightarrow \mathbb{R}^3$  or on the current configuration  $\mathbf{t}_b : \partial V \rightarrow \mathbb{R}^3$ . ( $\tilde{\mathbf{t}}_b = \mathbf{t}_b |\mathbf{J}\mathbf{F}^{-T} \mathbf{v}_R|$ ) Suppose that the applied traction  $\tilde{\mathbf{t}}_b$  is "dead" load, i.e., independent of deformation or time. Then its energetic contribution to the system free energy is given by

$$P^{\text{mech}}[\mathbf{y}] = - \int_{\partial V_R} \tilde{\mathbf{t}}_b \cdot \mathbf{y} = - \int_{\partial V} \mathbf{t}_b \cdot \mathbf{y}. \quad (2.29)$$

If the LCE body is in a transient state, the rate of mechanical work done to the body by the applied traction is given by

$$\dot{W}^{\text{mech}}[\mathbf{y}] = \int_{\partial V_R} \tilde{\mathbf{t}}_b \cdot \dot{\mathbf{y}} = \int_{\partial V} \mathbf{t}_b \cdot \dot{\mathbf{y}}. \quad (2.30)$$

2. Electrically, the boundary electrical potential is maintained at  $\xi_b : V_R \rightarrow \mathbb{R}$  by some external circuit. Its energetic contribution to the system free energy is identified as

$$P^{\text{elect}}[\mathbf{y}, \mathbf{p}] = \int_{\partial V_R} \xi_b \tilde{\mathbf{D}} \cdot \mathbf{v}_R = \int_{\partial V} \xi_b \mathbf{d} \cdot \mathbf{v} = \int_{\partial V} \xi_b (J \mathbf{F}^{-1} \mathbf{d}) \cdot \frac{\mathbf{F}^T \mathbf{v}}{J}. \quad (2.31)$$

In a transient state, the rate of electrical work done to the LCE body by the external circuit is given by

$$\dot{W}^{\text{elect}}[\mathbf{y}, \mathbf{p}] = - \int_{\partial V_R} \xi_b \left( \frac{d}{dt} \tilde{\mathbf{D}} \right) \cdot \mathbf{v}_R = - \int_{\partial V} \xi_b \frac{d}{dt} (J \mathbf{F}^{-1} \mathbf{d}) \cdot \frac{\mathbf{F}^T \mathbf{v}}{J}, \quad (2.32)$$

where  $\tilde{\mathbf{D}} = J \mathbf{F}^{-1} \mathbf{d}$  (resp.  $\mathbf{d}$ ) is the electrical displacement in reference (resp. current) configuration (Cf. Eq. (2.16)).

3. The nematic interaction is characterized by applied director couple on the boundary  $\tilde{\mathbf{s}}_b : \partial V_R \rightarrow \mathbb{R}^3$  or  $\mathbf{s}_b : \partial V \rightarrow \mathbb{R}^3$ . ( $\tilde{\mathbf{s}}_b = \mathbf{s}_b | J \mathbf{F}^{-T} \mathbf{v}_R$ ) Suppose the applied director couple  $\tilde{\mathbf{s}}$  is independent of deformation or time. Then its energetic contribution to the system free energy is identified as

$$P^{\text{nem}}[\mathbf{n}] = - \int_{\partial V_R} \tilde{\mathbf{s}}_b \cdot \mathbf{n} = - \int_{\partial V} \mathbf{s}_b \cdot \mathbf{n}, \quad (2.33)$$

and in a transient state, the rate of work done to the LCE body by the nematic loading device is given by

$$\dot{W}^{\text{nem}}[\mathbf{n}] = \int_{\partial V_R} \dot{\mathbf{n}} \cdot \tilde{\mathbf{s}}_b = \int_{\partial V} \dot{\mathbf{n}} \cdot \mathbf{s}_b, \quad (2.34)$$

Collecting terms in (2.29), (2.31) and (2.33), we identify the energetic contribution to the system free energy by the external loading devices as

$$\mathcal{P}^{\text{bc}}[\mathbf{y}, \mathbf{n}, \mathbf{p}] = \int_{\partial V_R} (-\tilde{\mathbf{t}}_b \cdot \mathbf{y} + \xi_b \tilde{\mathbf{D}} \cdot \mathbf{v}_R - \tilde{\mathbf{s}}_b \cdot \mathbf{n}). \quad (2.35)$$

We remark that the mechanical traction  $\tilde{\mathbf{t}}$  or  $\mathbf{t}$  and nematic director couple  $\tilde{\mathbf{s}}$  or  $\mathbf{s}$  are primitive concepts in the current framework. These quantities characterize the interaction between the LCE body or sub-body and the environment across the boundary and are hypothesized on any material surface/interface in the LCE body. As will be shown shortly (Cf. Section 3.1 and Eq. (3.11)) and in parallel to the classical Cauchy's theorem (Gurtin et al., 2010), this hypothesis implies the existence of mechanical stress tensor  $\boldsymbol{\sigma}$  and director couple tensor  $\mathbf{S}$ .

## 2.2. Variational principle and Euler–Lagrange equations

From the system free energy (2.2), we introduce the total free energy density function of the LCE body by collecting terms from Eqs. (2.3), (2.12), (2.18), (2.26) and (2.28) as

$$\Psi = W^{\text{elast}} + W^{\text{aniso}} + W^{\text{Frank}} + W^{\text{pol}} + W^{\text{flexo}} + W^{\text{opt}}. \quad (2.36)$$

Then the total free energy (2.2) of the system that includes the LCE body, electrical field, and boundary loading devices can be written as

$$\mathcal{F}^{\text{tot}}[Q, \mathbf{y}, \mathbf{n}, \mathbf{p}] = \int_{V_R} \Psi(Q, \nabla \mathbf{y}, \mathbf{n}, \nabla \mathbf{n}, \mathbf{p}) + \mathcal{E}^{\text{elect}}[\mathbf{y}, \mathbf{p}] + \mathcal{P}^{\text{bc}}[\mathbf{y}, \mathbf{n}, \mathbf{p}]. \quad (2.37)$$

We remark that the field energy  $\mathcal{E}^{\text{elect}}$  is nonlocal in the sense that it cannot be expressed as a single integral of a function of state variables  $(Q, \mathbf{y}, \mathbf{n}, \mathbf{p})$  and their derivatives, resulting in a separate treatment.

By the principle of minimum free energy, the equilibrium state of the system at a constant temperature is the state that minimizes the total free energy of the system. We use the standard calculus of variation to derive the associated Euler–Lagrange's equations. For a given state  $(Q, \mathbf{y}, \mathbf{n}, \mathbf{p})$ , an infinitesimal variation is defined as

$$(Q_\delta, \mathbf{y}_\delta, \mathbf{n}_\delta, \mathbf{p}_\delta) = (Q + \delta Q_1, \mathbf{y} + \delta \mathbf{y}_1, \mathbf{n} + \delta \mathbf{n}_1, \mathbf{p} + \delta \mathbf{p}_1),$$

where  $|\delta| \ll 1$  and  $(Q_1, \mathbf{y}_1, \mathbf{n}_1, \mathbf{p}_1)$  are arbitrary within the admissible space. By direct calculations, the first variation of elastic-anisotropic energy  $\mathcal{F}^{\text{el-an}}$  is given by

$$\begin{aligned} \left. \frac{d}{d\delta} \right|_{\delta=0} \mathcal{F}^{\text{el-an}}[Q_\delta, \mathbf{n}_\delta, \mathbf{y}_\delta] &= \int_{V_R} \left[ Q_1 \frac{\partial}{\partial Q} (W^{\text{elast}} + W^{\text{anis}}) \right. \\ &\quad \left. + J \mathbf{m}^{\text{elast}} \cdot \mathbf{n}_1 + (\boldsymbol{\Sigma}^{\text{elast}} + \boldsymbol{\Sigma}^{\text{anis}}) : \mathbf{F}_1 \right], \end{aligned} \quad (2.38)$$

where, from Eqs. (2.9), we find that

$$\begin{aligned}\Sigma^{\text{elast}} &= \frac{\partial W^{\text{elast}}}{\partial \mathbf{F}} = a_1 \mathbf{F} + a_2 \mathbf{n} \otimes \mathbf{F}^\top \mathbf{n}, \\ \Sigma^{\text{anis}} &= \frac{\partial W^{\text{anis}}}{\partial \mathbf{F}} = \mu_\beta (a_1 \mathbf{F} + a_2 \mathbf{F} \mathbf{N}_a \otimes \mathbf{N}_a),\end{aligned}\quad (2.39)$$

and

$$\mathbf{J} \mathbf{m}^{\text{elast}} := \frac{\partial W^{\text{elast}}}{\partial \mathbf{n}} = a_2 \mathbf{F} \mathbf{F}^\top \mathbf{n}.\quad (2.40)$$

By Eq. (2.13), the first variation of the Frank elasticity energy term is given by

$$\frac{d}{d\delta} \Big|_{\delta=0} \mathcal{F}^{\text{Frank}}[\mathbf{n}_\delta, \mathbf{y}_\delta] = \int_{V_R} \left( \Sigma^{\text{Frank}} : \mathbf{F}_1 + \tilde{\mathbf{S}}^{\text{Frank}} : \nabla \mathbf{n}_1 \right),\quad (2.41)$$

where

$$\begin{aligned}\tilde{\mathbf{S}}^{\text{Frank}} &= \frac{\partial W^{\text{Frank}}}{\partial \nabla \mathbf{n}} = K_F J \nabla \mathbf{n} \mathbf{F}^{-1} \mathbf{F}^{-\top}, \\ \Sigma^{\text{Frank}} &= \frac{\partial W^{\text{Frank}}}{\partial \mathbf{F}} = \frac{1}{2} J K_F \mathbf{F}^{-\top} |(\nabla \mathbf{n}) \mathbf{F}^{-1}|^2 - J K_F \mathbf{F}^{-\top} (\nabla \mathbf{n})^\top (\nabla \mathbf{n}) \mathbf{F}^{-1} \mathbf{F}^{-\top}.\end{aligned}\quad (2.42)$$

For the first variation of electrostatic energies, we combine the contributions of electric field and polarization (2.18), and boundary device (2.31). For brevity, the reader is referred to Liu (2014) for the detailed derivation of the first-variation of the electrical energy. Here we only present the final result:

$$\begin{aligned}\frac{d}{d\delta} \Big|_{\delta=0} \left( \mathcal{F}^{\text{elect}}[\mathbf{y}_\delta, \mathbf{n}_\delta, \mathbf{p}_\delta] + P^{\text{elect}}[\mathbf{y}_\delta, \mathbf{p}_\delta] \right) &= \int_{V_R} \left( J (\mathbf{F}^{-\top} \nabla \xi + \mathbf{e}^{\text{pol}}) \cdot \mathbf{p}_1 \right. \\ &\quad \left. + \mathbf{J} \mathbf{m}^{\text{pol}} \cdot \mathbf{n}_1 + \Sigma^{\text{MW}} : \mathbf{F}_1 \right),\end{aligned}\quad (2.43)$$

where

$$\begin{aligned}\mathbf{m}^{\text{pol}} &= A_1 (\mathbf{n} \cdot \mathbf{p}) \mathbf{p}, \quad \mathbf{e}^{\text{pol}} = (\mathbb{D}_n - \epsilon_0 \mathbf{I})^{-1} \mathbf{p}, \quad \Sigma^{\text{MW}} = J \sigma^{\text{MW}} \mathbf{F}^{-\top}, \\ \sigma^{\text{MW}} &= \nabla_y \xi \otimes \mathbb{D}_n \nabla_y \xi - \left[ \frac{\epsilon_0}{2} |\nabla_y \xi|^2 + (-\nabla_y \xi - \frac{\mathbf{e}^{\text{pol}}}{2}) \cdot \mathbf{p} \right] \mathbf{I}.\end{aligned}\quad (2.44)$$

By Eq. (2.26) the variation of the flexoelectric energy term is given as

$$\begin{aligned}\frac{d}{d\delta} \Big|_{\delta=0} \mathcal{F}^{\text{flexo}}[\mathbf{n}_\delta, \mathbf{y}_\delta, \mathbf{p}_\delta] &= \int_{V_R} \left[ \Sigma^{\text{flexo}} : \mathbf{F}_1 + \mathbf{J} \mathbf{e}^{\text{flexo}} \cdot \mathbf{p}_1 \right. \\ &\quad \left. + \mathbf{J} \mathbf{m}^{\text{flexo}} \cdot \mathbf{n}_1 + \tilde{\mathbf{S}}^{\text{flexo}} : \nabla \mathbf{n}_1 \right],\end{aligned}\quad (2.45)$$

where

$$\begin{aligned}\Sigma^{\text{flexo}} &= J f_s \mathbf{F}^{-\top} (\nabla \mathbf{n})^\top \mathbf{F}^{-\top} (\mathbf{p} \cdot \mathbf{n}) + J f_b \mathbf{F}^{-\top} (\nabla \mathbf{n})^\top \mathbf{p} \otimes \mathbf{F}^{-1} \mathbf{n} + J W^{\text{flexo}} \mathbf{F}^{-\top}, \\ \mathbf{e}^{\text{flexo}} &= -f_s (\nabla \mathbf{n} : \mathbf{F}^{-\top}) \mathbf{n} - f_b (\nabla \mathbf{n}) \mathbf{F}^{-1} \mathbf{n}, \\ \mathbf{m}^{\text{flexo}} &= -f_b \mathbf{F}^{-\top} (\nabla \mathbf{n})^\top \mathbf{p} - f_s (\nabla \mathbf{n} : \mathbf{F}^{-\top}) \mathbf{p}, \\ \tilde{\mathbf{S}}^{\text{flexo}} &= J \mathbf{S}^{\text{flexo}} \mathbf{F}^{-\top}, \quad \mathbf{S}^{\text{flexo}} = -f_s (\mathbf{p} \cdot \mathbf{n}) \mathbf{I} - f_b \mathbf{p} \otimes \mathbf{n}.\end{aligned}\quad (2.46)$$

Finally, by Eq. (2.28) the variation of the optical energy term can be written as

$$\frac{d}{d\delta} \Big|_{\delta=0} \mathcal{F}^{\text{opt}}[Q_\delta, \mathbf{n}_\delta] = \int_{V_R} \left[ \frac{\partial W^{\text{opt}}}{\partial Q} Q_1 + \mathbf{J} \mathbf{m}^{\text{opt}} \cdot \mathbf{n}_1 \right], \quad (\mathbf{J} \mathbf{m}^{\text{opt}} = \frac{\partial W^{\text{opt}}}{\partial \mathbf{n}}).\quad (2.47)$$

For brevity, we introduce the total (conservative) mechanical stress  $\Sigma^{\text{tot}}$ , total director couple tensor  $\tilde{\mathbf{S}}^{\text{tot}}$  (conjugate to  $\nabla \mathbf{n}$ ) and total director moment  $\mathbf{m}^{\text{tot}}$  (conjugate to  $\mathbf{n}$ ) as

$$\begin{aligned}\Sigma^{\text{tot}} &= \Sigma^{\text{elast}} + \Sigma^{\text{anis}} + \Sigma^{\text{Frank}} + \Sigma^{\text{flexo}} + \Sigma^{\text{MW}} = \frac{\partial \Psi}{\partial \mathbf{F}} + \Sigma^{\text{MW}}, \\ \tilde{\mathbf{S}}^{\text{tot}} &= \tilde{\mathbf{S}}^{\text{Frank}} + \tilde{\mathbf{S}}^{\text{flexo}} = \frac{\partial \Psi}{\partial \nabla \mathbf{n}}, \\ \mathbf{m}^{\text{tot}} &= \mathbf{m}^{\text{elast}} + \mathbf{m}^{\text{pol}} + \mathbf{m}^{\text{flexo}} + \mathbf{m}^{\text{opt}} = \frac{1}{J} \frac{\partial \Psi}{\partial \mathbf{n}}.\end{aligned}\quad (2.48)$$

Collecting all contributions from (2.38), (2.41), (2.43), (2.45) and (2.47), we find the first variation of the total free energy of the system as

$$\begin{aligned}\frac{d}{d\delta} \Big|_{\delta=0} \mathcal{F}^{\text{tot}}[Q + \delta Q_1, \mathbf{n} + \delta \mathbf{n}_1, \mathbf{F} + \delta \mathbf{F}_1, \mathbf{p} + \delta \mathbf{p}_1] &= - \int_{V_R} (\tilde{\mathbf{t}}_b \cdot \mathbf{y}_1 + \tilde{\mathbf{s}}_b \cdot \mathbf{n}) \\ &\quad \int_{V_R} \left\{ Q_1 \frac{\partial}{\partial Q} (W^{\text{opt}} + W^{\text{elast}} + W^{\text{anis}}) + \mathbf{F}_1 : \Sigma^{\text{tot}} \right. \\ &\quad \left. + \mathbf{J} \mathbf{p}_1 \cdot [\mathbf{F}^{-\top} \nabla \xi + \mathbf{e}^{\text{pol}} + \mathbf{e}^{\text{flexo}}] + \nabla \mathbf{n}_1 : \tilde{\mathbf{S}}^{\text{tot}} + \mathbf{J} \mathbf{n}_1 \cdot \mathbf{m}^{\text{tot}} \right\}.\end{aligned}\quad (2.49)$$

In account of incompressibility  $\det \mathbf{F} = 1$  and the unit director field  $|\mathbf{n}| = 1$ , we employ the method of Lagrange multiplier and add the following to the total free energy:

$$\mathcal{F}^{\text{Lag}}[\mathbf{y}, \mathbf{n}] = \int_{V_R} \left[ -\lambda_p (\det \mathbf{F} - 1) + \frac{1}{2} \lambda_n (|\mathbf{n}|^2 - 1) \right], \quad (2.50)$$

where  $\lambda_p, \lambda_n : V_R \rightarrow \mathbb{R}$  are scalar Lagrange multiplier fields. All together, we conclude that an equilibrium state necessarily satisfies the following Euler–Lagrange equation for state variables  $(Q, \mathbf{y}, \mathbf{n}, \mathbf{p}) : V_R \rightarrow \mathbb{R} \times \mathbb{R}^3 \times \mathbb{R}^3 \times \mathbb{R}^3$ :

$$\begin{cases} \frac{\partial}{\partial Q} (W^{\text{opt}} + W^{\text{elast}} + W^{\text{anis}}) = 0, \\ \text{div} (\boldsymbol{\Sigma}^{\text{tot}} - \lambda_p J \mathbf{F}^{-\text{T}}) = \mathbf{0}, \\ \mathbf{F}^{-\text{T}} \nabla \xi + \mathbf{e}^{\text{pol}} + \mathbf{e}^{\text{flexo}} = \mathbf{0}, \\ -\text{div} \tilde{\mathbf{S}}^{\text{tot}} + J \mathbf{m}^{\text{tot}} + \lambda_n \mathbf{n} = \mathbf{0}. \end{cases} \quad (2.51)$$

The boundary conditions are given as

$$(\boldsymbol{\Sigma}^{\text{tot}} - \lambda_p J \mathbf{F}^{-\text{T}}) \mathbf{v}_R = \tilde{\mathbf{t}}_b, \quad \tilde{\mathbf{S}}^{\text{tot}} \mathbf{v}_R = \tilde{\mathbf{s}}_b, \quad \xi = \xi_b \quad \text{on} \quad \partial V_R. \quad (2.52)$$

In summary, we obtain that a system of nonlinear partial differential equations (2.51), together with the Maxwell equation (2.16) and boundary conditions (2.52), for the state variables  $(Q, \mathbf{y}, \mathbf{n}, \mathbf{p})$  and electrical potential  $\xi$ , which may be solved to determine the equilibrium states of the photo-flexoelectric LCE body. We remark that boundary conditions other than Eq. (2.52) can also be applied, e.g., Dirichlet-type boundary conditions on  $(\mathbf{y}, \mathbf{n})$  or Neumann-type boundary conditions on  $\tilde{\mathbf{D}}$  on part of the boundary  $\partial V_R$ .

**Remark 2 (Elasticity-Dominating Photoactive LCEs).** In many applications of LCEs, it is the elastic energy (2.3) and photo-nematic coupling energy that dominate the responses of the LCE body. In this regime, the effects of electrical field and Frank elasticity on the director field or elastic fields are negligible. Nevertheless, the director field, electrical and optical properties of the LCE body do depend on elastic fields. In particular, the optical refraction index, can be actively controlled by mechanical loadings. For a simplified model in this regime, we write the total free energy of the system as

$$\begin{aligned} \mathcal{F}^{\text{tot}}[\mathbf{y}, \mathbf{n}, \mathbf{p}] = & \underbrace{\mathcal{F}^{\text{el-an}}[Q, \mathbf{y}, \mathbf{n}] + \mathcal{F}^{\text{opt}}[Q, \mathbf{n}] + \mathcal{P}^{\text{mech}}[\mathbf{y}]}_{\text{dominating terms}} \\ & + \mathcal{F}^{\text{Frank}}[\mathbf{y}, \mathbf{n}] + \mathcal{P}^{\text{nem}}[\mathbf{n}] + \mathcal{F}^{\text{elect}}[\mathbf{y}, \mathbf{n}, \mathbf{p}] + \mathcal{F}^{\text{flexo}}[\mathbf{y}, \mathbf{n}, \mathbf{p}] + \mathcal{P}^{\text{elect}}[\mathbf{y}, \mathbf{p}]. \end{aligned}$$

The dominating energy terms dictate the deformation and director field  $(\mathbf{y}, \mathbf{n})$ :

$$\min_{(\mathbf{y}, \mathbf{n})} \{ \mathcal{F}^{\text{el-an}}[\mathbf{y}, \mathbf{n}] + \mathcal{F}^{\text{opt}}[Q, \mathbf{n}] + \mathcal{P}^{\text{mech}}[\mathbf{y}] \},$$

implying the Euler–Lagrange equation:

$$\begin{cases} \frac{\partial}{\partial Q} (W^{\text{opt}} + W^{\text{elast}} + W^{\text{anis}}) = 0, \\ \frac{\partial}{\partial \mathbf{n}} (W^{\text{opt}} + W^{\text{elast}} + W^{\text{anis}}) = \lambda_n \mathbf{n}, \\ \text{div} \left[ \frac{\partial}{\partial \mathbf{F}} (W^{\text{elast}} + W^{\text{anis}}) - \lambda_p J \mathbf{F}^{-\text{T}} \right] = \mathbf{0}. \end{cases} \quad (2.53)$$

Upon obtaining the equilibrium  $(Q, \mathbf{y}, \mathbf{n})$  for some appropriate boundary conditions, we can determine the electrical field and polarization by minimizing the remaining energy terms over admissible polarization:

$$\min_{\mathbf{p}} \{ \mathcal{F}^{\text{elect}}[\mathbf{y}, \mathbf{n}, \mathbf{p}] + \mathcal{F}^{\text{flexo}}[\mathbf{y}, \mathbf{n}, \mathbf{p}] + \mathcal{P}^{\text{elect}}[\mathbf{y}, \mathbf{p}] \},$$

which implies the governing equation for the electrical field:

$$\begin{cases} -\nabla_y \xi = -f_s(\text{div} \mathbf{n}) \mathbf{n} - f_b(\nabla \mathbf{n}) \mathbf{n} + (\mathbb{D}_{\mathbf{n}} - \epsilon_0 \mathbf{I})^{-1} \mathbf{p}, \\ \text{div}(-\epsilon_0 \nabla_y \xi + \mathbf{p}) = 0. \end{cases} \quad (2.54)$$

From the right-hand-side of (2.54)<sub>1</sub>, we may claim flexoelectricity gives rise to electrical field  $\mathbf{e}^{\text{flexo}} = -f_s(\text{div} \mathbf{n}) \mathbf{n} - f_b(\nabla \mathbf{n}) \mathbf{n}$ .

**Remark 3 (Restrictions on Flexoelectric Coefficients).** Frank elasticity coefficient (2.26), dielectric coefficients (2.22) and flexoelectric coefficients in (2.26) need to satisfy certain inequalities for thermodynamic stability. To see this, we collect energy terms in the total free energy  $\Psi$  (Cf. (2.36)) of the LCE body pertaining to  $(\mathbf{n}, \nabla_y \mathbf{n}, \mathbf{p})$ :

$$\begin{aligned} E(\mathbf{n}, \nabla_y \mathbf{n}, \mathbf{p}) = & \frac{1}{2} K_F |\nabla_y \mathbf{n}|^2 + A_1 \frac{1}{2} (\mathbf{p} \cdot \mathbf{n})^2 + A_2 \frac{1}{2} (\mathbf{p} \cdot \mathbf{p}) \\ & - f_s(\nabla_y \cdot \mathbf{n})(\mathbf{p} \cdot \mathbf{n}) - f_b(\nabla_y \mathbf{n})^{\text{T}} \mathbf{p} \cdot \mathbf{n}. \end{aligned} \quad (2.55)$$

We remark that the nonlocal field energy  $\mathcal{E}^{\text{elect}}$  can be neglected in this analysis by constructing pole-free domains with piecewise constant polarization  $\mathbf{p}$ . Let  $\mathbf{p}_n = (\mathbf{p} \cdot \mathbf{n})\mathbf{n}$  and  $\mathbf{p}_t = \mathbf{p} - \mathbf{p}_n$ . For a thermodynamically stable model, we shall require the energy (2.55) be non-negative for any  $(\mathbf{n}, \nabla_y \mathbf{n}, \mathbf{p}) \in S^2 \times \mathbb{R}^{3 \times 3} \times \mathbb{R}^3$ :

$$E = \frac{1}{2} K_F |\nabla_y \mathbf{n}|^2 + (A_1 + A_2) \frac{1}{2} |\mathbf{p}_n|^2 + A_2 \frac{1}{2} |\mathbf{p}_t|^2 - f_s (\nabla_y \cdot \mathbf{n}) (\mathbf{p}_n \cdot \mathbf{n}) - 2f_b (\mathbf{p}_t + \mathbf{p}_n) \cdot \left( \frac{\nabla_y \mathbf{n} - (\nabla_y \mathbf{n})^\top}{2} \right) \mathbf{n} \geq 0. \quad (2.56)$$

Denote by

$$\nabla_y^{\text{dev}} \mathbf{n} = \text{Sym}(\nabla_y \mathbf{n}) - \frac{1}{3} (\nabla_y \cdot \mathbf{n}) \mathbf{I}.$$

Then we have

$$|\nabla_y \mathbf{n}|^2 = |\nabla_y^{\text{dev}} \mathbf{n}|^2 + \frac{1}{3} (\nabla_y \cdot \mathbf{n})^2 + |\text{Skw} \nabla_y \mathbf{n}|^2. \quad (2.57)$$

By completing squares, we rewrite eqn. (2.56) as

$$E = \frac{1}{2} K_F |\nabla_y^{\text{dev}} \mathbf{n}|^2 + \left( \frac{1}{6} K_F - \frac{3}{2} \frac{f_s^2}{A_1 + A_2} \right) (\nabla_y \cdot \mathbf{n})^2 + \frac{1}{2} \left( K_F - \frac{4f_b^2}{A_1 + A_2} - \frac{4f_b^2}{A_2} \right) |\text{Skw}(\nabla_y \mathbf{n})|^2 + \frac{A_1 + A_2}{2} \left[ (\mathbf{p}_n \otimes \mathbf{n}) - \frac{f_s}{A_1 + A_2} (\nabla_y \cdot \mathbf{n}) \mathbf{I} - \frac{2f_b}{A_1 + A_2} \text{Skw}(\nabla_y \mathbf{n}) \right]^2 + \frac{A_2}{2} \left[ (\mathbf{p}_t \otimes \mathbf{n}) - \frac{2f_b}{A_2} \text{Skw}(\nabla_y \mathbf{n}) \right]^2 \geq 0$$

Therefore, the Frank constant, dielectric and flexoelectric coefficients necessarily satisfy that

$$K_F \geq 4 \frac{f_b^2}{A_2 + A_1} + 4 \frac{f_b^2}{A_2}, \quad K_F \geq 9 \frac{f_s^2}{A_1 + A_2}, \quad K_F > 0, \quad (2.58)$$

$$A_1, A_1 + A_2 > 0 \quad \Leftrightarrow \quad \epsilon_a, \epsilon_c > \epsilon_0.$$

### 3. Dynamical models: photo-flexoelectric LCEs with dissipation

In this section, we construct a dynamical model to describe behavior of LCEs undergoing dissipative processes by the Coleman-Noll's procedure. It has been shown that consideration of dissipation is necessary for understanding the dynamical photo-electro-mechanical behavior of LCEs (Corbett and Warner, 2009b). Recently, Xu and Huo (2021) used the continuum model proposed by Zhang et al. (2019), which was originally based on dissipation principle for viscoelastic solids with micro-order, and extended it to dielectric LCEs to study Fréedericksz transition. Here, we extend Ericksen–Leslie liquid crystal dynamical theory to photo-flexo-dielectric LCEs with leaking currents. There are various formulations of dynamical models of LCEs available in the literature (Ericksen, 1961; Leslie, 1966, 1968, 1979, 1992). We have mostly followed the formulation presented in the Ericksen (1961), Leslie (1979) and Stewart (2019).

For simplicity, we assume the order parameter  $Q$  remains constant and that the thermodynamic state of the LCE body is described by time-dependent state variables  $(\mathbf{y}, \mathbf{n}, \mathbf{p})$ . Consider an arbitrary sub-body of the LCE body. With an abuse of notation, the reference (resp. configuration) of the sub-body is still denoted by  $V_R$  (resp.  $V$ ). Recall that  $\mathbf{v}_R$  (resp.  $\mathbf{v} = J\mathbf{F}^{-\top} \mathbf{v}_R / |J\mathbf{F}^{-\top} \mathbf{v}_R|$ ) represents the unit outward normal to the material surface in the reference (resp. current) configuration. Throughout this section, superposed dot ( $\dot{\cdot}$ ) denotes the total/material derivative with respect to time  $t$ . As it will be shown in due course, it will be instructive to present formulation in the current configuration instead of the reference configuration.

For the sub-body  $V$ , the electro-mechanical-nematic interactions between the sub-body and the environment are described from Eqs. (2.29)–(2.34). Collecting terms in Eqs. (2.30), (2.32) and (2.34), we identify the total rate of work done to the sub-body by the externally applied mechanical, electrical and nematic “forces” as

$$\dot{W}^{\text{tot}}[\mathbf{y}, \mathbf{n}, \mathbf{p}] = \int_{\partial V} \left( \dot{\mathbf{y}} \cdot \mathbf{t} + \dot{\mathbf{n}} \cdot \mathbf{s} - \xi \frac{d}{dt} (J\mathbf{F}^{-1} \mathbf{d}) \cdot \frac{\mathbf{F}^\top \mathbf{v}}{J} \right), \quad (3.1)$$

where the subscript “ $b$ ” is dropped in  $\mathbf{t}, \mathbf{s}, \xi$  is dropped to emphasize that  $V$  can actually be any sub-body of the overall LCE body.

For a thermodynamically consistent model for dissipative dynamical processes, we first define mechanical stress tensor  $\sigma$  and director couple tensor  $\mathbf{S}$  based on the principle of frame-indifference and the primitive concept of mechanical traction  $\mathbf{t}$  and director couple  $\mathbf{s}$  on any interface in the LCE body. This is necessary since the mechanical stress tensor and director couple tensor in prior sections are conservative, relying on the premise of the existence of free energy functions (Cf. Eq. (2.48)).

By Eq. (2.36), we identify the free energy density of the LCE body in the current configuration is given by  $\psi = \Psi/J$ . In account of the energy contribution of the electrical field, the total free energy of the LCE body and the electrical field is given by

$$\mathcal{U}^{\text{tot}}[\mathbf{y}, \mathbf{n}, \mathbf{p}] = \int_V \psi + \mathcal{E}^{\text{elect}}[\mathbf{y}, \mathbf{n}], \quad \mathcal{E}^{\text{elect}} = \int_V \frac{\epsilon_0}{2} |\nabla_y \xi|^2. \quad (3.2)$$

Let  $\rho_0$  be the mass density in the current configuration,  $\mathbf{v} = \dot{\mathbf{y}}$  the velocity, and  $\boldsymbol{\iota} = -\rho_0\dot{\mathbf{v}}$  the inertial force. In a dynamical process, the rate of energy dissipation can be expressed as

$$\begin{aligned} \dot{D} &= \dot{W}^{\text{tot}} - \dot{U}^{\text{tot}} - \frac{d}{dt} \int_V \frac{1}{2} \rho_0 |\dot{\mathbf{y}}|^2 \\ &= \int_{\partial V} \left( \dot{\mathbf{y}} \cdot \mathbf{t} + \dot{\mathbf{n}} \cdot \mathbf{s} - \xi \frac{d}{dt} (J \mathbf{F}^{-1} \mathbf{d}) \cdot \frac{\mathbf{F}^T \mathbf{v}}{J} \right) - \dot{U}^{\text{tot}} + \int_V \dot{\mathbf{y}} \cdot \boldsymbol{\iota}, \end{aligned} \quad (3.3)$$

where the conservation of mass  $\frac{d}{dt}(\rho_0 J) \equiv 0$  has been used in the last equality.

### 3.1. Balance laws for linear and angular momentum

The balance laws for linear and angular momentum can be obtained by appealing to the principle of frame-indifference, which will also facilitate the definitions of mechanical stress tensor and director couple tensor in dynamical dissipative processes. In essence, this is an application of Noether's theorem for LCE bodies. Suppose that the motion  $\mathbf{y} = \mathbf{y}(\mathbf{x}, t)$  and  $\mathbf{n} = \mathbf{n}(\mathbf{x}, t)$  of the LCE body is superimposed by a rigid-body motion in the sense that the new motion is given by

$$\mathbf{y}^*(\mathbf{x}, t) = \mathbf{Q}(t)\mathbf{y}(\mathbf{x}, t) + \mathbf{c}(t) \quad \text{and} \quad \mathbf{n}^*(\mathbf{x}, t) = \mathbf{Q}(t)\mathbf{n}(\mathbf{x}, t), \quad (3.4)$$

where  $\mathbf{Q}(t) \in SO(3)$  is a rotation matrix and  $\mathbf{c}(t) \in \mathbb{R}^3$  is a translation vector. From a passive viewpoint, the new motion (3.4) corresponds to a change of frame from  $O \rightarrow O^*$  such a material point with coordinates  $\mathbf{y}$  and director  $\mathbf{n}$  with respect to frame  $O$  is represented by coordinates  $\mathbf{y}^*$  and director  $\mathbf{n}^*$  with respect to the new frame  $O^*$ .

The principle of frame indifference asserts that the rate of change of free energy and rate of change of dissipation are invariant with respect to a superimposed rigid-body motion or equivalently, a change of frame from  $O \rightarrow O^*$ . To see the consequence of the principle of frame indifference, by Eq. (3.4) we notice that

$$\dot{\mathbf{y}}^* = \mathbf{Q}\dot{\mathbf{y}} + \dot{\mathbf{Q}}\mathbf{y} + \dot{\mathbf{c}} \quad \text{and} \quad \dot{\mathbf{n}}^* = \mathbf{Q}\dot{\mathbf{n}} + \dot{\mathbf{Q}}\mathbf{n}. \quad (3.5)$$

Here and subsequently, superposed  $(\ )^*$  denotes transformation due to the change of frame  $O \rightarrow O^*$ . As vectors, the mechanical traction  $\mathbf{t}$ , nematic director  $\mathbf{n}$ , unit normal  $\mathbf{v}$ , polarization  $\mathbf{p}$ , director couple  $\mathbf{s}$  and inertial force  $\boldsymbol{\iota}$  shall transform as (Gurtin et al., 2010):

$$(\mathbf{t}^*, \mathbf{n}^*, \mathbf{v}^*, \mathbf{d}^*, \mathbf{p}^*, \mathbf{s}^*, \boldsymbol{\iota}^*) = \mathbf{Q}(\mathbf{t}, \mathbf{n}, \mathbf{v}, \mathbf{d}, \mathbf{p}, \mathbf{s}, \boldsymbol{\iota}). \quad (3.6)$$

We remark that the inertial force  $\boldsymbol{\iota}^* \neq -\rho_0\dot{\mathbf{v}}^*$  since the frame  $O^*$  (Cf. Eq. (3.4)) is not an inertial frame. Also, the deformation gradient and strain rate transform as

$$\mathbf{F}^* = \nabla \mathbf{y}^* = \mathbf{Q}\nabla \mathbf{y} = \mathbf{Q}\mathbf{F} \quad \text{and} \quad \dot{\mathbf{F}}^* = \dot{\mathbf{Q}}\mathbf{F} + \mathbf{Q}\dot{\mathbf{F}}. \quad (3.7)$$

With respect to the new frame  $O^*$ , the energy balance relation parallel to Eq. (3.3) can be written as:

$$\dot{D}^* = \int_{\partial V} \left( \dot{\mathbf{y}}^* \cdot \mathbf{t}^* + \dot{\mathbf{n}}^* \cdot \mathbf{s}^* - \xi \frac{d}{dt} (J \mathbf{F}^{*-1} \mathbf{d}^*) \cdot \frac{\mathbf{F}^{*T} \mathbf{v}^*}{J} \right) - (\dot{U}^{\text{tot}})^* + \int_V \dot{\mathbf{y}}^* \cdot \boldsymbol{\iota}^*, \quad (3.8)$$

where  $\dot{D}^* = \dot{D}$  and  $(\dot{U}^{\text{tot}})^* = \dot{U}^{\text{tot}}$  by the principle of frame indifference. Inserting Eqs. (3.5) and (3.6) into Eq. (3.8) we obtain

$$\begin{aligned} \dot{D} &= \int_{\partial V} \left( (\dot{\mathbf{y}} + \mathbf{Q}^T \dot{\mathbf{Q}}\mathbf{y} + \mathbf{Q}^T \dot{\mathbf{c}}) \cdot \mathbf{t} + (\dot{\mathbf{n}} + \mathbf{Q}^T \dot{\mathbf{Q}}\mathbf{n}) \cdot \mathbf{s} - \xi \frac{d}{dt} (J \mathbf{F}^{-1} \mathbf{d}) \cdot \frac{\mathbf{F}^T \mathbf{v}}{J} \right) - \dot{U}^{\text{tot}} \\ &\quad + \int_V (\dot{\mathbf{y}} + \mathbf{Q}^T \dot{\mathbf{Q}}\mathbf{y} + \mathbf{Q}^T \dot{\mathbf{c}}) \cdot \boldsymbol{\iota}. \end{aligned} \quad (3.9)$$

Note that  $\mathbf{Q}^T \dot{\mathbf{Q}}$  is skew-symmetric and as a result there exist a vector of angular velocity  $\boldsymbol{\omega} \in \mathbb{R}^3$  such that  $\mathbf{Q}^T \dot{\mathbf{Q}} = \boldsymbol{\omega} \times$ . In addition, we notice the algebraic identities:

$$(\mathbf{Q}^T \dot{\mathbf{Q}}\mathbf{y}) \cdot \mathbf{t} = (\boldsymbol{\omega} \times \mathbf{y}) \cdot \mathbf{t} = \boldsymbol{\omega} \cdot (\mathbf{y} \times \mathbf{t}).$$

Subtracting Eq. (3.3) from (3.9), we obtain

$$\int_{\partial V} \left( \dot{\mathbf{c}}' \cdot \mathbf{t} + \boldsymbol{\omega} \cdot (\mathbf{y} \times \mathbf{t} + \mathbf{n} \times \mathbf{s}) \right) + \int_V \left( -\dot{\mathbf{c}}' \cdot \rho_0 \dot{\mathbf{v}} - \boldsymbol{\omega} \cdot (\mathbf{y} \times \rho_0 \dot{\mathbf{v}}) \right) = 0,$$

where  $\dot{\mathbf{c}}' = \mathbf{Q}^T \dot{\mathbf{c}}$ . The above equation holds for arbitrary angular velocity  $\boldsymbol{\omega} \in \mathbb{R}^3$  and translational velocity  $\dot{\mathbf{c}}' \in \mathbb{R}^3$ . Therefore, we obtain the conservation laws associated with the symmetry of frame-indifference:

$$\int_V \rho_0 \dot{\mathbf{v}} = \int_{\partial V} \mathbf{t}, \quad \int_V \mathbf{y} \times \rho_0 \dot{\mathbf{v}} = \int_{\partial V} (\mathbf{y} \times \mathbf{t} + \mathbf{n} \times \mathbf{s}), \quad (3.10)$$

which can be respectively recognized as the balance of linear momentum and balance of angular momentum.

We remark that the mechanical traction  $\mathbf{t}$  and director couple  $\mathbf{s}$  on  $\partial V$  characterizes the interactions between the environment and the sub-body  $V$  and in principle, could depend on the unit normal  $\mathbf{v}$  on  $\partial V$  in a general fashion. Applying Eq. (3.10) to infinitesimal tetrahedron (Leigh, 1968; Stewart, 2019; Gurtin et al., 2010), the classical Cauchy's argument implies that  $\mathbf{t}$  and  $\mathbf{s}$  must linearly

depend on the unit normal  $\mathbf{v}$  and there exist normal-independent mechanical stress tensor field  $\boldsymbol{\sigma} : V \rightarrow \mathbb{R}^{3 \times 3}$  and director couple tensor field  $\mathbf{S} : V \rightarrow \mathbb{R}^{3 \times 3}$  such that

$$\mathbf{t} = \boldsymbol{\sigma} \mathbf{v} \quad \text{and} \quad \mathbf{s} = \mathbf{S} \mathbf{v} \quad \text{on} \quad \partial V. \quad (3.11)$$

Inserting Eq. (3.11) into Eq. (3.10), by the divergence theorem we obtain the differential form of balance laws (3.10) in terms of the tensor fields  $(\boldsymbol{\sigma}, \mathbf{S})$ :

$$\operatorname{div}_y \boldsymbol{\sigma} = \rho_0 \dot{\mathbf{v}} \quad \text{and} \quad \operatorname{Skw} (\boldsymbol{\sigma} + \mathbf{S}(\nabla_y \mathbf{n})^\top + (\operatorname{div}_y \mathbf{S}) \otimes \mathbf{n}) = 0. \quad (3.12)$$

**Remark 4 (Symmetry of Stress Tensor and Director Couple Tensor).** It is well-known that the balance of angular momentum implies the symmetry of Cauchy stress tensor for classical materials, which can also be obtained by the frame-indifference of free energy and dissipation potential (Rahmati et al., 2023). In the current setting of LCEs, we observe that at the absence of boundary mechanical traction and director couple ( $\tilde{\mathbf{t}}_b = \tilde{\mathbf{s}}_b = 0$ ),

$$\mathcal{F}^{\text{tot}}[\mathbf{Q}\mathbf{y}, \mathbf{Q}\mathbf{n}, \mathbf{Q}\mathbf{p}] = \mathcal{F}^{\text{tot}}[\mathbf{y}, \mathbf{n}, \mathbf{p}].$$

Consider infinitesimal rotations with  $\mathbf{Q} = \mathbf{I} + \delta \boldsymbol{\theta}$  for some skew-symmetric  $\boldsymbol{\theta} \in \mathbb{R}^{3 \times 3}$ . By Eq. (2.49) we find that

$$0 = \frac{d}{d\delta} \Big|_{\delta=0} \mathcal{F}^{\text{tot}} [\mathbf{n} + \delta \boldsymbol{\theta} \mathbf{n}, \mathbf{y} + \delta \boldsymbol{\theta} \mathbf{y}, \mathbf{p} + \delta \boldsymbol{\theta} \mathbf{p}] = \int_V \left\{ \boldsymbol{\theta} : \left( \frac{1}{J} \boldsymbol{\Sigma}^{\text{tot}} \mathbf{F}^\top + (\nabla_y \boldsymbol{\xi} + \mathbf{e}^{\text{pol}} + \mathbf{e}^{\text{flexo}}) \otimes \mathbf{p} + \frac{1}{J} \tilde{\mathbf{S}}^{\text{tot}} (\nabla \mathbf{n})^\top + \mathbf{m}^{\text{tot}} \otimes \mathbf{n} \right) \right\}. \quad (3.13)$$

Therefore, we shall have

$$\operatorname{Skw} \left( \frac{1}{J} \boldsymbol{\Sigma}^{\text{tot}} \mathbf{F}^\top + (\nabla_y \boldsymbol{\xi} + \mathbf{e}^{\text{pol}} + \mathbf{e}^{\text{flexo}}) \otimes \mathbf{p} + \frac{1}{J} \tilde{\mathbf{S}}^{\text{tot}} (\nabla \mathbf{n})^\top + \mathbf{m}^{\text{tot}} \otimes \mathbf{n} \right) = 0. \quad (3.14)$$

By the last two equations of (2.51), we see that Eq. (3.14) coincides with the second of Eq. (3.12) upon recognizing the relation:

$$\boldsymbol{\sigma} = \frac{1}{J} \boldsymbol{\Sigma}^{\text{tot}} \mathbf{F}^\top, \quad \mathbf{S} = \frac{1}{J} \tilde{\mathbf{S}}^{\text{tot}} \mathbf{F}^\top = \frac{1}{J} \frac{\partial \Psi}{\partial \nabla \mathbf{n}} \mathbf{F}^\top, \quad (3.15)$$

and that the last of Eq. (2.51) is equivalent to  $-\operatorname{div}_y \mathbf{S} + \mathbf{m}^{\text{tot}} + \frac{1}{J} \lambda_n \mathbf{n} = 0$ .

### 3.2. Constitutive models for dissipative dynamic processes

We use the Second Law of thermodynamics and the principle of frame-indifference to formulate constitutive models for the dissipative processes in LCEs. By the Second Law, the rate of energy dissipation shall be non-negative for *any* isothermal processes:

$$\dot{D} = \dot{W}^{\text{tot}} - \dot{U}^{\text{tot}} - \frac{d}{dt} \int_V \rho_0 |\mathbf{v}|^2 \geq 0 \quad (3.16)$$

Assuming material incompressibility ( $J \equiv 1$ ), by Eq. (3.2) the rate of change of free energy of the LCE body and field energy can be expressed as

$$\dot{U}^{\text{tot}} = \frac{d}{dt} \int_V \psi(\nabla_y \mathbf{n}, \nabla \mathbf{n}, \mathbf{p}) + \frac{d}{dt} \mathcal{E}^{\text{elect}}[\mathbf{y}, \mathbf{p}]. \quad (3.17)$$

Recall that

$$\dot{\mathbf{F}} = \nabla \dot{\mathbf{y}} = (\nabla_y \mathbf{v}) \mathbf{F} = \mathbf{L} \mathbf{F} \quad \text{and} \quad \nabla \dot{\mathbf{n}} = (\nabla_y \dot{\mathbf{n}}) \mathbf{F}. \quad (3.18)$$

Direct calculation yields

$$\dot{\psi}(\nabla_y \mathbf{n}, \nabla \mathbf{n}, \mathbf{p}) = \frac{\partial \psi}{\partial \mathbf{F}} : \dot{\mathbf{F}} + \frac{\partial \psi}{\partial \mathbf{n}} \cdot \dot{\mathbf{n}} + \frac{\partial \psi}{\partial \nabla \mathbf{n}} : \nabla \dot{\mathbf{n}} + \frac{\partial \psi}{\partial \mathbf{p}} \cdot \dot{\mathbf{p}}. \quad (3.19)$$

Inserting Eqs. (3.18) and (3.19) into Eq. (3.17), by Eq. (2.44) we find that

$$\dot{U}^{\text{tot}} = \int_V \left\{ \left( \frac{1}{J} \frac{\partial \Psi}{\partial \mathbf{F}} \mathbf{F}^\top + \boldsymbol{\sigma}^{\text{MW}} \right) : \mathbf{L} + \frac{\partial \psi}{\partial \mathbf{n}} \cdot \dot{\mathbf{n}} + \frac{\partial \psi}{\partial \nabla \mathbf{n}} \mathbf{F}^\top : \nabla_y \dot{\mathbf{n}} + (\nabla_y \boldsymbol{\xi} + \frac{\partial \psi}{\partial \mathbf{p}}) \cdot \dot{\mathbf{p}} \right\} - \int_{\partial V_R} \tilde{\boldsymbol{\xi}} \tilde{\mathbf{D}} \cdot \mathbf{v}_R. \quad (3.20)$$

Moreover, inserting Eq. (3.11) into (3.1) we obtain

$$\begin{aligned} \dot{W}^{\text{tot}} &= \int_V [\boldsymbol{\sigma} : \mathbf{L} + \dot{\mathbf{y}} \cdot (\operatorname{div}_y \boldsymbol{\sigma}) + \mathbf{S} : \nabla_y \dot{\mathbf{n}} + (\operatorname{div}_y \mathbf{S}) \cdot \dot{\mathbf{n}}] - \int_{\partial V_R} \tilde{\boldsymbol{\xi}} \tilde{\mathbf{D}} \cdot \mathbf{v}_R \\ &= \int_V [\boldsymbol{\sigma} : \mathbf{L} - \dot{\mathbf{y}} \cdot \boldsymbol{\iota} + \mathbf{S} : \nabla_y \dot{\mathbf{n}} + (\operatorname{div}_y \mathbf{S}) \cdot \dot{\mathbf{n}}] - \int_{\partial V_R} \tilde{\boldsymbol{\xi}} \tilde{\mathbf{D}} \cdot \mathbf{v}_R \end{aligned} \quad (3.21)$$

Inserting Eqs. (3.20) and (3.21) into (3.16), we find the rate of energy dissipation of the system as

$$\begin{aligned} \dot{D} = & \int_V \left( \boldsymbol{\sigma} - \boldsymbol{\sigma}^{\text{MW}} - \frac{1}{J} \frac{\partial \Psi}{\partial \mathbf{F}} \mathbf{F}^\top \right) : \mathbf{L} \\ & + \left( \mathbf{S} - \frac{\partial \psi}{\partial \nabla \mathbf{n}} \mathbf{F}^\top \right) : \nabla_y \dot{\mathbf{n}} + \left( \text{div}_y \mathbf{S} - \frac{\partial \psi}{\partial \mathbf{n}} \right) \cdot \dot{\mathbf{n}} \\ & + \left( -\frac{\partial \psi}{\partial \mathbf{p}} - \nabla_y \xi \right) \cdot \dot{\mathbf{p}} \geq 0, \end{aligned} \quad (3.22)$$

where the inequality follows from the Second Law of thermodynamics. To guarantee the inequality (3.22) for any physical processes, we postulate that

$$\mathbf{S} = \frac{\partial \psi}{\partial \nabla \mathbf{n}} \mathbf{F}^\top,$$

and require that

$$\dot{D} = \int_V (\boldsymbol{\sigma}^{\text{visc}} : \mathbf{L} + \mathbf{s}^{\text{visc}} \cdot \dot{\mathbf{n}} + \mathbf{e}^{\text{visc}} \cdot \dot{\mathbf{p}}) \geq 0, \quad (3.23)$$

where the dissipative ‘‘forces’’ are defined as

$$\begin{aligned} \boldsymbol{\sigma}^{\text{visc}} & := \boldsymbol{\sigma} - \left( \boldsymbol{\sigma}^{\text{MW}} + \frac{1}{J} \frac{\partial \Psi}{\partial \mathbf{F}} \mathbf{F}^\top \right) + \lambda_p \mathbf{I}, \\ \mathbf{s}^{\text{visc}} & := \text{div}_y \mathbf{S} - \frac{\partial \psi}{\partial \mathbf{n}} - \lambda_n \mathbf{n}, \\ \mathbf{e}^{\text{visc}} & := -\frac{\partial \psi}{\partial \mathbf{p}} - \nabla_y \xi. \end{aligned} \quad (3.24)$$

We remark that the terms  $\lambda_p \mathbf{I}$  and  $\lambda_n \mathbf{n}$  in Eq. (3.24) arise from the constraint  $J = 1$  and  $|\mathbf{n}| = 1$ . Physically, we recognize  $\boldsymbol{\sigma}^{\text{visc}}$  as the viscous mechanical stress,  $\mathbf{s}^{\text{visc}}$  as the viscous director couple, and  $\mathbf{e}^{\text{visc}}$  as the current-generating electrical field.

To formulate a constitutive model, i.e., some relationship between the rate of change of state variables  $(\mathbf{L}, \dot{\mathbf{n}}, \dot{\mathbf{p}})$  and their conjugates  $(\boldsymbol{\sigma}^{\text{visc}}, \mathbf{s}^{\text{visc}}, \mathbf{e}^{\text{visc}})$ , we postulate that the rate of dissipation is local and given by a dissipation potential  $\Phi^{\text{visc}}$ :

$$\dot{D} = \int_V \Phi^{\text{visc}}(\mathbf{F}, \mathbf{n}; \mathbf{L}, \dot{\mathbf{n}}, \dot{\mathbf{p}}), \quad (3.25)$$

where, for simplicity, we have assumed that the dissipation potential  $\Phi^{\text{visc}}$  depends on deformation gradient  $\mathbf{F}$ , director  $\mathbf{n}$ , strain rate  $\mathbf{L}$ , and rate of change of director and polarization  $(\dot{\mathbf{n}}, \dot{\mathbf{p}})$ . For reasonable physical behaviors, the following restrictions should be placed on the functional form of dissipation potential  $\Phi^{\text{visc}}$ .

1. Non-negativity. By the Second Law of thermodynamics, it should holds

$$\Phi^{\text{visc}}(\mathbf{F}, \mathbf{n}; \mathbf{L}, \dot{\mathbf{n}}, \dot{\mathbf{p}}) \geq 0 \quad \forall (\mathbf{F}, \mathbf{n}; \mathbf{L}, \dot{\mathbf{n}}, \dot{\mathbf{p}}) \in \mathbb{R}^{3 \times 3} \times S^2 \times \mathbb{R}^{3 \times 3} \times \mathbb{R}^3 \times \mathbb{R}^3. \quad (3.26)$$

2. Stationary/equilibrium states do not dissipate energy:

$$\Phi^{\text{visc}}(\mathbf{F}, \mathbf{n}; \mathbf{0}, \mathbf{0}, \mathbf{0}) = 0 \quad \forall (\mathbf{F}, \mathbf{n}) \in \mathbb{R}^{3 \times 3} \times S^2. \quad (3.27)$$

3. Frame-indifference. Recall that upon a change of frame  $O \rightarrow O^*$ , the state variables and relevant quantities transform as Eqs. (3.4), (3.5) and (3.6). In particular, we have

$$(\mathbf{F}^*, \mathbf{n}^*; \mathbf{L}^*, \dot{\mathbf{n}}^*, \dot{\mathbf{p}}^*) = (\mathbf{Q}\mathbf{F}, \mathbf{Q}\mathbf{n}; \mathbf{Q}\mathbf{L}\mathbf{Q}^\top + \dot{\mathbf{Q}}\mathbf{Q}^\top, \mathbf{Q}\dot{\mathbf{n}} + \dot{\mathbf{Q}}\mathbf{n}, \mathbf{Q}\dot{\mathbf{p}} + \dot{\mathbf{Q}}\mathbf{p}).$$

Therefore, the invariance of  $\dot{D}$  implies that for any  $\mathbf{Q}(t)$ ,

$$\begin{aligned} \Phi^{\text{visc}}(\mathbf{F}, \mathbf{n}; \mathbf{L}, \dot{\mathbf{n}}, \dot{\mathbf{p}}) & = \Phi^{\text{visc}}(\mathbf{F}^*, \mathbf{n}^*; \mathbf{L}^*, \dot{\mathbf{n}}^*, \dot{\mathbf{p}}^*) \\ & = \Phi^{\text{visc}}(\mathbf{Q}\mathbf{F}, \mathbf{Q}\mathbf{n}; \mathbf{Q}\mathbf{L}\mathbf{Q}^\top + \dot{\mathbf{Q}}\mathbf{Q}^\top, \mathbf{Q}\dot{\mathbf{n}} + \dot{\mathbf{Q}}\mathbf{n}, \mathbf{Q}\dot{\mathbf{p}} + \dot{\mathbf{Q}}\mathbf{p}). \end{aligned} \quad (3.28)$$

Let

$$\mathbf{D} = \text{Sym}(\mathbf{L}) = \frac{1}{2}(\mathbf{L} + \mathbf{L}^\top) \quad \text{and} \quad \mathbf{W} = \text{Skw}(\mathbf{L}) = \frac{1}{2}(\mathbf{L} - \mathbf{L}^\top) \quad (3.29)$$

the symmetric and skew-symmetric part of spatial strain rate  $\mathbf{L}$ , respectively. By Eqs. (3.7) and (3.29), it is straightforward to verify that

$$(\mathbf{D}^*, (\nabla_y \mathbf{n})^*) = \mathbf{Q}(\mathbf{D}, \nabla_y \mathbf{n})\mathbf{Q}^\top, \quad \mathbf{W}^* = \mathbf{Q}\mathbf{W}\mathbf{Q}^\top + \dot{\mathbf{Q}}\mathbf{Q}^\top. \quad (3.30)$$

where  $\nabla_y \mathbf{n} = (\nabla \mathbf{n})\mathbf{F}^{-1}$  is the spatial director gradient. Further, we define the co-rotational rate of change of nematic director and polarization as

$$(\dot{\mathbf{n}}, \dot{\mathbf{p}}) = (\dot{\mathbf{n}} - \mathbf{W}\mathbf{n}, \dot{\mathbf{p}} - \mathbf{W}\mathbf{p}). \quad (3.31)$$

In contrast to  $(\dot{\mathbf{n}}, \dot{\mathbf{p}})$ , co-rotational rate of change of nematic director and polarization are frame in-different or covariant in the sense that

$$(\dot{\mathbf{n}}^*, \dot{\mathbf{p}}^*) = \mathbf{Q}(\dot{\mathbf{n}}, \dot{\mathbf{p}}).$$

Choose  $\dot{\mathbf{Q}}$  such that

$$\mathbf{Q}\mathbf{W}\mathbf{Q}^\top + \dot{\mathbf{Q}}\mathbf{Q}^\top = 0, \quad \text{i.e.,} \quad \dot{\mathbf{Q}} = -\mathbf{Q}\mathbf{W}.$$

Immediately, we find that

$$\begin{aligned} \mathbf{Q}\mathbf{L}\mathbf{Q}^\top + \dot{\mathbf{Q}}\mathbf{Q}^\top &= \mathbf{Q}\mathbf{D}\mathbf{Q}^\top + \mathbf{Q}\mathbf{W}\mathbf{Q}^\top + \dot{\mathbf{Q}}\mathbf{Q}^\top = \mathbf{Q}\mathbf{D}\mathbf{Q}^\top, \\ (\mathbf{Q}\dot{\mathbf{n}} + \dot{\mathbf{Q}}\mathbf{n}, \mathbf{Q}\dot{\mathbf{p}} + \dot{\mathbf{Q}}\mathbf{p}) &= (\mathbf{Q}\dot{\mathbf{n}} - \mathbf{Q}\mathbf{W}\mathbf{n}, \mathbf{Q}\dot{\mathbf{p}} - \mathbf{Q}\mathbf{W}\mathbf{p}) = \mathbf{Q}(\dot{\mathbf{n}}, \dot{\mathbf{p}}). \end{aligned}$$

Inserting the above equations into Eq. (3.28) we obtain

$$\Phi^{\text{visc}}(\mathbf{F}, \mathbf{n}; \mathbf{L}, \dot{\mathbf{n}}, \dot{\mathbf{p}}) = \Phi^{\text{visc}}(\mathbf{Q}\mathbf{F}, \mathbf{Q}\mathbf{n}; \mathbf{Q}\mathbf{D}\mathbf{Q}^\top, \mathbf{Q}\dot{\mathbf{n}}, \mathbf{Q}\dot{\mathbf{p}}) \quad \forall \mathbf{Q} \in \text{SO}(3). \quad (3.32)$$

Let  $\mathbf{Q}_F \in \text{SO}(3)$  be the rigid rotation in the polar decomposition, i.e.,  $\mathbf{Q}_F^\top \mathbf{U} = \mathbf{F}$  and  $\mathbf{U} = (\mathbf{F}^\top \mathbf{F})^{1/2}$ . Setting  $\mathbf{Q} = \mathbf{Q}_F$  in (3.32) we obtain

$$\Phi^{\text{visc}}(\mathbf{F}, \mathbf{n}; \mathbf{L}, \dot{\mathbf{n}}, \dot{\mathbf{p}}) = \Phi^{\text{visc}}(\mathbf{U}, \mathbf{Q}_F \mathbf{n}; \mathbf{Q}_F \mathbf{D} \mathbf{Q}_F^\top, \mathbf{Q}_F \dot{\mathbf{n}}, \mathbf{Q}_F \dot{\mathbf{p}}). \quad (3.33)$$

Evaluating (3.33) at  $\mathbf{U} = \mathbf{I}$  (and hence  $\mathbf{F} = \mathbf{Q}_F^\top$ ), we have

$$\Phi^{\text{visc}}(\mathbf{Q}_F^\top, \mathbf{n}; \mathbf{L}, \dot{\mathbf{n}}, \dot{\mathbf{p}}) = \Phi^{\text{visc}}(\mathbf{I}, \mathbf{Q}_F \mathbf{n}; \mathbf{Q}_F \mathbf{D} \mathbf{Q}_F^\top, \mathbf{Q}_F \dot{\mathbf{n}}, \mathbf{Q}_F \dot{\mathbf{p}}). \quad (3.34)$$

4. Material symmetry. Without loss of generality, choosing the reference configuration the same as the current configuration, i.e.,  $\mathbf{Q}_F = \mathbf{I}$ , we can write (3.34) as

$$\Phi^{\text{visc}}(\mathbf{I}, \mathbf{n}; \mathbf{L}, \dot{\mathbf{n}}, \dot{\mathbf{p}}) = \Phi^{\text{visc}}(\mathbf{I}, \mathbf{n}; \mathbf{D}, \dot{\mathbf{n}}, \dot{\mathbf{p}}). \quad (3.35)$$

Suppose that the LCE admits material symmetries, meaning that  $\Phi^{\text{visc}}$  is invariant with respect to a change of reference configuration  $\mathbf{x} \rightarrow \mathbf{x}' = \mathbf{R}\mathbf{x}$  for  $\mathbf{R} \in \mathcal{G} :=$  material symmetry group. Under this transformation, we have

$$(\mathbf{F}, \mathbf{L}, \mathbf{n}, \dot{\mathbf{n}}, \dot{\mathbf{p}}) \rightarrow (\mathbf{F}', \mathbf{L}', \mathbf{n}', \dot{\mathbf{n}}', \dot{\mathbf{p}}') = (\mathbf{R}\mathbf{F}, \mathbf{L}, \mathbf{n}, \dot{\mathbf{n}}, \dot{\mathbf{p}}),$$

and the invariance of  $\Phi^{\text{visc}}$  implies that  $\forall \mathbf{R} \in \mathcal{G}$ ,

$$\begin{aligned} \Phi^{\text{visc}}(\mathbf{I}, \mathbf{n}; \mathbf{L}, \dot{\mathbf{n}}, \dot{\mathbf{p}}) &= \Phi^{\text{visc}}(\mathbf{R}, \mathbf{n}; \mathbf{L}, \dot{\mathbf{n}}, \dot{\mathbf{p}}) \\ &= \Phi^{\text{visc}}(\mathbf{I}, \mathbf{n}; \mathbf{D}, \dot{\mathbf{n}}, \dot{\mathbf{p}}) = \Phi^{\text{visc}}(\mathbf{I}, \mathbf{R}^\top \mathbf{n}; \mathbf{R}^\top \mathbf{D} \mathbf{R}, \mathbf{R}^\top \dot{\mathbf{n}}, \mathbf{R}^\top \dot{\mathbf{p}}), \end{aligned} \quad (3.36)$$

where the last equality follows from Eqs. (3.34) and (3.35).

We now construct a simple but nontrivial constitutive model for dissipative processes in flexoelectric LCEs that are consistent with the restrictions discussed above. Comparing Eq. (3.23) with Eq. (3.25), we conclude that

$$\begin{aligned} \Phi^{\text{visc}}(\mathbf{I}, \mathbf{L}, \mathbf{n}, \dot{\mathbf{n}}, \dot{\mathbf{p}}) &= \sigma^{\text{visc}} : \mathbf{L} + \mathbf{s}^{\text{visc}} \cdot \dot{\mathbf{n}} + \mathbf{e}^{\text{visc}} \cdot \dot{\mathbf{p}} \\ &= \Phi^{\text{visc}}(\mathbf{I}, \mathbf{D}, \mathbf{n}, \dot{\mathbf{n}}, \dot{\mathbf{p}}) = \sigma_{\text{sym}}^{\text{visc}} : \mathbf{D} + \mathbf{s}^{\text{visc}} \cdot \dot{\mathbf{n}} + \mathbf{e}^{\text{visc}} \cdot \dot{\mathbf{p}}, \end{aligned} \quad (3.37)$$

where the second line follows from Eq. (3.36), and

$$\sigma_{\text{sym}}^{\text{visc}} = \text{Sym}(\sigma^{\text{visc}}) \quad (\text{resp.} \quad \sigma_{\text{skw}}^{\text{visc}} = \text{Skw}(\sigma^{\text{visc}}))$$

is the symmetric (resp. skew-symmetric) part of stress tensor  $\sigma^{\text{visc}}$ . Comparing two expressions on the second column in Eq. (3.37), by Eq. (3.31) we conclude that

$$\sigma_{\text{skw}}^{\text{visc}} = -\text{Skw}(\mathbf{s}^{\text{visc}} \otimes \mathbf{n} + \mathbf{e}^{\text{visc}} \otimes \mathbf{p}). \quad (3.38)$$

Further, to maintain the invariance of  $\Phi^{\text{visc}}$ , the viscous stress  $\sigma_{\text{sym}}^{\text{visc}}$ , director couple  $\mathbf{s}^{\text{visc}}$  and current-generating electric field  $\mathbf{e}^{\text{visc}}$  shall follow the usual transformation rules under the change of frame  $O \rightarrow O^*$ :

$$(\sigma_{\text{sym}}^{\text{visc}}, \mathbf{s}^{\text{visc}}, \mathbf{e}^{\text{visc}}) \rightarrow (\mathbf{Q}\sigma_{\text{sym}}^{\text{visc}}\mathbf{Q}^\top, \mathbf{Q}\mathbf{s}^{\text{visc}}, \mathbf{Q}\mathbf{e}^{\text{visc}}). \quad (3.39)$$

We remark that the symmetry (3.38) and the transformation (3.39) also follows from the definition of viscous stress and director couple in (3.24), the definition (3.11) of total mechanical stress and director couple, and the balance of angular momentum (3.12)<sub>2</sub>.

To proceed further with a minimum nontrivial constitutive model for dissipative processes, by (3.37) we postulate a linear relation between the ‘‘forces’’ and ‘‘rates’’:

$$\begin{bmatrix} \sigma_{\text{sym}}^{\text{visc}} \\ \mathbf{s}^{\text{visc}} \\ \mathbf{e}^{\text{visc}} \end{bmatrix} = \begin{bmatrix} \mathbf{C}_{\mathbf{n}} & \mathbf{B}_{\mathbf{n}} & \mathbf{A}_{\mathbf{n}} \\ \mathbf{B}_{\mathbf{n}}^\top & \mathbf{H}_{\mathbf{n}} & \mathbf{E}_{\mathbf{n}} \\ \mathbf{A}_{\mathbf{n}}^\top & \mathbf{E}_{\mathbf{n}}^\top & \mathbf{G}_{\mathbf{n}} \end{bmatrix} \begin{bmatrix} \mathbf{D} \\ \dot{\mathbf{n}} \\ \dot{\mathbf{p}} \end{bmatrix} \Leftrightarrow \quad (3.40)$$

$$\begin{cases} (\boldsymbol{\sigma}_{\text{sym}}^{\text{visc}})_{ij} = (\mathbb{C}_n)_{ijkl}(\mathbf{D})_{kl} + (\mathbb{B}_n)_{ijk}(\dot{\mathbf{n}})_k + (\mathbb{A}_n)_{ijk}(\dot{\mathbf{p}})_k, \\ (\mathbf{s}^{\text{visc}})_i = (\mathbb{B}_n)_{jki}(\mathbf{D})_{jk} + (\mathbb{H}_n)_{ij}(\dot{\mathbf{n}})_j + (\mathbb{E}_n)_{ij}(\dot{\mathbf{p}})_j, \\ (\mathbf{e}^{\text{visc}})_i = (\mathbb{A}_n)_{jki}(\mathbf{D})_{jk} + (\mathbb{E}_n)_{ji}(\dot{\mathbf{n}})_j + (\mathbb{G}_n)_{ij}(\dot{\mathbf{p}})_j, \end{cases} \quad (3.41)$$

where the coefficients  $\mathbb{B}_n, \mathbb{C}_n, \mathbb{H}_n$  in general depend on the local director  $\mathbf{n}$ , and admit the following symmetries:

$$\begin{aligned} (\mathbb{C}_n)_{ijkl} &= (\mathbb{C}_n)_{klij} = (\mathbb{C}_n)_{ijlk}, & (\mathbb{B}_n)_{ijk} &= (\mathbb{B}_n)_{jik}, & (\mathbb{A}_n)_{ijk} &= (\mathbb{A}_n)_{jik} \\ (\mathbb{H}_n)_{ij} &= (\mathbb{H}_n)_{ji}, & (\mathbb{G}_n)_{ij} &= (\mathbb{G}_n)_{ji}. \end{aligned} \quad (3.42)$$

By Eqs. (3.37) and (3.50), the dissipation potential  $\Phi^{\text{visc}}$  is a quadratic form of  $(\mathbf{D}, \dot{\mathbf{n}}, \dot{\mathbf{p}})$ :

$$\Phi^{\text{visc}}(\mathbf{I}, \mathbf{n}; \mathbf{D}, \dot{\mathbf{n}}, \dot{\mathbf{p}}) = \begin{bmatrix} \mathbf{D} \\ \dot{\mathbf{n}} \\ \dot{\mathbf{p}} \end{bmatrix}^T \begin{bmatrix} \mathbb{C}_n & \mathbb{B}_n & \mathbb{A}_n \\ \mathbb{B}_n^T & \mathbb{H}_n & \mathbb{E}_n \\ \mathbb{A}_n^T & \mathbb{E}_n^T & \mathbb{G}_n \end{bmatrix} \begin{bmatrix} \mathbf{D} \\ \dot{\mathbf{n}} \\ \dot{\mathbf{p}} \end{bmatrix}. \quad (3.43)$$

Furthermore, from a microscopic viewpoint, nematic liquid crystal elastomers are locally transversely isotropic with material symmetry group given by

$$\mathcal{G} = \{\mathbf{R} \in SO(3) : \mathbf{R}\mathbf{n} = \mathbf{n}\}. \quad (3.44)$$

Therefore, from Eq. (3.36) we see that the coefficients  $\mathbb{A}_n, \mathbb{B}_n, \mathbb{C}_n, \mathbb{E}_n, \mathbb{G}_n, \mathbb{H}_n$  necessarily satisfy

$$\begin{aligned} \Phi^{\text{visc}}(\mathbf{I}, \mathbf{n}; \mathbf{D}, \dot{\mathbf{n}}, \dot{\mathbf{p}}) &= \Phi^{\text{visc}}(\mathbf{I}, \mathbf{R}^T \mathbf{n}; \mathbf{R}^T \mathbf{D} \mathbf{R}, \mathbf{R}^T \dot{\mathbf{n}}, \mathbf{R}^T \dot{\mathbf{p}}) \quad \forall \mathbf{R} \in \mathcal{G} \Rightarrow \\ (\mathbb{C}_n)_{ijkl} &= (\mathbb{C}_n)_{i'j'k'l'} R_{i'i'} R_{j'j'} R_{k'k'} R_{l'l'}, \\ (\mathbb{B}_n)_{ijk} &= (\mathbb{B}_n)_{i'j'k'} R_{i'i'} R_{j'j'} R_{k'k'}, & (\mathbb{A}_n)_{ijk} &= (\mathbb{A}_n)_{i'j'k'} R_{i'i'} R_{j'j'} R_{k'k'}, \\ (\mathbb{H}_n, \mathbb{E}_n, \mathbb{G}_n)_{ij} &= (\mathbb{H}_n, \mathbb{E}_n, \mathbb{G}_n)_{i'j'} R_{i'i'} R_{j'j'}. \end{aligned} \quad (3.45)$$

By the standard argument as in Gurtin et al. (2010), general transversely isotropic tensors  $\mathbb{A}_n, \mathbb{B}_n, \mathbb{C}_n, \mathbb{E}_n, \mathbb{G}_n, \mathbb{H}_n$  are such that  $(D_n = \mathbf{n} \cdot \mathbf{D}\mathbf{n}, \dot{\mathbf{n}}_n = (\dot{\mathbf{n}} \cdot \mathbf{n})\mathbf{n} = 0, \dot{\mathbf{p}}_n = (\dot{\mathbf{p}} \cdot \mathbf{n})\mathbf{n})$

$$\begin{aligned} \mathbf{D} : \mathbb{C}_n \mathbf{D} &= C_{3333}(D_n)^2 + C_{1313}|\mathbf{D}\mathbf{n} - D_n \mathbf{n}|^2 + C_{1133}(\text{Tr} \mathbf{D} - D_n)D_n \\ &\quad + C_{1212}|\mathbf{D} - \mathbf{n} \otimes \mathbf{D}\mathbf{n} - (\mathbf{D}\mathbf{n}) \otimes \mathbf{n} + D_n \mathbf{n} \otimes \mathbf{n}|^2 + C_{1122}(\text{Tr} \mathbf{D} - D_n)^2, \\ \mathbf{D} : \mathbb{B}_n \dot{\mathbf{n}} &= B_{311}(\mathbf{D}\mathbf{n} - D_n \mathbf{n}) \cdot (\dot{\mathbf{n}} - \dot{\mathbf{n}}_n) + B_{113}(\text{Tr} \mathbf{D} - D_n)(\dot{\mathbf{n}} \cdot \mathbf{n}) + B_{333}D_n(\dot{\mathbf{n}} \cdot \mathbf{n}), \\ \mathbf{D} : \mathbb{A}_n \dot{\mathbf{p}} &= A_{311}(\mathbf{D}\mathbf{n} - D_n \mathbf{n}) \cdot (\dot{\mathbf{p}} - \dot{\mathbf{p}}_n) + A_{113}(\text{Tr} \mathbf{D} - D_n)(\dot{\mathbf{p}} \cdot \mathbf{n}) + A_{333}D_n(\dot{\mathbf{p}} \cdot \mathbf{n}), \end{aligned} \quad (3.46)$$

and

$$\begin{aligned} \dot{\mathbf{n}} \cdot \mathbb{H}_n \dot{\mathbf{n}} &= H_{11}|\dot{\mathbf{n}} - \dot{\mathbf{n}}_n|^2 + H_{33}|\dot{\mathbf{n}}_n|^2, \\ \dot{\mathbf{n}} \cdot \mathbb{E}_n \dot{\mathbf{p}} &= E_{11}(\dot{\mathbf{n}} - \dot{\mathbf{n}}_n) \cdot (\dot{\mathbf{p}} - \dot{\mathbf{p}}_n) + E_{33}\dot{\mathbf{n}}_n \cdot \dot{\mathbf{p}}_n, \\ \dot{\mathbf{p}} \cdot \mathbb{G}_n \dot{\mathbf{p}} &= G_{11}|\dot{\mathbf{p}} - \dot{\mathbf{p}}_n|^2 + G_{33}|\dot{\mathbf{p}}_n|^2. \end{aligned} \quad (3.47)$$

Using the constraints

$$\dot{\mathbf{n}} \cdot \mathbf{n} = \dot{\mathbf{n}} \cdot \mathbf{n} - \mathbf{n} \cdot \mathbf{W}\mathbf{n} = 0 \quad \text{and} \quad \text{Tr} \mathbf{D} = 0,$$

we find that the quadratic form (3.43) of dissipation potential can be simply written as

$$\begin{aligned} \Phi^{\text{visc}}(\mathbf{I}, \mathbf{D}, \mathbf{n}, \dot{\mathbf{n}}, \dot{\mathbf{p}}) &= \alpha_1(\mathbf{n} \cdot \mathbf{D}\mathbf{n})^2 + \alpha_2|\mathbf{D}\mathbf{n}|^2 + \alpha_3|\mathbf{D}|^2 + 2\alpha_4\dot{\mathbf{n}} \cdot \mathbf{D}\mathbf{n} + \alpha_5|\dot{\mathbf{n}}|^2 \\ &\quad + 2\alpha_6\dot{\mathbf{n}} \cdot \dot{\mathbf{p}} + \alpha_7|\dot{\mathbf{p}} - \dot{\mathbf{p}}_n|^2 + \alpha_8|\dot{\mathbf{p}}_n|^2 + 2\alpha_9 D_n(\dot{\mathbf{p}} \cdot \mathbf{n}) + 2\alpha_{10}\mathbf{n} \cdot \mathbf{D}(\dot{\mathbf{p}} - \dot{\mathbf{p}}_n), \end{aligned} \quad (3.48)$$

where  $\alpha_1 = C_{3333} - C_{1313} - C_{1133} + C_{1212} + C_{1122}$ ,  $\alpha_2 = C_{1313} - 2C_{1212}$ ,  $\alpha_3 = C_{1212}$ ,  $\alpha_4 = B_{311}$ ,  $\alpha_5 = H_{11}$ ,  $\alpha_6 = E_{11}$ ,  $\alpha_7 = G_{11}$ ,  $\alpha_8 = G_{33}$ ,  $\alpha_9 = A_{333} - A_{113}$ , and  $\alpha_{10} = A_{311}$ . For simplicity, assume  $\alpha_7 = \alpha_8$  and  $\alpha_9 = 0$ . Then, the positivity of  $\Phi^{\text{visc}}$  implies that

$$\alpha_{1,2,3,5,7,8} > 0, \quad \alpha_6^2 \leq \alpha_7 \alpha_5, \quad \alpha_4^2 \leq (\alpha_2 + 2\alpha_3)\alpha_5, \quad \alpha_{10}^2 \leq (\alpha_2 + 2\alpha_3)\alpha_7. \quad (3.49)$$

Consequently, for transversely isotropic LCEs the ‘‘forces’’ and ‘‘rates’’ are related by

$$\begin{bmatrix} \boldsymbol{\sigma}_{\text{sym}}^{\text{visc}} \\ \mathbf{s}^{\text{visc}} \\ \mathbf{e}^{\text{visc}} \end{bmatrix} = \begin{bmatrix} \alpha_1 D_n \mathbf{n} \otimes \mathbf{n} + \alpha_2 \text{Sym}(\mathbf{D}\mathbf{n} \otimes \mathbf{n}) + \alpha_3 \mathbf{D} + \text{Sym}((\alpha_4 \dot{\mathbf{n}} + \alpha_{10}(\dot{\mathbf{p}} - \dot{\mathbf{p}}_n)) \otimes \mathbf{n}) \\ \alpha_4 \mathbf{D}\mathbf{n} + \alpha_5 \dot{\mathbf{n}} + \alpha_6 \dot{\mathbf{p}} \\ \alpha_6 \dot{\mathbf{n}} + \alpha_7 \dot{\mathbf{p}} + \alpha_{10}(\mathbf{D}\mathbf{n} - D_n \mathbf{n}) \end{bmatrix}. \quad (3.50)$$

From (3.38), we have

$$\begin{aligned} \boldsymbol{\sigma}_{\text{skw}}^{\text{visc}} &= -\text{Skw}((\alpha_4 \mathbf{D}\mathbf{n} + \alpha_5 \dot{\mathbf{n}} + \alpha_6 \dot{\mathbf{p}}) \otimes \mathbf{n}) \\ &\quad - \text{Skw}((\alpha_6 \dot{\mathbf{n}} + \alpha_7 \dot{\mathbf{p}} + \alpha_{10}(\mathbf{D}\mathbf{n} - D_n \mathbf{n})) \otimes \mathbf{p}). \end{aligned} \quad (3.51)$$

We remark that at the absence of dissipative electrical currents (i.e.,  $\mathbb{E}_{\mathbf{n}} = \mathbb{G}_{\mathbf{n}} \equiv 0$ ), the five viscosities  $\alpha_{1,2,3,4,5}$  can be one-to-one linearly mapped to the Leslie viscosities in the classical dynamical model for liquid crystals.

Collecting all together, we obtain the dynamical governing equations for evolution of states of flexoelectric LCEs:

$$\begin{cases} \operatorname{div}_y \boldsymbol{\sigma} = \rho_0 \dot{\mathbf{v}}, & \text{(balance of linear momentum),} \\ \operatorname{Skw}(\boldsymbol{\sigma} + \mathbf{S}(\nabla_y \mathbf{n})^\top + (\operatorname{div}_y \mathbf{S}) \otimes \mathbf{n}) = \mathbf{0} & \text{(balance of angular momentum),} \\ (\operatorname{div}_y \mathbf{S}) = \mathbf{m}^{\text{tot}} + \lambda_{\mathbf{n}} \mathbf{n} + \mathbf{s}^{\text{visc}} & \text{(balance of director couple),} \\ \operatorname{div}_y(-\epsilon_0 \nabla_y \xi + \mathbf{p}) = 0 & \text{(Maxwell's equation),} \end{cases} \quad (3.52)$$

where the constitutive model are prescribed by the free energy function and dissipation potential with

$$\begin{aligned} \boldsymbol{\sigma} &= \left( \boldsymbol{\sigma}^{\text{MW}} + \frac{1}{J} \frac{\partial \Psi}{\partial \mathbf{F}} \mathbf{F}^\top \right) + \lambda_p \mathbf{I} + \boldsymbol{\sigma}^{\text{visc}}, \\ \mathbf{S} &= \frac{\partial \Psi}{\partial \nabla \mathbf{n}} \mathbf{F}^\top, \quad \mathbf{m}^{\text{tot}} = \frac{\partial \Psi}{\partial \mathbf{n}}, \quad -\nabla_y \xi = \frac{\partial \Psi}{\partial \mathbf{p}} + \mathbf{e}^{\text{visc}}, \end{aligned} \quad (3.53)$$

and dissipative “forces” given by (3.50) and (3.51). Further, we note that by (3.14), the balance of angular momentum in Eq. (3.52)<sub>2</sub> is equivalent to (3.38) upon recognizing that

$$\boldsymbol{\sigma} = \frac{1}{J} \left( \frac{\partial \Psi}{\partial \mathbf{F}} + \boldsymbol{\Sigma}^{\text{MW}} \right) \mathbf{F}^\top + \boldsymbol{\sigma}^{\text{visc}} \quad \text{and} \quad \mathbf{S} = \frac{1}{J} \tilde{\mathbf{S}}^{\text{tot}} \mathbf{F}^\top = \frac{1}{J} \frac{\partial \Psi}{\partial \nabla \mathbf{n}} \mathbf{F}^\top. \quad (3.54)$$

Upon specifying boundary conditions for  $(\mathbf{y}, \mathbf{n})$  and electrical potential  $\xi$  on  $\partial V$ , Eqs. (3.52) and (3.53) can be solved to determine the evolution of states of the flexoelectric LCE bodies.

#### 4. Asymptotic theories

The equilibrium and dynamical models discussed in prior sections are fully nonlinear and not amenable for explicit solutions. In practice, the loading conditions (i.e., the prescribed boundary conditions) and material constants may be controlled such that the response of the LCE body is in a particular regime that can be well approximated by an asymptotic theory. We are therefore motivated to consider a few asymptotic models for photo-flexoelectric LCEs to facilitate physical insights and analytical solutions in this section.

**Remark 5 (Non-dimensionalization).** Different asymptotic regimes should be described by some relevant dimensionless parameters of material constants and loading conditions. As presentation of the equations in a dimensionless manner simplifies interpretation of the problem and ease numerical solution, we identify the following dimensionless variables

$$\begin{aligned} \bar{\mathbf{p}} &:= \frac{\mathbf{p}}{\sqrt{\epsilon_0 \mu}}, \quad \bar{\xi} := \frac{\xi}{H} \sqrt{\frac{\epsilon_0}{\mu}}, \quad \bar{A}_1 := \epsilon_0 A_1, \quad \bar{A}_2 := \epsilon_0 A_2, \\ \bar{f}_b &:= \frac{f_b}{H} \sqrt{\frac{\epsilon_0}{\mu}}, \quad \bar{f}_s := \frac{f_s}{H} \sqrt{\frac{\epsilon_0}{\mu}}, \quad \bar{K}_F := \frac{K_F}{\mu H^2}, \quad \bar{\mu}_\beta := \frac{\mu_\beta}{\mu}, \quad \bar{\kappa} := \frac{\kappa}{\mu}, \end{aligned} \quad (4.1)$$

where  $H$  is the characteristic length of the LCE body. We identify dimensionless gradient operators as

$$\bar{\nabla} := H \nabla, \quad \bar{\nabla}_y := H \nabla_y. \quad (4.2)$$

From this point forward, we will only use dimensionless equations. For brevity and with an abuse of notation, we will drop the over-bar ( $\bar{\cdot}$ ); the reader should assume that all material property coefficients are dimensionless.

##### 4.1. Asymptotic expansions

We will consider the competitions between various terms in the total free energy (2.2). Let  $\mathbf{u} : V_R \rightarrow \mathbb{R}^3$  be the displacement ( $\nabla \mathbf{u} = \mathbf{F} - \mathbf{I}$ ). We introduce three scaling parameters  $\epsilon_i$  ( $i = 1, 2, 3$ ), i.e., the orders of magnitude of  $(\nabla \mathbf{u}, \nabla \mathbf{n}, \mathbf{p})$ :

$$|\nabla \mathbf{u}| \sim \epsilon_1, \quad |\nabla \mathbf{n}| \sim \epsilon_2, \quad |\mathbf{p}| \sim \epsilon_3, \quad (4.3)$$

and for an integer index  $\alpha = (\alpha_1, \alpha_2, \alpha_3) \in \mathbb{Z}^3$ , denote by  $\epsilon^\alpha = \epsilon_1^{\alpha_1} \epsilon_2^{\alpha_2} \epsilon_3^{\alpha_3}$ . Suppose that these scaling parameters  $\epsilon_i$  ( $i = 1, 2, 3$ ) are independent of each other. Omitting the boundary contributions from mechanical and nematic loadings for the moment (i.e.,  $\tilde{\mathbf{t}}_b = \tilde{\mathbf{s}}_b = 0$ ), we aim to formally write the dimensionless total free energy (2.2) or (2.37) as a sum of terms of distinct orders:

$$\mathcal{F}^{\text{tot}}[\mathbf{y}, \mathbf{n}, \mathbf{p}] = \mathcal{F}^{\text{opt}}[\mathbf{n}] + \sum_{\alpha} \mathcal{F}^{(\alpha)}[\mathbf{u}, \mathbf{n}, \mathbf{p}], \quad (4.4)$$

where  $\mathcal{F}^{(\alpha)}[\mathbf{u}, \mathbf{n}, \mathbf{p}] \sim \epsilon^\alpha$ . Note that the order of magnitude of the photo-nematic coupling energy  $\mathcal{F}^{\text{opt}}[\mathbf{n}]$  depends on the light intensity of external sources, and is therefore treated separately.

To proceed, we first consider elastic energy (2.4) and (2.6). Let  $\gamma = a^{1/3} - 1$ , where the material constant  $a$  is used in Eqs. (2.5) and (2.6). Suppose that  $|\gamma| \sim |\nabla \mathbf{u}| \sim \epsilon_1$ . Keeping terms up to  $O(\epsilon_1^2)$ , we have

$$\begin{aligned} (\mathbf{F}_{\mathbf{n}} \mathbf{F}_{\mathbf{n}}^\top)^{-1} &= (1 + \gamma) \mathbf{I} - 3\gamma \mathbf{n} \otimes \mathbf{n} + 3\gamma^2 \mathbf{n} \otimes \mathbf{n} + o(\epsilon_1^2), \\ (\mathbf{F}_{\mathbf{N}}^\top \mathbf{F}_{\mathbf{N}})^{-1} &= (1 + \gamma) \mathbf{I} - 3\gamma \mathbf{N} \otimes \mathbf{N} + 3\gamma^2 \mathbf{N} \otimes \mathbf{N} + o(\epsilon_1^2). \end{aligned} \quad (4.5)$$

Recall that  $\mathbf{F} = \mathbf{I} + \nabla \mathbf{u}$  and  $|\nabla \mathbf{u}| \sim \varepsilon_1 \ll 1$ . Expanding the energy densities (2.4) and (2.6) and truncating at  $O(\varepsilon_1^2)$ , within an additive constant we have

$$\begin{aligned} W^{\text{elast}} &= \left. \frac{\partial W^{\text{elast}}}{\partial \mathbf{F}} \right|_{\mathbf{F}=\mathbf{I}} : \nabla \mathbf{u} + \frac{1}{2} \nabla \mathbf{u} : \left. \frac{\partial^2 W^{\text{elast}}}{\partial \mathbf{F} \partial \mathbf{F}} \right|_{\mathbf{F}=\mathbf{I}} \nabla \mathbf{u} + o(\varepsilon_1^2), \\ W^{\text{anis}} &= \left. \frac{\partial W^{\text{anis}}}{\partial \mathbf{F}} \right|_{\mathbf{F}=\mathbf{I}} : \nabla \mathbf{u} + \frac{1}{2} \nabla \mathbf{u} : \left. \frac{\partial^2 W^{\text{anis}}}{\partial \mathbf{F} \partial \mathbf{F}} \right|_{\mathbf{F}=\mathbf{I}} \nabla \mathbf{u} + o(\varepsilon_1^2). \end{aligned} \quad (4.6)$$

Inserting Eqs. (4.5) into (2.4) and (2.6), within a constant and by (4.6) we write the elastic/anisotropic energies as follows:

$$W^{\text{elast}} + W^{\text{anis}} = \psi^{\text{el-an}}(\mathbf{E}, \mathbf{n}) + o(\varepsilon_1^2), \quad (4.7)$$

where

$$\begin{aligned} \psi^{\text{el-an}}(\mathbf{E}, \mathbf{n}) &= \mu |\mathbf{E}_d - \mathbf{E}^*(\mathbf{n})|^2 + \frac{1}{2} \kappa (\text{Tr}(\mathbf{E}))^2 + \mu_\beta |\mathbf{E}_d - \mathbf{E}^*(\mathbf{N})|^2, \\ \mathbf{E} &= \frac{\nabla \mathbf{u} + (\nabla \mathbf{u})^\top}{2}, \quad \mathbf{E}_d = \mathbf{E} - \frac{1}{3} \text{Tr} \mathbf{E}, \quad \mathbf{E}^*(\mathbf{n}) = \frac{3\gamma}{2} \left( \mathbf{n} \otimes \mathbf{n} - \frac{1}{3} \mathbf{I} \right). \end{aligned} \quad (4.8)$$

Similarly, the Frank elasticity energy (2.12) can be expanded as

$$W^{\text{Frank}} = \frac{1}{2} K_F J |\nabla \mathbf{n} \mathbf{F}^{-1}|^2 = \frac{1}{2} K_F |\nabla \mathbf{n}|^2 + \sigma^{\text{Frank}} : \nabla \mathbf{u} + o(\varepsilon_1 \varepsilon_2^2), \quad (4.9)$$

where (Cf. Eq. (2.42))

$$\sigma^{\text{Frank}} = \frac{1}{2} K_F |\nabla \mathbf{n}|^2 \mathbf{I} - K_F (\nabla \mathbf{n})^\top \nabla \mathbf{n}. \quad (4.10)$$

Let (Cf. Eq. (2.45)–(2.46))

$$\begin{aligned} \sigma^{\text{flexo}} &= f_s(\mathbf{p} \cdot \mathbf{n})(\nabla \mathbf{n})^\top + f_b((\nabla \mathbf{n})^\top \mathbf{p}) \otimes \mathbf{n} + ((\mathbf{n} \otimes \mathbf{p}) \cdot \mathbb{F}(\nabla \mathbf{n})) \mathbf{I} \quad (\sim \varepsilon_2 \varepsilon_3), \\ \mathbf{e}^{\text{flexo}} &= -f_s(\text{div} \mathbf{n}) \mathbf{n} - f_b(\nabla \mathbf{n}) \mathbf{n} \quad (\sim \varepsilon_2), \\ \mathbf{m}^{\text{flexo}} &= -f_s(\text{div} \mathbf{n}) \mathbf{p} - f_b(\nabla \mathbf{n})^\top \mathbf{p} \quad (\sim \varepsilon_2 \varepsilon_3), \\ \mathbf{S}^{\text{flexo}} &= -f_s(\mathbf{n} \cdot \mathbf{p}) \mathbf{I} - f_b \mathbf{n} \otimes \mathbf{p} \quad (\sim \varepsilon_3). \end{aligned} \quad (4.11)$$

The flexoelectric energy (2.26) can be expanded as

$$\begin{aligned} W^{\text{flexo}} &= \underbrace{(\mathbf{n} \otimes \mathbf{p}) \cdot \mathbb{F}(\nabla \mathbf{n})}_{= \mathbf{e}^{\text{flexo}} \cdot \mathbf{p} = \mathbf{m}^{\text{flexo}} \cdot \mathbf{n} = \mathbf{S}^{\text{flexo}} : \nabla \mathbf{n}} + \sigma^{\text{flexo}} : \nabla \mathbf{u} + o(\varepsilon_1 \varepsilon_2 \varepsilon_3), \end{aligned} \quad (4.12)$$

The electrical energy term (2.18) can be expanded as (Cf. Eq. (2.43))

$$P^{\text{elect}} + P^{\text{elect}} = \int_{V_R} \left[ \frac{\varepsilon_0}{2} |\nabla \xi|^2 + \frac{1}{2} \mathbf{p} \cdot (\mathbb{D}_{\mathbf{n}} - \varepsilon_0 \mathbf{I})^{-1} \mathbf{p} + \sigma^{\text{MW}} : \nabla \mathbf{u} \right] + o(\varepsilon_1 \varepsilon_3^2), \quad (4.13)$$

where (Cf. Eq. (2.44))

$$\begin{aligned} \mathbf{e}^{\text{pol}} &= (\mathbb{D}_{\mathbf{n}} - \varepsilon_0 \mathbf{I})^{-1} \mathbf{p} \quad (\sim \varepsilon_3), \\ \sigma^{\text{MW}} &= \nabla \xi \otimes \mathbb{D}_{\mathbf{n}} \nabla \xi - \left[ \frac{\varepsilon_0}{2} |\nabla \xi|^2 + (-\nabla \xi - \frac{1}{2} \mathbf{e}^{\text{pol}}) \cdot \mathbf{p} \right] \mathbf{I} \quad (\sim \varepsilon_3^2). \end{aligned} \quad (4.14)$$

In summary, by Eqs. (4.7), (4.9), (4.12) and (4.13) the leading terms of the total free energy in the expansion (4.4) can be identified as

$$\begin{aligned} F^{(2,0,0)}[\mathbf{u}, \mathbf{n}] &= \int_{V_R} \left[ \mu |\mathbf{E}_d - \mathbf{E}^*(\mathbf{n})|^2 + \frac{1}{2} \kappa (\text{Tr}(\mathbf{E}))^2 + \mu_\beta |\mathbf{E}_d - \mathbf{E}^*(\mathbf{N})|^2 \right], \\ F^{(0,2,0)}[\mathbf{n}] &= \int_{V_R} \frac{1}{2} K_F |\nabla \mathbf{n}|^2, \quad F^{(1,2,0)}[\mathbf{u}, \mathbf{n}] = \int_{V_R} \sigma^{\text{Frank}} : \nabla \mathbf{u}, \\ F^{(0,0,2)}[\mathbf{n}, \mathbf{p}] &= \int_{V_R} \left[ \frac{\varepsilon_0}{2} |\nabla \xi|^2 + \frac{1}{2} \mathbf{p} \cdot (\mathbb{D}_{\mathbf{n}} - \varepsilon_0 \mathbf{I})^{-1} \mathbf{p} \right], \\ F^{(1,0,2)}[\mathbf{u}, \mathbf{n}, \mathbf{p}] &= \int_{V_R} \nabla \mathbf{u} : \sigma^{\text{MW}}, \\ F^{(0,1,1)}[\mathbf{n}, \mathbf{p}] &= \int_{V_R} (\mathbf{n} \otimes \mathbf{p}) \cdot \mathbb{F}(\nabla \mathbf{n}), \quad F^{(1,1,1)}[\mathbf{u}, \mathbf{n}, \mathbf{p}] = \int_{V_R} \nabla \mathbf{u} : \sigma^{\text{flexo}}. \end{aligned} \quad (4.15)$$

We are now ready to formally derive asymptotic theories in various regimes.

#### 4.2. Liquid crystals ( $\mu \sim \kappa \sim \mu_\beta \sim 0$ )

In this regime, the (regular) elasticity is negligible and the LCE is actually liquid with trivial shear modulus. Therefore, it is more convenient to use Eulerian description or equivalently choose the reference configuration the same as the current configuration (i.e.,  $\mathbf{y} = \mathbf{x}$  and hence displacement  $\mathbf{u} = 0$ ). The total free energy of the system in this regime is given by (setting  $\tilde{\mathbf{i}}_b = \tilde{\mathbf{s}}_b = 0$ )

$$\begin{aligned}
 \mathcal{F}^{\text{tot}}[\mathbf{p}, \mathbf{n}] &= \mathcal{F}^{\text{opt}}[\mathbf{n}] + F^{(0,2,0)}[\mathbf{n}] + F^{(0,0,2)}[\mathbf{n}, \mathbf{p}] + F^{(0,1,1)}[\mathbf{n}, \mathbf{p}] \\
 &= \mathcal{F}^{\text{opt}}[\mathbf{n}] + \int_V \left[ \frac{1}{2} K_F |\nabla \mathbf{n}|^2 + (\mathbf{n} \otimes \mathbf{p}) \cdot \mathbb{F}(\nabla \mathbf{n}) \right. \\
 &\quad \left. + \frac{\epsilon_0}{2} |\nabla \xi|^2 + \frac{1}{2} \mathbf{p} \cdot (\mathbb{D}_{\mathbf{n}} - \epsilon_0 \mathbf{I})^{-1} \mathbf{p} \right].
 \end{aligned} \tag{4.16}$$

From Eqs. (2.51) and (3.52) and in account of the special conditions (i.e.,  $\mathbf{y} = \mathbf{x}$  and  $\mathcal{F}^{\text{el-an}} = 0$ ), we obtain the following simplified theories for flexoelectric liquid crystals.

**Equilibrium States.** By directly using Eq. (2.51) or repeating the first-variation calculation for Eq. (4.16), we can obtain the governing equation for an equilibrium state of a photo-flexoelectric liquid crystal body. In particular, by Eqs. (2.44), (2.46), (2.51)<sub>3</sub>, (4.11) and (4.14) we find that

$$\begin{aligned}
 -\nabla \xi &= \mathbf{e}^{\text{flexo}} + \mathbf{e}^{\text{pol}} = -f_s(\text{div} \mathbf{n}) \mathbf{n} - f_b(\nabla \mathbf{n}) \mathbf{n} + (\mathbb{D}_{\mathbf{n}} - \epsilon_0 \mathbf{I})^{-1} \mathbf{p}, \\
 \mathbf{m}^{\text{tot}} &= \mathbf{m}^{\text{flexo}} + \mathbf{m}^{\text{pol}} + \mathbf{m}^{\text{opt}} = (\mathbb{F}(\nabla \mathbf{n})) \mathbf{p} + A_1(\mathbf{n} \cdot \mathbf{p}) \mathbf{p} + \frac{\partial W^{\text{opt}}}{\partial \mathbf{n}}.
 \end{aligned} \tag{4.17}$$

Therefore, the governing equations for  $(\mathbf{n}, \mathbf{p})$  is as follows:

$$\begin{cases} \text{div}(-\epsilon_0 \nabla \xi + \mathbf{p}) = 0 & \text{(Maxwell equation),} \\ -\text{div}(K_F \nabla \mathbf{n} + \mathbb{F}(\mathbf{n} \otimes \mathbf{p})) + \mathbf{m}^{\text{tot}} + \lambda_{\mathbf{n}} \mathbf{n} = 0 & \text{(Balance of director couples).} \end{cases} \tag{4.18}$$

**Remark 6 (Liquid Crystals in Electrical Fields Without Photo-Flexoelectric Coupling).** If the flexoelectricity and photo-nematic coupling are neglected ( $\mathcal{F}^{\text{flexo}} = \mathcal{F}^{\text{opt}} = 0$ ), by (4.17) we have

$$\begin{aligned}
 \mathbf{p} &= -(\mathbb{D}_{\mathbf{n}} - \epsilon_0 \mathbf{I}) \nabla \xi, \\
 \mathbf{m}^{\text{pol}} &= -(\epsilon_c - \epsilon_a)(\mathbf{n} \cdot \nabla \xi) \nabla \xi - \frac{(\epsilon_c - \epsilon_a)^2}{\epsilon_a - \epsilon_0} (\mathbf{n} \cdot \nabla \xi)^2 \mathbf{n}.
 \end{aligned} \tag{4.19}$$

Therefore, the total free energy (4.16) can also be written as (setting  $\tilde{\mathbf{t}}_b = \tilde{\mathbf{s}}_b = 0$ )

$$\begin{aligned}
 \mathcal{F}^{\text{tot}}[\mathbf{p}, \mathbf{n}] &= \int_V \left( \frac{1}{2} K_F |\nabla \mathbf{n}|^2 - \frac{1}{2} \nabla \xi \cdot \mathbb{D}_{\mathbf{n}} \nabla \xi \right) \\
 &= \frac{1}{2} \int_V \left( K_F |\nabla \mathbf{n}|^2 - \epsilon_a |\nabla \xi|^2 - (\epsilon_c - \epsilon_a)(\mathbf{n} \cdot \nabla \xi)^2 \right).
 \end{aligned} \tag{4.20}$$

In addition, we can rewrite (4.18) as

$$\begin{cases} \text{div}(-\mathbb{D}_{\mathbf{n}} \nabla \xi) = 0 & \text{(Maxwell equation),} \\ -\text{div}(K_F \nabla \mathbf{n}) - (\epsilon_c - \epsilon_a)(\mathbf{n} \cdot \nabla \xi) \nabla \xi + \lambda'_{\mathbf{n}} \mathbf{n} = 0 & \text{(Balance of director couples),} \end{cases} \tag{4.21}$$

where the second term in Eq. (4.19)<sub>2</sub> is merged with the Lagrange multiplier  $\lambda_{\mathbf{n}}$ . Qualitatively, by Eq. (4.20) we see the effect of electric field on the director field: the director field tends to align with (resp. perpendicular to) the electric field  $-\nabla \xi$  if  $\epsilon_c > \epsilon_a$  (resp.  $\epsilon_c < \epsilon_a$ ).

**Dynamical Models.** In account of the additional viscous “forces” (3.24) in dynamical processes, the dynamical governing equations for photo-flexoelectric LCs would be the same as (3.52). The constitutive relations between  $(\sigma, \mathbf{S}, -\nabla \xi)$  and  $(\mathbf{F}, \mathbf{n}, \mathbf{p}; \mathbf{D}, \dot{\mathbf{n}}, \dot{\mathbf{p}})$  are now given by

$$\begin{aligned}
 \sigma &= -\lambda_p \mathbf{I} + \sigma^{\text{MW}} + \sigma^{\text{visc}}, \\
 \mathbf{S} &= K_F \nabla \mathbf{n} + \mathbb{F}(\mathbf{n} \otimes \mathbf{p}), \\
 -\nabla \xi &= -f_s(\text{div} \mathbf{n}) \mathbf{n} - f_b(\nabla \mathbf{n}) \mathbf{n} + (\mathbb{D}_{\mathbf{n}} - \epsilon_0 \mathbf{I})^{-1} \mathbf{p} + \mathbf{e}^{\text{visc}},
 \end{aligned} \tag{4.22}$$

and dissipative “forces” given by Eqs. (3.50) and (3.51).

**Remark 7 (Dynamical Ericksen–Leslie Theory for Liquid Crystals).** At the absence of photo-flexoelectricity and electrical fields (i.e.,  $\mathcal{F}^{\text{tot}} = \mathcal{F}^{\text{Frank}}$  and  $\mathbb{A}_{\mathbf{n}} = \mathbb{E}_{\mathbf{n}} = \mathbb{G}_{\mathbf{n}} = \mathbb{H}_{\mathbf{n}} = 0$ ), the model prescribed by Eqs. (3.52), (4.22), (3.50) and (3.51) is simplified as

$$\begin{cases} \text{div}_y \sigma = \rho_0 \dot{\mathbf{v}}, & \text{Tr}(\mathbf{D}) = 0, & \sigma = -\lambda_p \mathbf{I} + \mathbb{C}_{\mathbf{n}} \mathbf{D} + \sigma_{\text{skw}}^{\text{visc}}, \\ \sigma_{\text{skw}}^{\text{visc}} = -\alpha_4 \text{Skw}((\mathbf{D}\mathbf{n}) \otimes \mathbf{n}) - \alpha_5 \text{Skw}(\dot{\mathbf{n}} \otimes \mathbf{n}), & & \\ K_F \text{div} \nabla \mathbf{n} = \lambda_{\mathbf{n}} \mathbf{n} + \mathbf{s}^{\text{visc}}, & \mathbf{s}^{\text{visc}} = \alpha_4 \mathbf{D}\mathbf{n} + \alpha_5 \dot{\mathbf{n}}, & \end{cases} \tag{4.23}$$

which recovers the classical Ericksen–Leslie’s equations for liquid crystals (Ericksen, 1961; Leslie, 1966, 1968; Stewart, 2019). In particular, the coefficients  $\alpha_{1,2,3,4,5}$  can be one-to-one linearly mapped to the conventional Leslie viscosities.

**Remark 8 (Dynamical Model for Liquid Crystals in Electrical Fields).** At the absence of photo-flexoelectricity, we consider the dynamical responses of liquid crystals with  $\mathcal{F}^{\text{tot}} = \mathcal{F}^{\text{Frank}} + \mathcal{F}^{\text{elect}}$ . Then the model prescribed by (3.52), (4.22), (3.50) and (3.51) is simplified as

$$\begin{cases} \operatorname{div}(-\epsilon_0 \nabla \xi + \mathbf{p}) = 0, & -\nabla \xi = (\mathbb{D}_{\mathbf{n}} - \epsilon_0 \mathbf{I})^{-1} \mathbf{p} + \mathbf{e}^{\text{visc}}, \\ \mathbf{e}^{\text{visc}} = \alpha_6 \dot{\mathbf{n}} + \alpha_7 \dot{\mathbf{p}} + \alpha_{10} (\mathbf{D}\mathbf{n} - D_{\mathbf{n}}\mathbf{n}), \\ \operatorname{div}_y \boldsymbol{\sigma} = \rho_0 \dot{\mathbf{v}}, & \operatorname{Tr}(\mathbf{D}) = 0, & \boldsymbol{\sigma} = -\lambda_p \mathbf{I} + \boldsymbol{\sigma}^{\text{MW}} + \mathbf{C}_{\mathbf{n}} \mathbf{D} + \boldsymbol{\sigma}_{\text{skw}}^{\text{visc}}, \\ \boldsymbol{\sigma}_{\text{skw}}^{\text{visc}} = -\text{Skw}(\mathbf{s}^{\text{visc}} \otimes \mathbf{n} + \mathbf{e}^{\text{visc}} \otimes \mathbf{p}), \\ K_F \operatorname{div} \nabla \mathbf{n} = \lambda_{\mathbf{n}} \mathbf{n} + \mathbf{m}^{\text{pol}} + \mathbf{s}^{\text{visc}}, & \mathbf{s}^{\text{visc}} = \alpha_4 \mathbf{D}\mathbf{n} + \alpha_5 \dot{\mathbf{n}} + \alpha_6 \dot{\mathbf{p}}. \end{cases} \quad (4.24)$$

Further, suppose that the applied electrical field  $\mathbf{E}_0 \in \mathbb{R}^3$  (i.e., the boundary potential is given by  $\xi_b = -\mathbf{E}_0 \mathbf{x}$  on  $\partial V$ ) is uniform and much larger than the stray field in the sense that

$$|\mathbf{E}_0| \gg |-\nabla \xi - \mathbf{E}_0|, \quad (4.25)$$

by Eq. (4.19)<sub>2</sub> we see that the couple on the direction  $\mathbf{n}$  is approximately given by

$$-\mathbf{m}^{\text{pol}} \approx (\epsilon_c - \epsilon_a)(\mathbf{n} \cdot \mathbf{E}_0)\mathbf{E}_0.$$

In addition, if we neglect the flow problem (i.e.,  $\mathbf{v} = 0$ ), the anisotropy of dielectric tensor (i.e.,  $\epsilon_a = \epsilon_c = \epsilon$  and  $\mathbb{D}_{\mathbf{n}} = \epsilon \mathbf{I}$ ), and the coupling between  $(\dot{\mathbf{n}}, \dot{\mathbf{p}})$  (i.e.,  $\alpha_6 = 0$ ), the two evolutionary equations for  $(\mathbf{n}(\mathbf{x}, t), \mathbf{p}(\mathbf{x}, t))$  in Eq. (4.24) are decoupled and can be written as

$$\begin{cases} \alpha_5 \dot{\mathbf{n}} = K_F \operatorname{div} \nabla \mathbf{n} - \lambda_{\mathbf{n}} \mathbf{n} + (\epsilon_c - \epsilon_a)(\mathbf{n} \cdot \mathbf{E}_0)\mathbf{E}_0, \\ \frac{d}{dt}(\operatorname{div} \mathbf{p}) = \operatorname{div} \left( -\frac{\epsilon}{(\epsilon - \epsilon_0)\alpha_7} \nabla \xi \right). \end{cases} \quad (4.26)$$

We recognize the second of (4.26) as the conservation of charges with electrical conductivity  $\frac{\epsilon}{(\epsilon - \epsilon_0)\alpha_7}$  and Ohm's law

$$\mathbf{j}_e = -\frac{\epsilon}{(\epsilon - \epsilon_0)\alpha_7} \nabla \xi.$$

If the Frank elasticity is neglected ( $K_F = 0$ ), the first of (4.26) can be written as

$$\alpha_5 \dot{\mathbf{n}} = (\epsilon_c - \epsilon_a)(\mathbf{n} \cdot \mathbf{E}_0)\mathbf{E}_0 + \lambda_{\mathbf{n}} \mathbf{n} \Leftrightarrow \alpha_5 \dot{\theta} = -(\epsilon_c - \epsilon_a)|\mathbf{E}_0|^2 \cos \theta \sin \theta, \quad (4.27)$$

where  $\theta$  is the angle between  $\mathbf{n}$  and  $\mathbf{E}_0$ . Once again, we see that the director field tends to align with (resp. perpendicular to) the electric field  $\mathbf{E}_0$  if  $\epsilon_c > \epsilon_a$  (resp.  $\epsilon_c < \epsilon_a$ ).

**Remark 9 (Dynamical Model for Photo-Flexoelectric Liquid Crystals Without Flow).** Suppose that the flow problem can be neglected. Physically, this means each LC molecule is anchored at a fixed position but the director is free to rotate. For simplicity, we neglect the dissipation due to electrical currents, i.e., set  $\mathbb{A}_{\mathbf{n}} = \mathbb{E}_{\mathbf{n}} = \mathbb{G}_{\mathbf{n}} = 0$  in Eq. (3.50). Then the model prescribed by (3.52), (4.22), (3.50) and (3.51) is simplified as

$$\begin{cases} \operatorname{div}(-\epsilon_0 \nabla \xi + \mathbf{p}) = 0, \\ -\nabla \xi = -f_s(\operatorname{div} \mathbf{n})\mathbf{n} - f_b(\nabla \mathbf{n})\mathbf{n} + (\mathbb{D}_{\mathbf{n}} - \epsilon_0 \mathbf{I})^{-1} \mathbf{p} \\ \operatorname{div}(K_F \nabla \mathbf{n} + \mathbb{F}(\mathbf{n} \otimes \mathbf{p})) = \lambda_{\mathbf{n}} \mathbf{n} + \mathbf{m}^{\text{tot}} + \alpha_5 \dot{\mathbf{n}}, \\ \mathbf{m}^{\text{tot}} = (\mathbb{F}(\nabla \mathbf{n}))\mathbf{p} + A_1(\mathbf{n} \cdot \mathbf{p})\mathbf{p} + \frac{\partial W^{\text{opt}}}{\partial \mathbf{n}}, \end{cases} \quad (4.28)$$

which determines the evolution of director field  $\mathbf{n} = \mathbf{n}(\mathbf{x}, t)$  at the presence of flexoelectricity and electrical fields. If the stray field is negligible (Cf. Eq. (4.25)), the evolution equation (4.26) may be simplified as

$$\operatorname{div}(K_F \nabla \mathbf{n} + \mathbb{F}(\mathbf{n} \otimes \mathbf{p})) = \lambda_{\mathbf{n}} \mathbf{n} + \mathbf{m}^{\text{tot}} + \alpha_5 \dot{\mathbf{n}}, \quad (4.29)$$

where  $\mathbf{p} = (\mathbb{D}_{\mathbf{n}} - \epsilon_0 \mathbf{I})[\mathbf{E}_0 + f_s(\operatorname{div} \mathbf{n})\mathbf{n} + f_b(\nabla \mathbf{n})\mathbf{n}]$  and  $\mathbf{m}^{\text{tot}} = (\mathbb{F}(\nabla \mathbf{n}))\mathbf{p} + A_1(\mathbf{n} \cdot \mathbf{p})\mathbf{p} + \mathbf{m}^{\text{opt}}$ .

### 4.3. Geometrically linear theories for LCEs

The fully nonlinear static and dynamic theories (Cf. (2.51) and (3.52)) for photo-flexoelectric LCEs are highly complex, offering limited insight into the underlying physics and first-order effects from various couplings. As a result, in this section we focus on geometrically linear models in the sense that the energetic dependence on  $\nabla \mathbf{u}$  is truncated at  $O(|\nabla \mathbf{u}|^2)$ . In the regime of small strain ( $|\nabla \mathbf{u}| \sim \epsilon_1 \ll 1$ ), it is no longer necessary to differentiate derivatives with respect to the Eulerian and Lagrangian variables.

We focus on the static theory and equilibrium responses. Dynamical models can be obtained by adding the viscous ‘‘forces’’ in (3.50) and (3.51) to the corresponding balance laws. With the leading quadratic elastic energy  $F^{(2,0,0)}[\mathbf{u}, \mathbf{n}]$  in Eq. (4.15) as the benchmark, there are a few cases that will be separately discussed below.

**Photo-flexoelectric LCEs.** Suppose that  $\varepsilon_2 \sim \varepsilon_3 \sim \varepsilon_1^{1/2}$ . From Eqs. (4.4) and (4.15), we have

$$\begin{aligned} \mathcal{F}^{\text{tot}}[\mathbf{u}, \mathbf{n}, \mathbf{p}] &= \mathcal{F}^{\text{opt}}[\mathbf{n}] + \underbrace{F^{(0,2,0)}[\mathbf{n}] + F^{(0,0,2)}[\mathbf{n}, \mathbf{p}] + F^{(0,1,1)}[\mathbf{n}, \mathbf{p}]}_{\sim O(\varepsilon_1)} \\ &+ \underbrace{F^{(2,0,0)}[\mathbf{u}, \mathbf{n}] + F^{(1,2,0)}[\mathbf{u}, \mathbf{n}] + F^{(1,0,2)}[\mathbf{u}, \mathbf{n}, \mathbf{p}] + F^{(1,1,1)}[\mathbf{u}, \mathbf{n}, \mathbf{p}]}_{\sim O(\varepsilon_1^2)}. \end{aligned}$$

Since  $\varepsilon_1 \ll 1$ , in the asymptotic limit the minimization problem  $\min_{\mathbf{u}, \mathbf{n}, \mathbf{p}} \mathcal{F}^{\text{tot}}[\mathbf{u}, \mathbf{n}, \mathbf{p}]$  is well-approximated by sequentially minimizing the dominating  $O(\varepsilon_1)$ -terms and then higher-order  $O(\varepsilon_1^2)$ -terms.

1.  $O(\varepsilon_1)$ -terms:

$$\min_{\mathbf{n}, \mathbf{p}} \left\{ F^{(0,2,0)}[\mathbf{n}] + F^{(0,0,2)}[\mathbf{n}, \mathbf{p}] + F^{(0,1,1)}[\mathbf{n}, \mathbf{p}] + \mathcal{F}^{\text{opt}}[\mathbf{n}] \right\} \quad (4.30)$$

where we have assumed that the photo-nematic coupling (2.28) is also of order  $O(\varepsilon_1)$ , i.e.,  $\mathbf{m}^{\text{opt}} \sim \varepsilon_1$ . The Euler–Lagrange equation associated with the variational principle (4.30) is the same as Eqs. (4.17) and (4.18). Upon specifying appropriate boundary conditions, Eqs. (4.17) and (4.18) determine the equilibrium profiles of director field and polarization ( $\mathbf{n}, \mathbf{p}$ ).

2.  $O(\varepsilon_1^2)$ -terms:

$$\min_{\mathbf{u}} \left\{ F^{(2,0,0)}[\mathbf{u}, \mathbf{n}] + F^{(1,2,0)}[\mathbf{u}, \mathbf{n}] + F^{(1,0,2)}[\mathbf{u}, \mathbf{n}, \mathbf{p}] + F^{(1,1,1)}[\mathbf{u}, \mathbf{n}, \mathbf{p}] \right\}, \quad (4.31)$$

The Euler–Lagrange equation associated with Eq. (4.31) is given by (Cf. Eq. (2.51)<sub>2</sub>)

$$\text{div}(\boldsymbol{\sigma}^{\text{el-an}} + \boldsymbol{\sigma}^{\text{Frank}} + \boldsymbol{\sigma}^{\text{flexo}} + \boldsymbol{\sigma}^{\text{MW}} - \lambda_p \mathbf{I}) = 0, \quad \boldsymbol{\sigma}^{\text{el-an}} = \frac{\partial \Psi^{\text{el-an}}(\mathbf{E}, \mathbf{n})}{\partial \mathbf{E}}.$$

where the stress  $\boldsymbol{\sigma}^{\text{Frank}}$  (Cf. (4.10)),  $\boldsymbol{\sigma}^{\text{flexo}}$  (Cf. (4.11)),  $\boldsymbol{\sigma}^{\text{MW}}$  (Cf. (4.14)) are determined by ( $\mathbf{n}, \mathbf{p}$ ), i.e., the minimization problem (4.30) to the dominating  $O(\varepsilon_1)$ -energy terms.

**Photo-dielectric LCEs.** Suppose that  $\varepsilon_3 \sim \varepsilon_1^{1/2}$  and  $\varepsilon_2 \ll \varepsilon_1$ . In this regime, we may neglect the Frank elasticity and flexoelectricity. From Eqs. (4.4) and (4.15), we have

$$\begin{aligned} \mathcal{F}^{\text{tot}}[\mathbf{u}, \mathbf{n}, \mathbf{p}] &= \mathcal{F}^{\text{opt}}[\mathbf{n}] + \underbrace{F^{(0,0,2)}[\mathbf{n}, \mathbf{p}]}_{\sim O(\varepsilon_1)} + \underbrace{F^{(2,0,0)}[\mathbf{u}, \mathbf{n}] + F^{(1,0,2)}[\mathbf{u}, \mathbf{n}, \mathbf{p}]}_{\sim O(\varepsilon_1^2)} \\ &+ \underbrace{F^{(0,1,1)}[\mathbf{n}, \mathbf{p}]}_{O(\varepsilon_2 \varepsilon_1^{1/2})} + \underbrace{F^{(0,2,0)}[\mathbf{n}] + F^{(1,2,0)}[\mathbf{u}, \mathbf{n}] + F^{(1,1,1)}[\mathbf{u}, \mathbf{n}, \mathbf{p}]}_{\sim o(\varepsilon_1^2)}. \end{aligned}$$

Therefore, if the photo-nematic coupling (2.28) is also of order  $O(\varepsilon_1)$ , i.e.,  $\mathbf{m}^{\text{opt}} \sim \varepsilon_1$ , the director and polarization ( $\mathbf{n}, \mathbf{p}$ ) is determined by the dominating  $O(\varepsilon_1)$ -terms:

$$\min_{\mathbf{n}, \mathbf{p}} \left\{ F^{(0,0,2)}[\mathbf{n}, \mathbf{p}] + \mathcal{F}^{\text{opt}}[\mathbf{n}] \right\}, \quad (4.32)$$

implying that (Cf. (4.18))

$$\begin{cases} \text{div}(-\mathbb{D}_n \nabla \xi) = 0 & \text{(Maxwell equation),} \\ \mathbf{m}^{\text{tot}} + \lambda_n \mathbf{n} = A_1(\mathbf{p} \cdot \mathbf{n})\mathbf{p} + \mathbf{m}^{\text{opt}} + \lambda_n \mathbf{n} = 0 & \text{(Balance of director couples).} \end{cases} \quad (4.33)$$

For  $O(\varepsilon_1^2)$ -terms, we have

$$\min_{\mathbf{u}} \left\{ F^{(2,0,0)}[\mathbf{u}, \mathbf{n}] + F^{(1,0,2)}[\mathbf{u}, \mathbf{n}, \mathbf{p}] \right\}, \quad (4.34)$$

implying

$$\text{div}(\boldsymbol{\sigma}^{\text{el-an}} + \boldsymbol{\sigma}^{\text{MW}} - \lambda_p \mathbf{I}) = 0, \quad \boldsymbol{\sigma}^{\text{el-an}} = \frac{\partial \Psi^{\text{el-an}}(\mathbf{E}, \mathbf{n})}{\partial \mathbf{E}}.$$

**Photo-nematic LCEs.** Suppose that  $\varepsilon_2 \sim \varepsilon_1^{1/2}$  and  $\varepsilon_3 \sim o(\varepsilon_1^{3/2})$ . In this regime, by Eqs. (4.4) and (4.15), we have

$$\begin{aligned} \mathcal{F}^{\text{tot}}[\mathbf{u}, \mathbf{n}, \mathbf{p}] &= \mathcal{F}^{\text{opt}}[\mathbf{n}] + \underbrace{F^{(0,2,0)}[\mathbf{n}]}_{\sim O(\varepsilon_1)} + \underbrace{F^{(2,0,0)}[\mathbf{u}, \mathbf{n}] + F^{(1,2,0)}[\mathbf{u}, \mathbf{n}]}_{\sim O(\varepsilon_1^2)} \\ &+ \underbrace{F^{(0,1,1)}[\mathbf{n}, \mathbf{p}] + F^{(0,0,2)}[\mathbf{n}, \mathbf{p}] + F^{(1,0,2)}[\mathbf{u}, \mathbf{n}, \mathbf{p}] + F^{(1,1,1)}[\mathbf{u}, \mathbf{n}, \mathbf{p}]}_{o(\varepsilon_1^2)}. \end{aligned}$$

Therefore, if the photo-nematic coupling (2.28) is also of order  $O(\varepsilon_1)$ , i.e.,  $\mathbf{m}^{\text{opt}} \sim \varepsilon_1$ , the director and polarization ( $\mathbf{n}, \mathbf{p}$ ) is determined by the dominating  $O(\varepsilon_1)$ -terms:

$$\min_{\mathbf{n}, \mathbf{p}} \left\{ F^{(0,2,0)}[\mathbf{n}] + \mathcal{F}^{\text{opt}}[\mathbf{n}] \right\}, \quad (4.35)$$

implying that (Cf. (4.18))

$$-\operatorname{div}(K_F \nabla \mathbf{n}) + \mathbf{m}^{\text{opt}} + \lambda_n \mathbf{n} = 0 \quad (\text{Balance of director couples}). \quad (4.36)$$

For  $O(\varepsilon_1^2)$ -terms, we have

$$\min_{\mathbf{u}} \left\{ F^{(2,0,0)}[\mathbf{u}, \mathbf{n}] + F^{(1,2,0)}[\mathbf{u}, \mathbf{n}] \right\}, \quad (4.37)$$

implying

$$\operatorname{div}(\boldsymbol{\sigma}^{\text{el-an}} + \boldsymbol{\sigma}^{\text{Frank}} - \lambda_p \mathbf{I}) = 0, \quad \boldsymbol{\sigma}^{\text{el-an}} = \frac{\partial \psi^{\text{el-an}}(\mathbf{E}, \mathbf{n})}{\partial \mathbf{E}}.$$

Finally, we can minimize the remaining lower-order terms over admissible polarization  $\mathbf{p}$  and determine the dielectric response of the body.

**Elasticity-dominating photo-flexoelectric LCEs.** Suppose that  $\varepsilon_1 \gg \varepsilon_2 \sim \varepsilon_3$ . In this regime, we may neglect the Frank elasticity and flexoelectricity for the elasticity problem. Formally, by Eqs. (4.4) and (4.15) we have

$$\begin{aligned} \mathcal{F}^{\text{tot}}[\mathbf{u}, \mathbf{n}, \mathbf{p}] &= \mathcal{F}^{\text{opt}}[\mathbf{n}] + \underbrace{F^{(2,0,0)}[\mathbf{u}, \mathbf{n}] + F^{(0,2,0)}[\mathbf{n}] + F^{(1,2,0)}[\mathbf{u}, \mathbf{n}]}_{\sim O(\varepsilon_1^2)} \\ &\quad + \underbrace{F^{(0,0,2)}[\mathbf{n}, \mathbf{p}] + F^{(0,1,1)}[\mathbf{n}, \mathbf{p}]}_{\sim O(\varepsilon_3^2)} + \underbrace{F^{(1,0,2)}[\mathbf{u}, \mathbf{n}, \mathbf{p}] + F^{(1,1,1)}[\mathbf{u}, \mathbf{n}, \mathbf{p}]}_{\sim O(\varepsilon_3^2)}. \end{aligned}$$

Therefore, if the opto-nematic coupling (2.28) is also of order  $O(\varepsilon_1^2)$ , the displacement and director  $(\mathbf{u}, \mathbf{n})$  is determined by

$$\min_{\mathbf{n}, \mathbf{p}} \left\{ F^{(2,0,0)}[\mathbf{u}, \mathbf{n}] + \mathcal{F}^{\text{opt}}[\mathbf{n}] \right\} \quad (4.38)$$

implying that  $(\boldsymbol{\sigma}^{\text{el-an}} = \frac{\partial \psi^{\text{el-an}}(\mathbf{E}, \mathbf{n})}{\partial \mathbf{E}})$ ,  $\mathbf{m}^{\text{elast}} = \frac{\partial \psi^{\text{el-an}}(\mathbf{E}, \mathbf{n})}{\partial \mathbf{n}} = a_2(\mathbf{I} + 2\mathbf{E})\mathbf{n}$

$$\begin{cases} \operatorname{div}(\boldsymbol{\sigma}^{\text{el-an}} - \lambda_p \mathbf{I}) = 0, & (\text{Balance of linear momentum}), \\ \mathbf{m}^{\text{elast}} + \mathbf{m}^{\text{opt}} + \lambda_n \mathbf{n} = 0 & (\text{Balance of director couples}). \end{cases} \quad (4.39)$$

For  $O(\varepsilon_3^2)$ -terms, we have

$$\min_{\mathbf{p}} \left\{ F^{(0,0,2)}[\mathbf{n}, \mathbf{p}] + F^{(0,1,1)}[\mathbf{n}, \mathbf{p}] \right\}, \quad (4.40)$$

implying the electrostatic problem:

$$\begin{cases} \operatorname{div}(-\varepsilon_0 \nabla \xi + \mathbf{p}) = 0, \\ -\nabla \xi = \mathbf{e}^{\text{flexo}} + \mathbf{e}^{\text{pol}} = -f_s(\operatorname{div} \mathbf{n})\mathbf{n} - f_b(\nabla \mathbf{n})\mathbf{n} + (\mathbb{D}_{\mathbf{n}} - \varepsilon_0 \mathbf{I})^{-1} \mathbf{p}. \end{cases}$$

where the director  $\mathbf{n}$  is determined by the minimization problem (4.38) to the dominating  $O(\varepsilon_1^2)$ -terms.

We remark that there are other scenarios where the Frank elasticity is comparable or dominating the regular elasticity. For brevity, we omit the discussions about these scenarios since the formal calculation of these asymptotic models is quite similar to what we have presented.

## 5. Results and discussion

### 5.1. Bending induced flexoelectric effect in LCEs

In this section, we study bending induced flexoelectricity using an approximate analytical approach. In the current setting, the flexoelectric effect is mediated by the director; strain gradient induces a non-uniform arrangement of nematic director, resulting in a polarization via the flexoelectric effect (Cf. Eq. (2.26)). Several theoretical studies on the bending deformation of LCEs exist in the literature (Corbett et al., 2008; Fu et al., 2016; Lin et al., 2012; Modes et al., 2010; Warner and Mahadevan, 2004; You et al., 2012; Pence, 2006). However, these studies mostly focus on the actuation induced in response to external stimuli (Warner and Mahadevan, 2004; Pence, 2006). There have been little attention paid to the director reorientation in bending deformation of LCEs (Liu et al., 2020; Xu et al., 2020) and there is no study on the bending induced flexoelectric response of the material. Recently, Liu et al. (2021) studied pure bending of LCEs using different constitutive relations and showed that, depending on the constitutive relation, there may be two different solutions for any given bending angle and there is a critical bending angle at which a  $\pi/2$  rotation of nematic director is reported distinguishing one solution from the other. We will use the constitutive relations given in Eqs. (2.9). We will also exploit the asymptotic theories presented earlier to arrive at a close-form solution.

As illustrated in Fig. 4(a), we consider an LCE beam with thickness  $2H$  and the length  $2L$  in the reference configuration. We use Cartesian coordinate system  $\{\mathbf{e}_x, \mathbf{e}_y, \mathbf{e}_z\}$  to denote material points in the reference configuration and cylindrical coordinate system  $\{\mathbf{e}_r, \mathbf{e}_\theta, \mathbf{e}_z\}$  for spatial points in the current configuration. In response to an applied bending moment  $M$ , the LCE undergoes a pure plane strain bending deformation (Cf. Fig. 4) such that any point initially located in the plane with normal  $\mathbf{e}_x$  (resp.  $\mathbf{e}_y$ ) is mapped

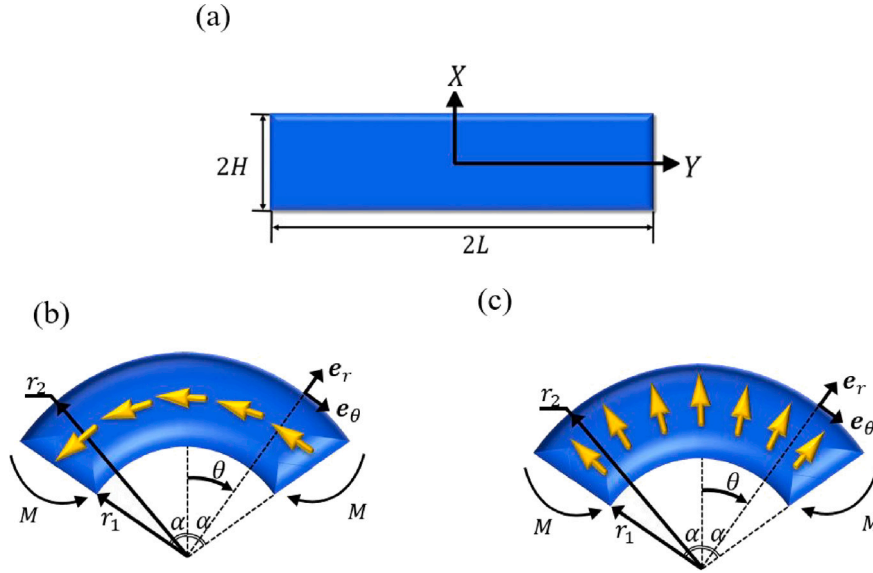


Fig. 4. Schematic of the LCE under bending deformation. The gold arrows show the direction of nematic directors. (a) Undeformed isotropic configuration. (b) Deformed configuration with  $\mathbf{n} = \mathbf{e}_\theta$  (case 1). (c) Deformed configuration with  $\mathbf{n} = \mathbf{e}_r$  (case 2).

to a point located in a plane with normal  $\mathbf{e}_r$  (resp.  $\mathbf{e}_\theta$ ). Suppose that the preferred direction  $\mathbf{N} = \mathbf{e}_X$  in the anisotropic energy (2.6). Assuming the material is incompressible ( $\det \mathbf{F} = 1$ ), we find the deformation and the deformation gradient tensor as Rivlin (1949)

$$r = \sqrt{2AX + B}, \quad \theta = \frac{Y}{A}, \quad (5.1)$$

$$\mathbf{F} = \frac{A}{r} \mathbf{e}_r \otimes \mathbf{e}_X + \frac{r}{A} \mathbf{e}_\theta \otimes \mathbf{e}_Y, \quad (5.2)$$

where  $A$  and  $B$  are unknown constants. We identify  $r_1 = r(X = -H)$ ,  $r_2 = r(X = H)$  and  $\alpha = \theta(Y = L)$  (see Fig. 4). Suppose that the (regular) elasticity dominates the contribution of Frank elasticity, electrical field and photo-flexoelectricity, i.e., the LCE body is in the regime discussed in Remark 2. Therefore, the equilibrium deformation and director field  $(\mathbf{y}, \mathbf{n})$  is dictated by

$$\min_{\mathbf{y}, \mathbf{n}} \left\{ \mathcal{F}^{\text{el-an}}[\mathbf{y}, \mathbf{n}] + \mathcal{P}^{\text{mech}}[\mathbf{y}] \right\}. \quad (5.3)$$

By Eqs. (2.3) and (2.9), first-variation with respect to director  $\mathbf{n}$  yields

$$\mathbf{F}\mathbf{F}^\top \mathbf{n} = \lambda_{\mathbf{n}} \mathbf{n}. \quad (5.4)$$

Substituting Eq. (5.2) into Eq. (5.4), we obtain two solutions for nematic director

$$\begin{cases} \mathbf{n} = \mathbf{e}_\theta & \text{Case 1,} \\ \mathbf{n} = \mathbf{e}_r & \text{Case 2.} \end{cases} \quad (5.5)$$

Throughout this paper, we refer to first solution as *case 1* and the second solution *case 2*. Note that  $\mathbf{N} = \mathbf{e}_X$  and the anisotropy behavior of the material tends to keep nematic directors aligned with the thickness direction. The bending deformation creates strain along the axis of the material (beam) and it may be energetically favorable for the nematic directors to reorient toward axis of the beam. The case 1 (shown in Fig. 4(b)) represents the situation where the nematic directors have rotated toward the axis of the beam while no reorientation is reported according to case 2 (shown in Fig. 4(c)). It is important to note that both solutions represent a uniform arrangement of nematic directors throughout the material. Liu et al. (2021) also obtained similar uniform solutions albeit using different constitutive relations. The reason for this behavior is that non-uniform arrangement of the nematic director induces shear deformation in the material. However, shear deformation is not allowed based on the kinematic constraint used in this work and in the work done of Liu et al. (2021) (see Eq. (5.1)). We will use a finite element model in the next sections in order to obtain more realistic results.

From (5.5), we have

$$\begin{cases} \nabla \mathbf{n} = -\frac{1}{A} \mathbf{e}_r \otimes \mathbf{e}_Y & \text{Case 1,} \\ \nabla \mathbf{n} = \frac{1}{A} \mathbf{e}_\theta \otimes \mathbf{e}_Y & \text{Case 2.} \end{cases} \quad (5.6)$$

Substituting Eqs. (5.5), (5.2) and (5.6) into (2.46), the flexoelectric polarization is obtained as

$$\begin{cases} \mathbf{e}^{\text{flexo}} = -\frac{f_b r}{A^2} \mathbf{e}_r & \text{Case 1,} \\ \mathbf{e}^{\text{flexo}} = -\frac{f_s}{r} \mathbf{e}_r & \text{Case 2.} \end{cases} \quad (5.7)$$

Eq. (5.7) illustrates that the flexoelectric effect predicted in the case 1 is based on  $f_b$ , which is due to bending reorientation of the nematic directors. In contrast, the flexoelectric effect predicted in the case 2 is based on  $f_s$ , which is due to splay reorientation of the nematic directors. We impose open-circuit electrical boundary condition for all the surfaces (i.e.,  $\mathbf{D} \cdot \mathbf{v}_R = 0$ ) and determine the flexoelectric effect generated electric field inside the material by substituting Eq. (5.7) into Eq. (2.54) and

$$\begin{cases} -\nabla \xi = -\frac{f_b(\epsilon_a - 1)}{A\epsilon_a} \mathbf{e}_X & \text{Case 1,} \\ -\nabla \xi = -\frac{A f_s(\epsilon_c - 1)}{r^2 \epsilon_c} \mathbf{e}_X & \text{Case 2.} \end{cases} \quad (5.8)$$

The above solutions show that the electric field generated in the LCE is roughly proportional to flexoelectric coefficient of the material multiplied by the curvature of the material ( $-\nabla \xi \propto f_b \kappa_0$  or  $-\nabla \xi \propto f_s \kappa_0$  where  $\kappa_0$  is the curvature of the material). We have previously shown that a very similar relationship (See D.9 in Rahmati et al., 2019) is obtained for the electric field generated in response to bending deformation of a flexoelectric Euler beam ( $-\nabla \xi \propto f \kappa_0$ , where  $f$  is the flexoelectric coefficient of the flexoelectric Euler beam). LCEs allow larger deformation which bodes well for a stronger flexoelectric effect.

We now determine which of the two solutions (case 1 and case 2) are energetically more favorable. Therefore, we need to fully solve the problem for unknowns  $A$  and  $B$  and then determine the free energy for each case. We introduce  $\Sigma^{\text{tot}}$  as

$$\Sigma^{\text{tot}} = \Sigma^{\text{elast}} + \Sigma^{\text{anis}} = \Sigma_{rX}^{\text{tot}} \mathbf{e}_r \otimes \mathbf{e}_X + \Sigma_{\theta Y}^{\text{tot}} \mathbf{e}_\theta \otimes \mathbf{e}_Y, \quad (5.9)$$

where  $\Sigma_{rX}^{\text{tot}}$  and  $\Sigma_{\theta Y}^{\text{tot}}$  can be obtained substituting Eq. (5.2) into Eqs. (2.39). By Eq. (2.53)<sub>2</sub> we obtain

$$\frac{d}{dX} \left( \Sigma_{rX}^{\text{tot}} - \lambda_p \frac{r}{A} \right) - \frac{1}{A} \left( \Sigma_{\theta Y}^{\text{tot}} - \lambda_p \frac{A}{r} \right) = 0. \quad (5.10)$$

Solving the Eq. (5.10) for the Lagrange multiplier  $\lambda_p$ , we have

$$\begin{cases} \lambda_p = a^{1/3} \frac{A^2}{2r^2} \left( 1 + \frac{\mu_\beta}{a} \right) - a^{-2/3} \frac{r^2}{2A^2} (1 + a\mu_\beta) + C_1 & \text{Case 1,} \\ \lambda_p = a^{-2/3} \frac{A^2}{2r^2} (1 + \mu_\beta) - a^{1/3} \frac{r^2}{2A^2} (1 + \mu_\beta) + C_1 & \text{Case 2,} \end{cases} \quad (5.11)$$

where  $C_1$  is the integration constant and can simply be determined from the free traction boundary condition on the surface  $X = -H$ ,

$$\Sigma_{rX}^{\text{tot}} - \lambda_p \frac{r}{A} \Big|_{X=-H} = 0. \quad (5.12)$$

We identify two unknown constants  $\lambda_b$  and  $\kappa_b$  as

$$\lambda_b = \frac{r_2 - r_1}{2H}, \quad \kappa_b = \frac{r_2 - r_1}{r_1}. \quad (5.13)$$

It is clear that  $\lambda_b$  is a measure for change of the thickness during bending deformation and  $\kappa_b$  is a dimensionless measure for the curvature. The unknowns  $A$  and  $B$  can be expressed in terms of  $\lambda_b$  and  $\kappa_b$  as

$$A = \frac{H \lambda_b^2 (2 + \kappa_b)}{\kappa_b}, \quad B = \frac{2H^2 \lambda_b^2 (2 + \kappa_b (2 + \kappa_b))}{\kappa_b^2} \quad (5.14)$$

The only two unknowns at this point are  $\lambda_b$  and  $\kappa_b$ . The free traction boundary condition on the surface  $X = H$  is used to determine  $\lambda_b$  in terms of  $\kappa_b$ :

$$\begin{cases} \lambda_b^4 = \frac{16(1+a\mu_\beta)(1+\kappa_b)^2}{(2+\kappa_b)^4(a+\mu_\beta)} & \text{Case 1,} \\ \lambda_b^4 = \frac{16a(1+\kappa_b)^2}{(2+\kappa_b)^4} & \text{Case 2.} \end{cases} \quad (5.15)$$

At this point, the only unknown is the dimensionless curvature  $\kappa_b$ . The relationship between the applied bending moment  $M$  and the curvature  $\kappa_b$  can be simply established by using traction boundary condition on the surface  $Y = \pm L$ . We can also determine the relationship between bending angle  $\alpha$  and curvature  $\kappa_b$  from the relation  $A = \frac{L}{\alpha}$  and the first of (5.14). Therefore, all quantities can be written in terms of the bending angle  $\alpha$ .

We now evaluate the total free energy. The difference between energy values between case 1 and case 2 ( $\Delta F = F_{\text{case 1}}^{\text{el-an}} - F_{\text{case 2}}^{\text{el-an}}$ ) is shown in Fig. 5. The negative values of the free energy difference  $\Delta F$  indicates that the case 1 has lower energy and therefore energetically favorable. We note that case 1 is always more favorable regardless of the material or geometrical parameters used. Therefore, within the limitations of our assumptions, bending deformation of the LCE always will lead to a  $\pi/2$  director reorientation. Also, we conclude that the electric field generated in the material is determined from case 1 which is given as  $-\nabla \xi = -f_b(\epsilon_a - 1)/(A\epsilon_a) \mathbf{e}_X$ .

We remark that these theoretical results are based on the assumption that there is no shear deformation in the LCE under bending deformation. Therefore, this model and models like in Liu et al. (2021) will be less accurate if the shear contribution is substantial.

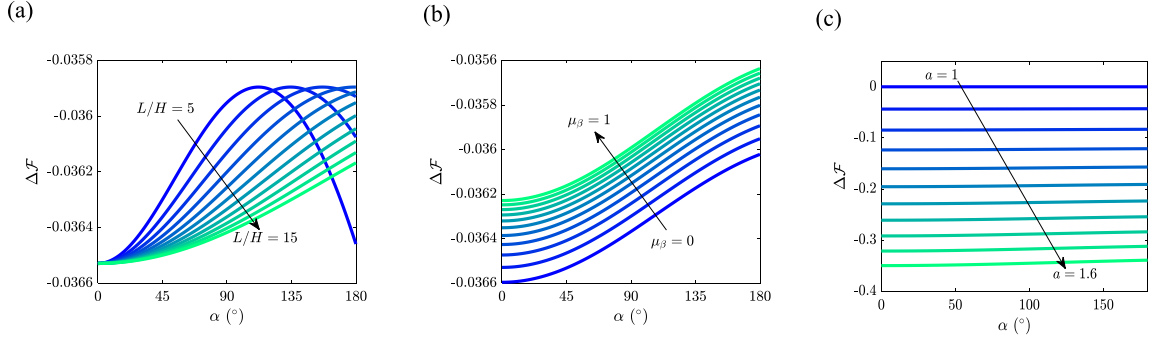


Fig. 5. The difference of free energy obtained using case 1 and case 2 versus bending angle for different (a) aspect ratios  $L/H$ , (b) the material property  $\mu_\beta$  and (c) the material property  $a$ .

## 5.2. Finite element implementation

Given the nonlinear nature of the governing equations and the myriad couplings, except for very simple boundary value problems, a computational approach is necessary. Accordingly, we briefly outline a finite element based procedure in this section that can be used with open source software. As the Eq. (2.51) is linear with respect to polarization and it is easier to express boundary condition in terms of electric potential, we determine polarization in terms of electric potential and will consider electric potential as the unknown field instead of polarization. The weak form of the equations are given as

$$\begin{aligned} \int_{V_R} \nabla w_1 \cdot \tilde{\mathbf{D}} &= 0, \\ \int_{V_R} \nabla w_2 : \left[ \frac{\partial \Psi}{\partial \mathbf{F}} + \Sigma^{MW} - \lambda_p J \mathbf{F}^{-T} \right] &= \int_{S_N} \tilde{\mathbf{t}}_a \cdot \mathbf{w}_2, \\ \int_{V_R} \nabla w_3 : \frac{\partial \Psi}{\partial \nabla \mathbf{n}} + \int_{V_R} \mathbf{w}_3 \cdot \left( \frac{\partial \Psi}{\partial \mathbf{n}} + \lambda_n \mathbf{n} \right) &= 0, \\ \int_{V_R} w_4 \frac{\partial \Psi}{\partial Q} &= 0, \\ \int_{V_R} w_5 (\mathbf{n} \cdot \mathbf{n} - 1) &= 0, \\ \int_{V_R} w_6 (\det \mathbf{F} - 1) &= 0. \end{aligned}$$

where  $(w_1, w_2, w_3, w_4, w_5, w_6)$  are arbitrary test functions. In subsequent section we use open source finite element package FeniCS to solve the above system of equations. We use Taylor-Hood element for the coupled nonlinear problem and employ quadratic interpolation for displacement, and linear interpolation for electric potential, nematic director, order parameter and Lagrange multipliers. A similar setting has been successfully used by Luo and Calderer (2012) to study behavior of LCE materials. We will compare and validate results of our model with the results presented by Luo and Calderer (2012).

## 5.3. Numerical results for photo-flexoelectric LCE bodies

The stretch deformation of a nematic LCE sheet is a well known problem that has been widely investigated experimentally (Küpfert and Finkelmann, 1994; Kundler and Finkelmann, 1995; Küpfert and Finkelmann, 1991) and theoretically (Verwey et al., 1996; Golubović and Lubensky, 1989; Conti et al., 2002; Mbanga et al., 2010). Experimental observation of stress–strain relationship for a clamped nematic LCE sheet under stretch reveals a *semi-soft* behavior. The semi-soft behavior indicates that the stress–strain diagram is composed of three different parts (Kundler and Finkelmann, 1995; Küpfert and Finkelmann, 1991; Conti et al., 2002). Initially, the material shows a relatively stiffer response under small strains in which nematic directors do not rotate. As strain increases, a soft response is observed accompanied by the reorientation nematic directors. Finally, once nematic directors are all aligned along the direction of maximum stretch, another stiff phase ensues. The theoretical prediction based on the model presented by Bladon, Terentjev, and Warner (BTW) (Gurtin et al., 2010) were able to predict formation of stripe domain instability but they were unable to capture the initial hard response. However, Conti et al. (2002) used the free energy presented by Verwey, Warner, and Terentjev (VWT) and successfully captured the formation of stripe domains and semi-soft behavior of LCEs. Luo and Calderer (2012) added Oseen–Frank energy expression to BTW energy and predicted a semi-soft behavior for LCE using a computational approach. Their results did not show formation of stripe domains as they used relatively large Frank elasticity coefficient. In this section, we have used the free energy proposed by DeSimone and Teresi (2009) along with the finite element framework explained earlier to study the flexoelectric behavior of NLCEs under stretch deformation. We also have included effects of Frank elasticity

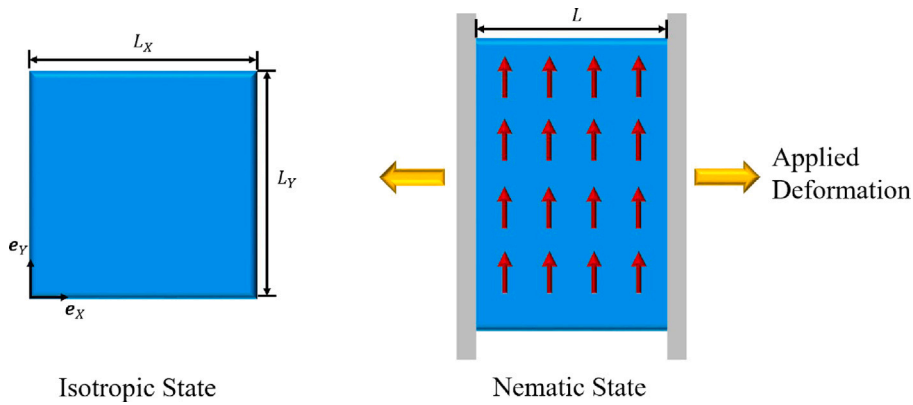


Fig. 6. Schematic of the simulated specimen in clamp pulling numerical experiment. The system is relaxed to a nematic state and then the boundary conditions are applied.

since both the latter and flexoelectricity are dominant at similar (smaller) length scales. We do not perform stability analysis and we do not report formation of stripe domain instabilities. We believe at small scales, Frank elasticity terms penalizes rotation of nematic directors and prevents creation of stripe domains. Also, even if stripe domains form, they are less germane to the goals of our current work.

Fig. 6 shows the schematic of the two dimensional sample simulated. In the reference state, the sample is in the isotropic state where the deformation is zero in the entire sample. After energy minimization in the initial state and in absence of any external loading, the sample is transformed into nematic state where all nematic directors are aligned along one random direction. Without loss of generality, we have chosen Y-direction as this direction (Fig. 6). In the next step and in order to simulate the clamp pulling experiment, we have constrained the deformation along Y-direction and the direction of nematic director on both vertical surfaces of the specimen to stay the same as the values observed in the nematic state and in the absence of any external loading on both vertical surfaces of the specimen. We then pull the specimen from both left and right end by applying uniform deformation  $\Delta L$  along X-direction.

### 5.3.1. Validation of FEA code

To validate our finite element code, and compare with the existing literature, we set electrical terms to zero and assume  $a_1 = 1$  and  $a_2 = -0.4$  in Eq. (2.11). Also, we set  $\bar{\mu}_\beta = 0$ ,  $\bar{\mu} = 2$ ,  $\bar{K}_F = 0.03$ . The simulated specimen has the dimensions of  $L_X = 1/\sqrt{0.5}$  and  $L_Y = 1$  (see Fig. 6). By doing so, our model reduces to the one presented in Luo and Calderer (2012). Due to symmetry we only simulate the upper right quarter of the figure and impose the same boundary conditions as in Luo and Calderer (2012). Fig. 7 shows our results and the results presented in Luo and Calderer (2012) for the deformed configurations of LCE under different strain along with the direction of nematic directors and the contours of BTW energy. It is seen that our results exactly match the ones presented by Luo and Calderer (2012).

### 5.3.2. Size effect on the semi-soft response of the material

We also investigate the effect of the Frank elasticity on the stress-strain behavior of NLCE. The stress-strain diagram for different values of  $\bar{K}_F$  has been plotted in Fig. 8 where stress values plotted is the average normal stress along X direction and we have set  $\bar{\mu}_\beta = 0.5$ . Our results are able to capture semi-soft behavior of the material. As expected, increase in the  $\bar{K}_F$  penalizes rotation of nematic director and delays the soft behavior of the material. Although the Frank elasticity coefficient  $K_F$  is itself a material property and is constant,  $\bar{K}_F$  changes with size. This graph shows that stress strain response of the LCE is indeed size-dependent.

### 5.3.3. Flexoelectric response of a LCE sheet under uni-axial stretch

As shown earlier, the rotation of nematic directors is observed in the clamp-pulling experiment. As flexoelectric behavior of LCEs depends on the rotation of director, we expect observation of a flexoelectric effect under clamp-pulling experiment of LCE at small enough size scale. Therefore, in the following, we “turn on” the effects of electrical terms by setting  $\bar{\epsilon}_a = 2.26$ ,  $\bar{\epsilon}_s = 4.52$ ,  $\bar{f}_b = 0.001$  and  $\bar{f}_s = 0.002$ . We will comment later on the values of flexoelectric coefficient but the magnitude of these values will not impact our qualitative conclusion in this section. The film is under open circuit condition ( $\bar{\mathbf{D}} \cdot \mathbf{N} = 0$ ) on all surfaces. Without loss of generality, we set electric potential on the point  $(L_X/2, 0)$  to zero in order to ease numerical convergence. Fig. 9 shows the contours of dimensionless electric potential plotted in the deformed configuration for different values of applied deformation. Also, the direction of nematic directors are depicted with black arrows. In the earlier stages of deformation, the rotation of nematic directors is negligible and generated electric potential due to the flexoelectric effect is also negligible. As strain increases, the gradient of nematic director field becomes larger and an electric potential difference becomes evident along the specimen. However, the electric potential difference is symmetric during all steps of loading. Our calculation show the volume average of dimensionless electric field in both X and Y directions remains zero at all steps of loading. From this, we can conclude that the flexoelectric effect may be present in the clamp-pulling experiment if conducted at small length scales. However, it will not be easily measurable as the average electric field is zero.

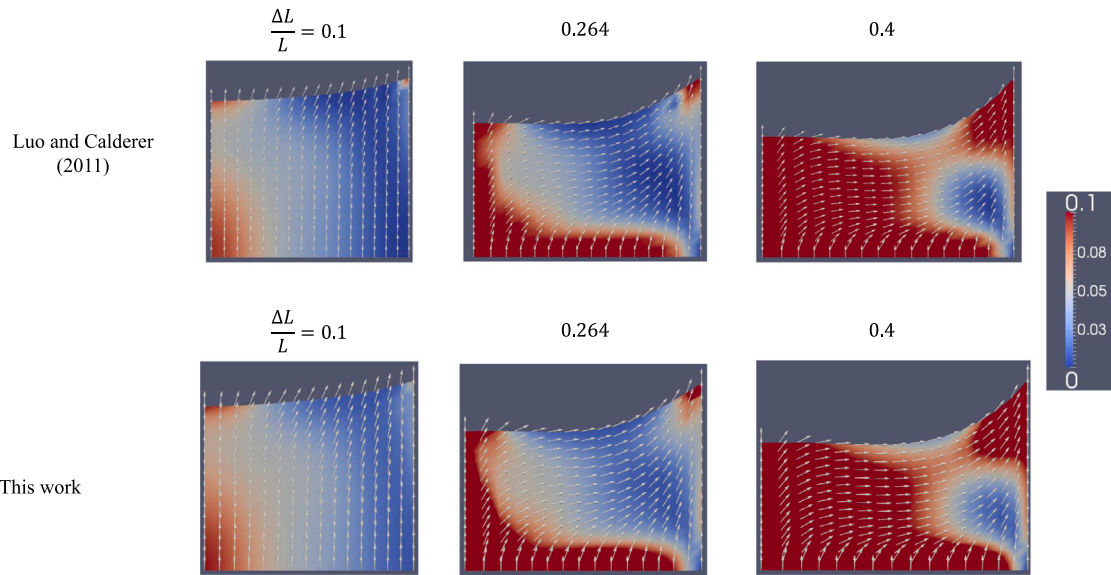


Fig. 7. Comparison of BTW energy contours, deformation and direction of nematic director between current study and the FEA results presented by Luo and Calderer (2012).

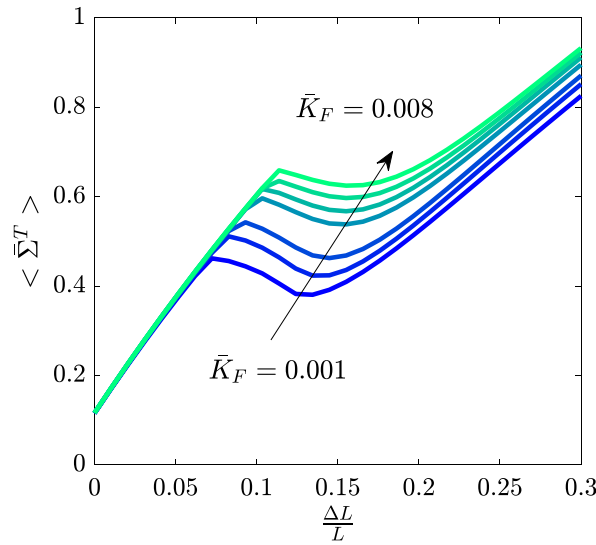


Fig. 8. The effect of the Frank elasticity coefficient on the semi-soft behavior of the LCE under clamp-pulling deformation.

#### 5.4. Finite element results for the flexoelectric effect in bending deformation of LCEs

Since the flexoelectric effect in LCEs is result of a non-zero gradient of nematic director fields and bending is arguably the simplest way to create non-uniform deformation and consequently non-zero gradient of nematic director field, we investigate flexoture deformation in this section. Photo-induced bending deformation of NLCEs have been widely studied. However, almost all these studies do not include director field reorientation in bending deformation. In addition, plate theories have been developed for NLCEs (Liu et al., 2020; Mihai and Goriely, 2020; Agostiniani and DeSimone, 2020) that can be used to study bending deformation of LCEs. However, as these models average out variations along the thickness directions, they are not suitable for studying the flexoelectric effect under bending deformation. We have used the free energy proposed by DeSimone and Teresi (2009) by setting  $a_1 = a^{1/3}$  and  $a_2 = -a^{1/3} \frac{a-1}{a}$ . Unless other wise stated we have assumed  $a = 1.05$ ,  $\mu = 30$  KPa,  $K_F = 10^{-11}$  J/m,  $\epsilon_a = 2.26$ ,  $\epsilon_c = 4.52$  and  $\mu_\beta = 0.1\mu$ . The size scale is set to be  $H = 10^{-6}$  m. As discussed earlier, the maximum value of the flexoelectric coefficient depends on the value of Frank elasticity term. The order of flexoelectric coefficient for LCEs is expected to be in the order of  $1/\epsilon_0$  pC/m (Rajapaksha et al., 2021). Therefore, we have set  $f_b \epsilon_0 = f_s \epsilon_0 = 1$  pC/N. We also identify volume average sign as  $\langle \cdot \rangle = \frac{1}{V} \int_V \cdot$

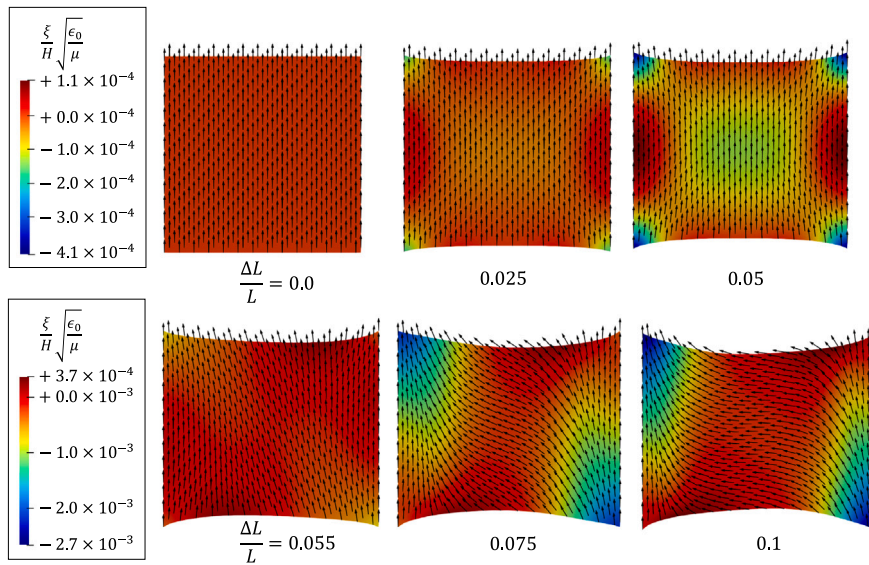


Fig. 9. Contours of the dimensionless electric potential in the deformed configuration under different stretch values. The black arrows show the direction of the nematic directors.

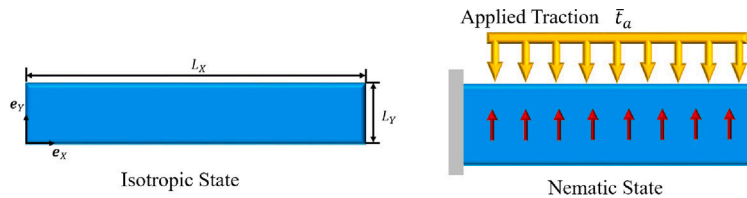


Fig. 10. The schematic of the simulated sample. We apply boundary conditions in the nematic state.

which will be used in this section to plot average electric field and average polarization generated in the material in response to bending.

The schematic of simulated sample is shown in Fig. 10. Similar to the stretch simulation, we apply boundary conditions on the material in the nematic state. We assume  $N_a = e_y$  and let the system relax from isotropic state to nematic state and then we constrain deformation and nematic director direction on the left side of the material (see Fig. 10). In order to create bending deformation, a dimensionless traction  $\bar{t}_a = -\bar{t}_a e_y$  is applied on the top surface of the material.

#### 5.4.1. Bending and splay flexoelectric effect

Two types of rotation of the nematic directors have been considered in the flexoelectric formulation: bending rotation characterized by  $f_b$  and splay rotation characterized by  $f_s$ . We remark that we must distinguish between the bending rotation of the nematic directors and the bending deformation of material itself. Here, we have used the same sign for both effects and we have used the same positive values for the both in order to ease the interpretation of the underlying physics behind the flexoelectric effect in LCEs. Our results show that both bending and splay rotations may occur under bending deformation.

Fig. 11 shows the average dimensionless electric field versus applied traction in presence and absence of each one of bending or splay flexoelectric effects. We observe that the average electric field along  $X$  direction is not negligible compare to average electric field generated along  $Y$  direction, specially under small loading ( $\bar{t}_a < 0.1$ ) where the major flexoelectric effect observed is an electric field generated along axis direction ( $X$  direction). This electric field is the result of bending rotation of nematic directors ( $f_b$  flexoelectric effect). We also see that (Cf. Fig. 11(a))  $f_b$  flexoelectric effect will lead to the generation of average electric field with positive value along the axis direction of the material ( $X$  direction) for all stages of loading while  $f_s$  flexoelectric effect generates negative electric field along the  $X$  direction. Therefore, there is a competition between these two effects. The  $f_b$  flexoelectric effect is dominant under small deformation and the  $f_s$  flexoelectric effect takes over for large deformations. Accordingly, Fig. 11(a) shows that, in presence of both  $f_b$  and  $f_s$  effects, as loading increases, the average electric field in  $X$  direction increases and peaks at a positive value and finally becomes increasingly negative. However, Fig. 11(b) shows both  $f_b$  and  $f_s$  effect will lead to a positive electric field along the thickness direction and these two effects intensify each other and the electric field in  $Y$  direction always increases as loading increases. It is important to note that we have assumed positive values for both  $f_b$  and  $f_s$ . If these two coefficients had opposite signs, we would see competition along  $Y$  direction instead of  $X$  direction.

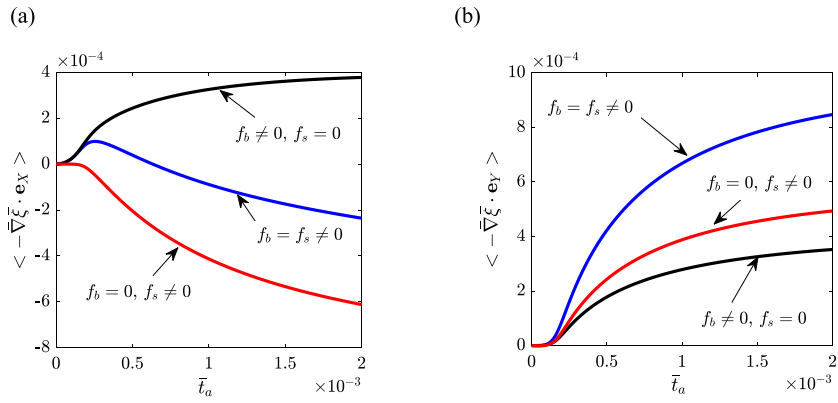


Fig. 11. Average dimensionless electric field along X (a) and Y (b) directions versus applied traction in presence and absence of bending and splay flexoelectric effects.

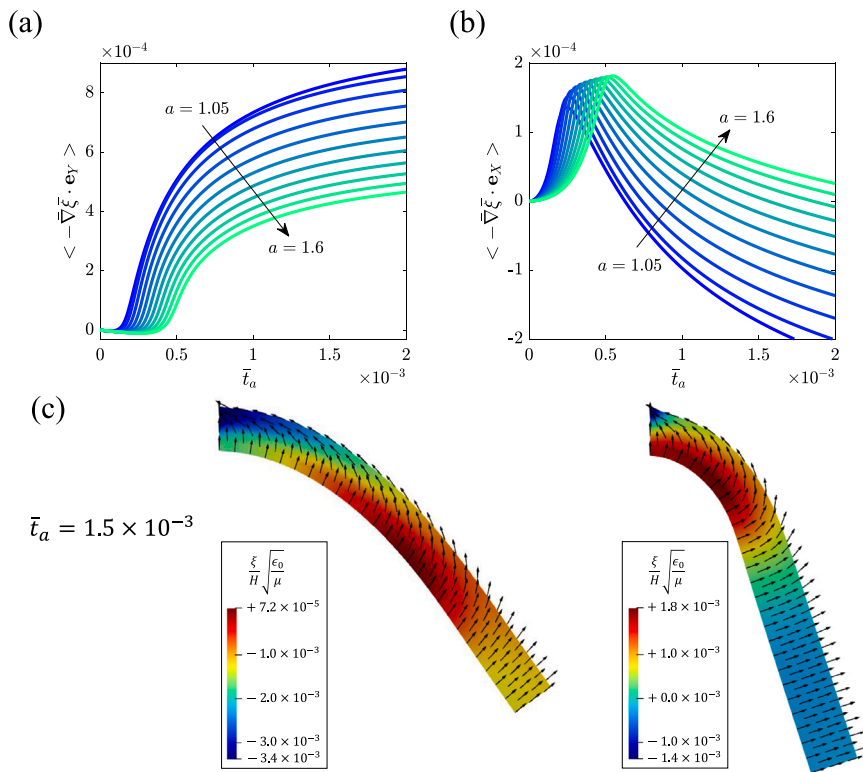
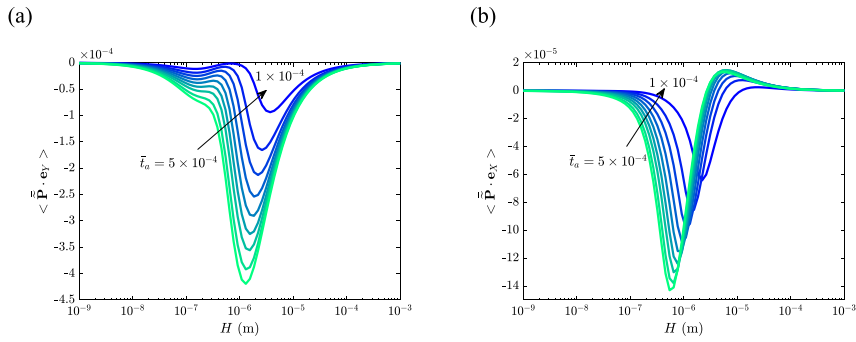


Fig. 12. Electric potential and average electric field generated in the material under bending deformation. (a) Average electric field in Y direction versus applied traction for different values of material parameter  $a$ . (b) Average electric field in X direction versus applied traction for different values of material parameter  $a$ . (c) Contours of dimensionless electric potential for two different materials one with  $a = 1.05$  shown on the left side and one with  $a = 1.6$  shown on the right side ( $\bar{t}_a = 1.5 \times 10^{-3}$  for both). Black arrows show the direction of nematic directors.

5.4.2. The effect of material parameter  $a$  in flexoelectric effect

Fig. 12 illustrates the effect of material parameter  $a$  on the bending induced flexoelectric behavior of the material. The magnitude of the material parameter  $a$  determines the magnitude of strain induced in the material as a result of alignment or rotation of nematic directors. For prolate nematic elastomers,  $a$  is always greater than one. Under small strain assumption, the magnitude of  $a$  is close to 1 while it could be larger for large deformations. DeSimone and coworkers used value of 1.05 in the DeSimone et al. (2007) and value of 1.88 in the Arroyo and DeSimone (2014).

Here, we have plotted average electric field along X and Y directions in Fig. 12(a) and 12(b) for values of  $a$  from 1.05 to 1.6. It is seen that as this material parameter increases, the flexoelectric effect becomes weaker. The reason for this behavior may be discerned from Fig. 12(c) where contours of dimensionless electric potential and direction of nematic directors has been plotted on



**Fig. 13.** Size effect in bending deformation induced flexoelectric effect. (a) Average polarization field along  $X$  direction versus characteristic length for materials under different magnitude of loading. (b) Average polarization field along  $Y$  direction versus characteristic length for materials under different magnitude of loading.

the deformed configuration of two materials one with  $a = 1.05$  (left) and one with  $a = 1.6$  (right), both under the same bending load. In order to interpret these figures we should note that the nematic directors tend to rotate toward the principal stretch direction in order to reduce elastic part of free energy  $W^{\text{elast}}$ . However, there are two factors which tend to avoid rotation of nematic director. The first factor is related to bending deformation of the material. Under bending deformation, the principal stretch direction is perpendicular to the thickness direction both above and below the neutral axis. The rotation of nematic director toward the principal stretch direction creates tension while external load tend to compress material points below the neutral axis. Therefore, external load opposes rotation of nematic director in the areas below the neutral axis which is under compression. This explains the reason that, for the points located near surface  $Y = 0$  in the deformed configuration, nematic directors have remained more or less parallel to the thickness in Fig. 12(c). The second factor is the anisotropic part of energy  $W^{\text{anisotropy}}$  which is minimized if nematic directors are parallel to the thickness direction of the material. The  $W^{\text{elast}}$  energy reduction induced due to rotation of nematic directors should overcome energy increase in  $W^{\text{anisotropy}}$  in order to observe rotation of nematic directors with respect to material points. This energy barrier against rotation is larger if the material parameter  $a$  is larger. Therefore, the flexoelectric effect is weaker in the materials with larger  $a$ . It is worthwhile to note that  $W^{\text{anisotropy}}$  will not restrict rotation of material points itself. Therefore, it does not restrict nematic director gradient induced as a result of rotation of material points. It means that it does not restrict the  $f_b$  flexoelectric effect while it will adversely impact the  $f_s$  flexoelectric effect. This is consistent with the behavior observed in Fig. 12(b) where it is seen that for the material with small values of  $a$ , the average electric field in X direction is negative while the opposite is true for the material with large  $a$ . This shows that increase in the value of the material parameter  $a$  may alter the flexoelectric mechanism from splay induced flexoelectric effect to bending induced flexoelectric effect in LCEs.

#### 5.4.3. Size effect in bending

Flexoelectricity in solids is often considerable at small nanosize scales while this effect is negligible at larger size scales (Krichen and Sharma, 2016; Ahmadpoor and Sharma, 2015). Here, we focus on this aspect in the context of flexure. The average polarization along X and Y directions versus characteristic length of the material has been plotted in Fig. 13(a) and Fig. 13(b), respectively. Both figures show a similar (and expected) trend where the flexoelectric effect is negligible at large size scales. As the characteristic length becomes smaller, the polarization increases and the flexoelectric effect reaches a maximum at around characteristic length  $H \approx 10^{-6}$ . The exact characteristic length in which bending deformation induced polarization reaches its maximum depends on the value of applied traction (Fig. 13).

Our observation can be reconciled by noting that the flexoelectric effect is linearly proportional to the inverse of characteristic length and the effect of Frank elasticity is quadratically proportional to the inverse of characteristic length. At very small size scales, Frank elasticity term becomes a major constraint which tends to keep nematic directors uniform and impedes the flexoelectric effect. To better illustrate this competition, consider Fig. 14 where the contours of dimensionless electric field and direction of nematic directors have been plotted in the deformed configuration of three materials at three different size scales. The applied dimensionless loading is the same across these three materials. For  $H = 10^{-3}$  m, the flexoelectric effect is substantively absent and the electric potential is zero everywhere. Both flexoelectric effect and the Frank elasticity effect are negligible at this large size scale. As size scale goes smaller to  $H = 10^{-6}$  m, an electric potential difference is observed across the material. For size scale  $H = 10^{-6}$  m, no gradient in the nematic field is reported. This is because the Frank elasticity effect is so dominant as to penalize any gradient in the nematic director field. Therefore, no flexoelectric effect is suppressed.

#### 5.5. Finite element results for photo-flexoelectric effect in NLCEs

It is well known that nematic LCEs containing azobenzene molecules can exhibit a large reversible photo induced strain (Finkelmann et al., 2001). Light illumination of a photo responsive LCE can lead to two kind of deformation. The first is the photo-induced phase transition and the second is the photo-induced reorientation of nematic directors (Pang et al., 2019). Photo-induced phase transition is due to absorption of photons by azobenzene molecules which lead to trans-cis photoisomerization, the

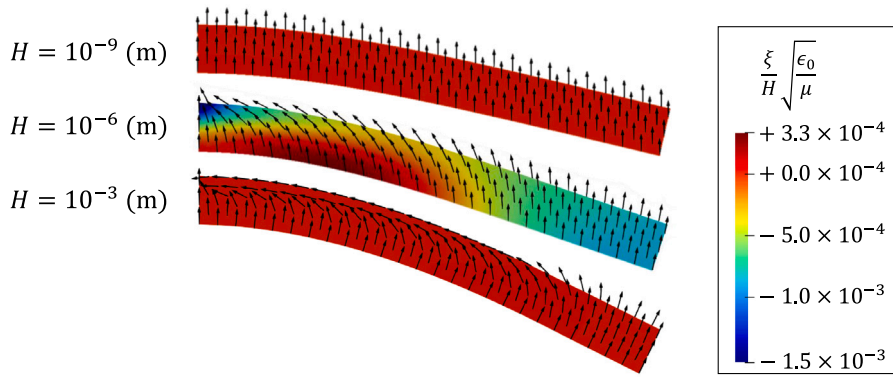


Fig. 14. Contours of the dimensionless electric field and directions of nematic director for three materials at three different size scale.

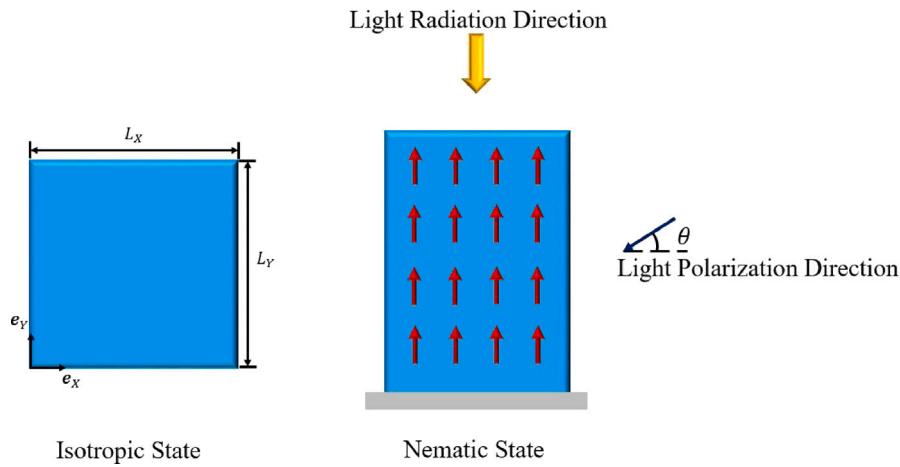


Fig. 15. Schematic of the specimen simulated for photo-flexoelectric analysis. The boundary conditions are applied in the nematic state.

disturbance of the orientational order and transformation of the material from nematic to isotropic state (Warner and Terentjev, 2007). The light induced reorientation effect, also known as the Weigert Effect (Weigert, 1919), is a result of repeated trans-cis-trans isomerization cycles in response to polarized light irradiation (Ube and Ikeda, 2014). Although experimental studies have studied photo-induced reorientation in nematic liquid crystal polymers (Hrozhyk et al., 2009; White et al., 2009; Luo et al., 2021), most theoretical studies have not considered light polarization direction dependent light induced reorientation effects (Jin et al., 2010; Warner and Mahadevan, 2004; Zhang and Huo, 2018; Warner et al., 2010; Lin et al., 2012; Corbett and Warner, 2007; You et al., 2012). Recently, Bai and Bhattacharya (2020), using the free energy developed by Corbett and Warner (2006), studied photomechanical coupling in a photoactive LCE under both light illumination and mechanical stress. They studied the effect of light polarization direction on the reorientation of nematic directors. Here, we have used the same free-energy and coupled it with electricity to study light induced flexoelectric effect.

In what follows, unless other wise stated, we have assumed  $a = 1.05$ ,  $\mu = 30$  KPa,  $K_F = 10^{-11}$  J/m,  $\epsilon_a = 2.26$ ,  $\epsilon_c = 4.52$ ,  $f_b \epsilon_0 = f_s \epsilon_0 = 1$  pC/N and  $\mu_\beta = \mu$ . The size scale is set to be  $H = 10^{-6}$  m. We further assume  $\bar{J}_n = 5$ ,  $f = \frac{1}{6}$  and  $\mu_n = 20\mu$ . For simplicity, we assume light intensity in the material is obtained using so-called Beer-Lambert law as follows

$$I = I_0 \exp\left(-\frac{X_2 - H}{d_p}\right). \quad (5.16)$$

In order to facilitate interpretation of results, we assume  $d_p = 0.1H$ . We also set  $I_0 = 0.5$ . It should be mentioned that the exact profile of the light and light intensity in each position in the material depends on the texture of the material. The polarization direction of light beam can be modified using a polarizer. Also, penetration depth of the material can be modified by addition of scattering particles such as microspheres (Firbank et al., 1995) or intralipid fat (Flock et al., 1992), or absorbing particles such as black ink in the solution of the material. Detailed description of manufacturing process of the material is beyond the scope of current work.

Similar to our discussion for the stretch and bending simulations, we set boundary conditions on the nematic state. Assuming  $\mathbf{N} = \mathbf{e}_y$ , we relax the system and then constrain the deformation and nematic directors on the bottom surface (Fig. 15).

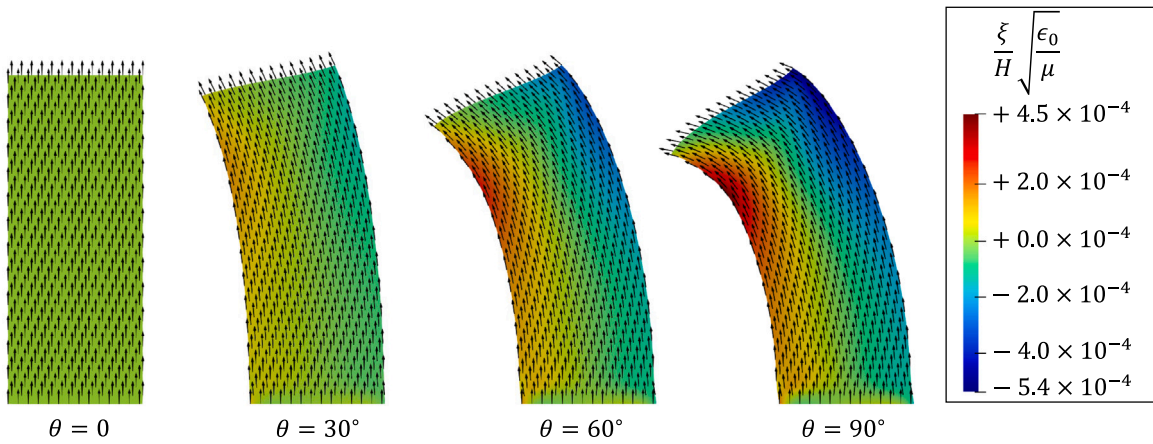


Fig. 16. Contours of dimensionless electric potential for material under polarized light irradiation with different polarization directions. The black arrows show the direction of nematic directors.

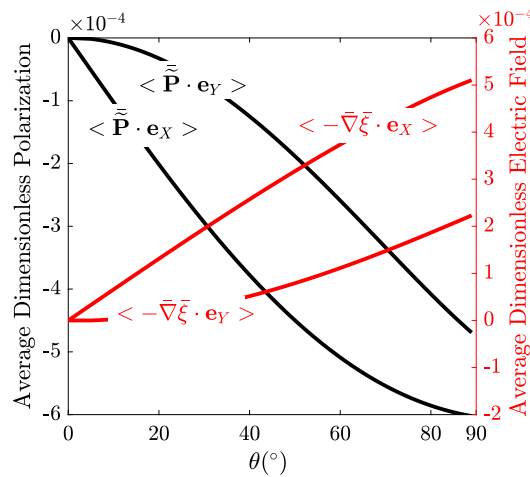


Fig. 17. Average dimensionless polarization and electric field induced in the material as result of polarized light irradiation with different polarization directions.

5.5.1. Effect of polarization direction of light on photo-flexoelectric effect

The contours of dimensionless electric potential along with direction of nematic directors are plotted in Fig. 16 for material under light with different polarization directions. We identify polarization direction of the material with  $\theta$ . Initially, we have set  $\theta = 0$ . As nematic directors tend to remain perpendicular to the polarization direction, no deformation and flexoelectric effect is observed in that case. We gradually increase  $\theta$  with step size of one degree and with that observe a reorientation of nematic directors. Fig. 16 shows that as  $\theta$  increases, the reorientation of nematic directors increases and as a result the flexoelectric effect becomes stronger and deformation becomes larger. The maximum director reorientation is reported in the region of the material which is close to light-facing surface (and thus is exposed to higher light intensity).

Average dimensionless polarization and dimensionless electric field versus light polarization direction in both  $X$  and  $Y$  directions are plotted in Fig. 17. Fig. 17 also shows that flexoelectric effect becomes stronger as  $\theta$  increases. Notably, light induced electric field and polarization is not negligible in  $X$  or  $Y$  directions. Moreover, this figure shows the electric field generated in the material in response to light-generated bending deformation, has the order of magnitude of 1. This is at least three order of magnitude greater than what could be predicted using the relationships given in Eq. (5.15) by the simplified analytical model. This signifies the importance on nonlinear effects due to large deformation of LCEs which could intensify flexoelectric response of the material up to several orders of magnitude. This means that although flexoelectric coefficient of LCEs are small compare to conventional solid dielectrics, nonlinear deformation of LCEs can significantly impact their flexoelectric response.

5.5.2. Effect of the material aspect ratio

The effect of materials aspect ratio on the light induced deformation along with distribution of order parameter  $Q$  is shown in Fig. 18 where aspect ratio is defined as  $\frac{L_x}{L_y}$  (see Fig. 15). Fig. 18 shows that the light induced deformation in materials with

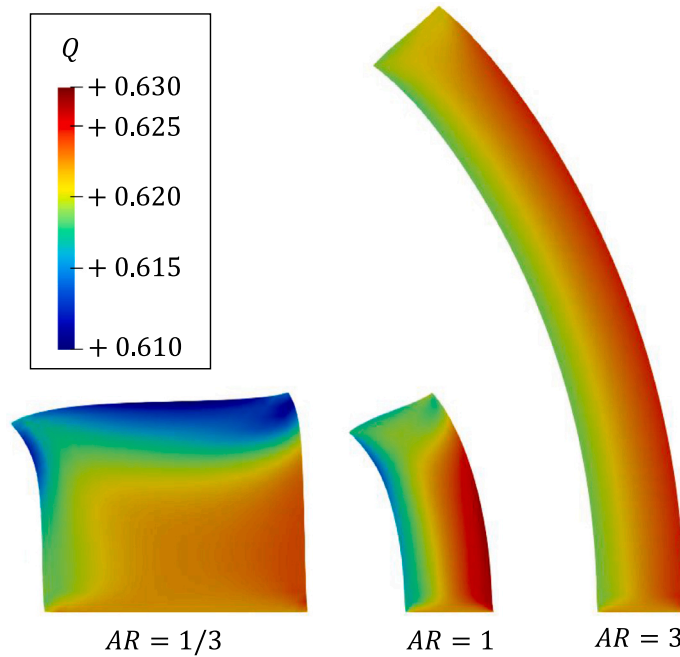


Fig. 18. Contours of order parameter  $Q$  for material with different aspect ratio (AR) under polarized light with  $\theta = \pi/4$ .

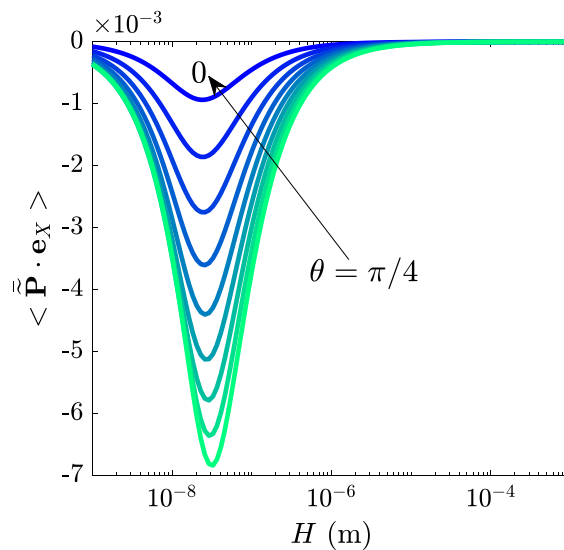


Fig. 19. Average dimensionless polarization along the  $X$  direction versus characteristic length of the material for photoactive LCE under light irradiation with different polarization directions.

smaller AR is shear-deformation dominated with flexure being more relevant for larger ARs. Also, contours of order parameter show that the variation of order parameter in the material is small and thus not closer to the transformation to isotropic phase, where  $Q = 0$ . This is because light intensity used in this section has been deliberately chosen to be small to avoid phase transition.

### 5.5.3. Size effect in photo-flexoelectric behavior of the material

The size effect in light induced flexoelectric effect in LCEs is studied in Figs. 19 and 20. Fig. 19 shows that at larger size scales, photo-flexoelectric effect is negligible. As size scale decreases, the light induced polarization increases until it peaks at size scale close to  $5 \times 10^{-8}$  and then again it decreases with further reduction in the value of size scale. This trend is similar to that for bending induced flexoelectric effect. Fig. 19 shows that for size scale  $H = 10^{-3}$  light induced rotation of nematic directors do not lead to any flexoelectric effect. Also, Fig. 19 shows that for smaller size scales of  $H = 10^{-6}$  and  $H = 5 \times 10^{-6}$ , the distribution of nematic

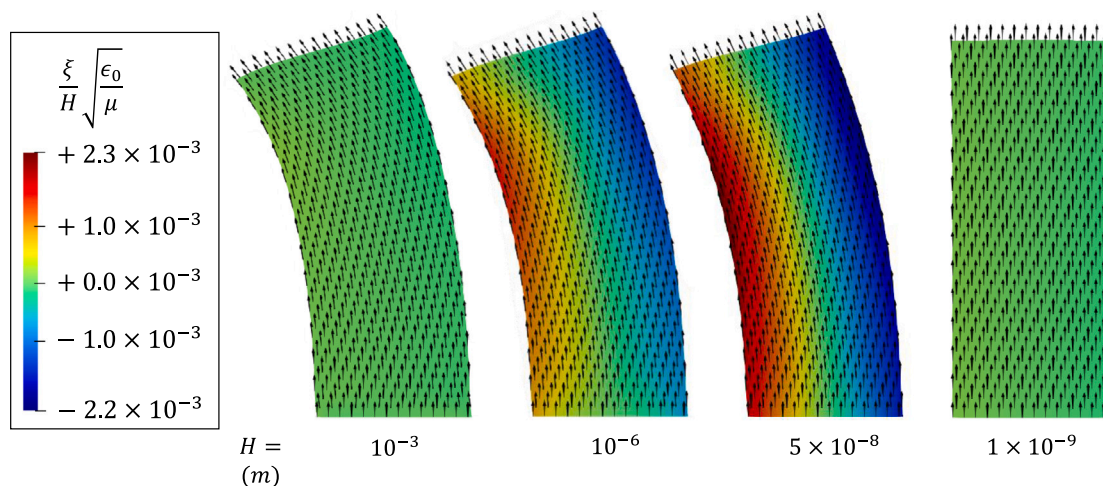


Fig. 20. Contours of dimensionless electric potential for materials with different characteristic length under polarized light with  $\theta = \pi/4$ .

director is similar to the distribution observed at the size scale  $H = 10^{-3}$  but flexoelectric effect is larger because the gradient of nematic director is larger at this size scale. However, Fig. 19 shows that there is no nematic director gradient due to the dominance of Frank elasticity.

## 6. Concluding remarks

Our developed theoretical and computational framework for photo-flexoelectricity represents a first attempt to systematically study the possibility of flexoelectricity-mediated direct conversion of light into electricity in liquid crystal elastomers. While the effect is certainly modest, it is nevertheless an exciting option to explore for wireless sensors and actuators. In particular, we expect efforts that could increase the light-electricity coupling to be an important future direction in the burgeoning field of architected and meta materials. The optical-electrical coupling could be potentially increased by several strategies including design of polymer chains at the microscopic scale (Grasinger et al., 2021; Khandagale et al., 2024; Grasinger and Dayal, 2021) and/or use of electret ideas (Liu and Sharma, 2018). Another possibility is the use of liquid inclusions that retain softness of the overall material but may provide a route to engineering further electromechanical coupling through capillary effects and use of ionic liquids (Krichen et al., 2019; Style et al., 2015b,a; Mathur et al., 2005). Instabilities triggered in the context of photo-flexoelectricity could also be a relevant field of study since the underlying materials are quite soft (Yang and Sharma, 2023). Finally, in recent works, using hard magnetics in soft matter have been used to implement another kind of modality for wireless actuation (Kim et al., 2018). Building on these works, magnetoelectric effect has also been designed in elastomers (Rahmati et al., 2023). The addition of magnetic order to LCEs may yet prove to be another mechanism to engineer an all-wireless magneto-electro-optical coupling.

## CRedit authorship contribution statement

**Amir Hossein Rahmati:** Writing – original draft, Methodology, Investigation, Formal analysis. **Kosar Mozaffari:** Formal analysis. **Liping Liu:** Writing – review & editing, Writing – original draft, Supervision, Methodology, Investigation, Formal analysis, Conceptualization. **Pradeep Sharma:** Writing – review & editing, Writing – original draft, Supervision, Resources, Project administration, Methodology, Investigation, Funding acquisition, Formal analysis, Conceptualization.

## Declaration of competing interest

The authors declare that they have no known competing financial interests or personal relationships that could have appeared to influence the work reported in this paper.

## Acknowledgments

L.L. gratefully acknowledges the support of National Science Foundation, USA DMS-2306254 and Simons travel grant. P.S. gratefully acknowledges the support of the Hugh Roy and Lillie Cranz Cullen Distinguished University Chair from the University of Houston, USA.

## Data availability

Data will be made available on request.

## References

- Abdollahi, A., Peco, C., Millán, D., Arroyo, M., Catalan, G., Arias, I., 2015. Fracture toughening and toughness asymmetry induced by flexoelectricity. *Phys. Rev. B* 92 (9), 094101.
- Acharya, A., Dayal, K., 2014. Continuum mechanics of line defects in liquid crystals and liquid crystal elastomers. *Quart. Appl. Math.* 72 (1), 33–64.
- Adler, J.H., Atherton, T.J., Benson, T.R., Emerson, D., MacLachlan, S.P., 2015. Energy minimization for liquid crystal equilibrium with electric and flexoelectric effects. *SIAM J. Sci. Comput.* 37 (5), S157–S176.
- Agostiniani, V., DeSimone, A., 2012. Ogden-type energies for nematic elastomers. *Int. J. Non-Linear Mech.* 47 (2), 402–412.
- Agostiniani, V., DeSimone, A., 2020. Rigorous derivation of active plate models for thin sheets of nematic elastomers. *Math. Mech. Solids* 25 (10), 1804–1830.
- Ahmadpoor, F., Sharma, P., 2015. Flexoelectricity in two-dimensional crystalline and biological membranes. *Nanoscale* 7 (40), 16555–16570.
- Anderson, D.R., Carlson, D.E., Fried, E., 1999. A continuum-mechanical theory for nematic elastomers. *J. Elasticity* 56 (1), 33–58.
- Annapoornan, R., Wang, Y., Cai, S., 2023. Harnessing soft elasticity of liquid crystal elastomers to achieve low voltage driven actuation. *Adv. Mater. Technol.* 8 (9), 2201969.
- Arroyo, M., DeSimone, A., 2014. Shape control of active surfaces inspired by the movement of euglenids. *J. Mech. Phys. Solids* 62, 99–112.
- Babaei, M., Gao, J., Clement, A., Dayal, K., Shankar, M.R., 2021. Torque-dense photomechanical actuation. *Soft Matter* 17 (5), 1258–1266.
- Bai, R., Bhattacharya, K., 2020. Photomechanical coupling in photoactive nematic elastomers. *J. Mech. Phys. Solids* 144, 104115.
- Bhaskar, U.K., Banerjee, N., Abdollahi, A., Solanas, E., Rijnders, G., Catalan, G., 2016. Flexoelectric MEMS: towards an electromechanical strain diode. *Nanoscale* 8 (3), 1293–1298.
- Biggins, J., Warner, M., Bhattacharya, K., 2012. Elasticity of polydomain liquid crystal elastomers. *J. Mech. Phys. Solids* 60 (4), 573–590.
- Bisoyi, H.K., Urbas, A.M., Li, Q., 2019. Soft materials driven by photothermal effect and their applications. *Photoactive Functional Soft Materials: Preparation, Properties, and Applications*. Wiley Online Library, pp. 1–44.
- Bladon, P., Terentjev, E., Warner, M., 1993. Transitions and instabilities in liquid crystal elastomers. *Phys. Rev. E* 47 (6), R3838.
- Bladon, P., Terentjev, E.M., Warner, M., 1994. Deformation-induced orientational transitions in liquid crystals elastomer. *J. Phys. II* 4 (1), 75–91.
- Brand, H.R., Pleiner, H., 1994. Electrohydrodynamics of nematic liquid crystalline elastomers. *Phys. A* 208 (3–4), 359–372.
- Brannum, M.T., Steele, A.M., Venetos, M.C., Korley, L.T., Wnek, G.E., White, T.J., 2019. Light control with liquid crystalline elastomers. *Adv. Opt. Mater.* 7 (6), 1801683.
- Breneman, K.D., Brownell, W.E., Rabbitt, R.D., 2009. Hair cell bundles: flexoelectric motors of the inner ear. *PLoS One* 4 (4), e5201.
- Brighenti, R., McMahan, C.G., Cosma, M.P., Kotikian, A., Lewis, J.A., Daraio, C., 2021. A micromechanical-based model of stimulus responsive liquid crystal elastomers. *Int. J. Solids Struct.* 219, 92–105.
- Buka, A., Éber, N., 2013. Flexoelectricity in Liquid Crystals: Theory, Experiments and Applications. World Scientific.
- Calleja, R.D., Díaz-Boñis, P., Llovera-Segovia, P., Quijano, A., 2014. On the nonlinear behaviour of nematic single crystal elastomers under biaxial mechanic and electrical force fields. *Eur. Phys. J. E* 37 (7), 1–13.
- Camacho-Lopez, M., Finkelmann, H., Palfy-Muhoray, P., Shelley, M., 2004. Fast liquid-crystal elastomer swims into the dark. *Nat. Mater.* 3 (5), 307–310.
- Catalan, G., Lubk, A., Vlooswijk, A., Snoeck, E., Magen, C., Janssens, A., Rispen, G., Rijnders, G., Blank, D.H., Noheda, B., 2011. Flexoelectric rotation of polarization in ferroelectric thin films. *Nat. Mater.* 10 (12), 963–967.
- Chambers, M., Verduzco, R., Gleeson, J.T., Sprunt, S., Jakli, A., 2009. Flexoelectricity of a calamitic liquid crystal elastomer swollen with a bent-core liquid crystal. *J. Mater. Chem.* 19 (42), 7909–7913.
- Chanda, M., Roy, S.K., 2006. *Plastics Technology Handbook*. CRC Press.
- Chen, Y.-C., Fried, E., 2006. Uniaxial nematic elastomers: constitutive framework and a simple application. *Proc. R. Soc. A: Math. Phys. Eng. Sci.* 462 (2068), 1295–1314.
- Chen, M., Gao, M., Bai, L., Zheng, H., Qi, H.J., Zhou, K., 2023. Recent advances in 4D printing of liquid crystal elastomers. *Adv. Mater.* 35 (23), 2209566.
- Cheung, D.L., Clark, S.J., Wilson, M.R., 2004. Calculation of flexoelectric coefficients for a nematic liquid crystal by atomistic simulation. *J. Chem. Phys.* 121 (18), 9131–9139.
- Codony, D., Gupta, P., Marco, O., Arias, I., 2021. Modeling flexoelectricity in soft dielectrics at finite deformation. *J. Mech. Phys. Solids* 146, 104182.
- Cohen, N., Dayal, K., deBotton, G., 2016. Electroelasticity of polymer networks. *J. Mech. Phys. Solids* 92, 105–126.
- Conti, S., DeSimone, A., Dolzmann, G., 2002. Semisoft elasticity and director reorientation in stretched sheets of nematic elastomers. *Phys. Rev. E* 66 (6), 061710.
- Corbett, D., Van Oosten, C., Warner, M., 2008. Nonlinear dynamics of optical absorption of intense beams. *Phys. Rev. A* 78 (1), 013823.
- Corbett, D., Warner, M., 2006. Nonlinear photoresponse of disordered elastomers. *Phys. Rev. Lett.* 96 (23), 237802.
- Corbett, D., Warner, M., 2007. Linear and nonlinear photoinduced deformations of cantilevers. *Phys. Rev. Lett.* 99 (17), 174302.
- Corbett, D., Warner, M., 2009a. Deformation and rotations of free nematic elastomers in response to electric fields. *Soft Matter* 5 (7), 1433–1439.
- Corbett, D., Warner, M., 2009b. Electromechanical elongation of nematic elastomers for actuation. *Sensors Actuators A* 149 (1), 120–129.
- Davidson, Z.S., Shahsavan, H., Aghakhani, A., Guo, Y., Hines, L., Xia, Y., Yang, S., Sitti, M., 2019. Monolithic shape-programmable dielectric liquid crystal elastomer actuators. *Sci. Adv.* 5 (11), eaay0855.
- De Gennes, P.-G., Prost, J., 1993. *The Physics of Liquid Crystals*. (83), Oxford University Press.
- Deng, Q., Ahmadpoor, F., Brownell, W.E., Sharma, P., 2019. The collusion of flexoelectricity and hopf bifurcation in the hearing mechanism. *J. Mech. Phys. Solids* 130, 245–261.
- Deng, Q., Kammoun, M., Erturk, A., Sharma, P., 2014a. Nanoscale flexoelectric energy harvesting. *Int. J. Solids Struct.* 51 (18), 3218–3225.
- Deng, Q., Liu, L., Sharma, P., 2014b. Flexoelectricity in soft materials and biological membranes. *J. Mech. Phys. Solids* 62, 209–227.
- Deng, Q., Liu, L., Sharma, P., 2017. A continuum theory of flexoelectricity. In: *Flexoelectricity in Solids: From Theory To Applications*. World Scientific, pp. 111–167.
- DeSimone, A., 2010. Nematic elastomers: modelling, analysis, and numerical simulations. In: *Poly-, Quasi-and Rank-One Convexity in Applied Mechanics*. Springer, pp. 241–264.
- DeSimone, A., 2011. Electro-mechanical response of nematic elastomers: an introduction. In: *Mechanics and Electrodynamics of Magneto-and Electro-Elastic Materials*. Springer, pp. 231–266.
- DeSimone, A., DiCarlo, A., Teresi, L., 2007. Critical voltages and blocking stresses in nematic gels. *Eur. Phys. J. E* 24 (3), 303–310.
- DeSimone, A., Teresi, L., 2009. Elastic energies for nematic elastomers. *Eur. Phys. J. E* 29 (2), 191–204.
- Díaz-Calleja, R., Díaz-Boñis, P., 2014. Electromechanical behaviour of biaxially stretched nematic liquid single crystal elastomers. *Int. J. Non-Linear Mech.* 64, 26–32.

- Diaz-Calleja, R., Llovera-Segovia, P., Riande, E., Quijano López, A., 2013. Mechanic and electromechanic effects in biaxially stretched liquid crystal elastomers. *Appl. Phys. Lett.* 102 (5), 052901.
- Dong, L., Zhao, Y., 2018. Photothermally driven liquid crystal polymer actuators. *Mater. Chem. Front.* 2 (11), 1932–1943.
- Dunn, M.L., 2007. Photomechanics of mono- and polydomain liquid crystal elastomer films. *J. Appl. Phys.* 102 (1), 013506.
- Elston, S.J., 2008. Flexoelectricity in nematic domain walls. *Phys. Rev. E* 78 (1), 011701.
- Ericksen, J.L., 1961. Conservation laws for liquid crystals. *Trans. Soc. Rheol.* 5 (1), 23–34.
- Eringen, A.C., 2000. A unified continuum theory for electrodynamic of polymeric liquid crystals. *Internat. J. Engrg. Sci.* 38 (9–10), 959–987.
- Ferrantini, C., Pioner, J.M., Martella, D., Coppini, R., Piroddi, N., Paoli, P., Calamai, M., Pavone, F.S., Wiersma, D.S., Tesi, C., et al., 2019. Development of light-responsive liquid crystalline elastomers to assist cardiac contraction. *Circ. Res.* 124 (8), e44–e54.
- Finkelmann, H., Nishikawa, E., Pereira, G., Warner, M., 2001. A new opto-mechanical effect in solids. *Phys. Rev. Lett.* 87 (1), 015501.
- Firbank, M., Oda, M., Delpy, D.T., 1995. An improved design for a stable and reproducible phantom material for use in near-infrared spectroscopy and imaging. *Phys. Med. Biol.* 40 (5), 955.
- Flock, S.T., Jacques, S.L., Wilson, B.C., Star, W.M., van Gemert, M.J., 1992. Optical properties of intralipid: a phantom medium for light propagation studies. *Lasers Surg. Med.* 12 (5), 510–519.
- Fowler, H.E., Rothmund, P., Keplinger, C., White, T.J., 2021. Liquid crystal elastomers with enhanced directional actuation to electric fields. *Adv. Mater.* 33 (43), 2103806.
- Frank, F.C., 1958. I. Liquid crystals. On the theory of liquid crystals. *Discuss. Faraday Soc.* 25, 19–28.
- Fu, C., Xu, Y., Xu, F., Huo, Y., 2016. Light-induced bending and buckling of large-deflected liquid crystalline polymer plates. *Int. J. Appl. Mech.* 8 (07), 1640007.
- Fukunaga, A., Urayama, K., Takigawa, T., DeSimone, A., Teresi, L., 2008. Dynamics of electro-opto-mechanical effects in swollen nematic elastomers. *Macromolecules* 41 (23), 9389–9396.
- Gennes, P.D., 1980. In: Helfrich, W., Heppke, G. (Eds.), *Liquid Crystals of One- and Two-Dimensional Order*. Springer, Berlin, p. 231ff.
- Gennes, P.D., 1982. In: Ciferri, A., Krigbaum, W., Meyer, R. (Eds.), *Polymer Liquid Crystals*. Academic Press, New York.
- Giannakopoulos, A.E., Rosakis, A.J., 2020. Dynamics of flexoelectric materials: subsonic, intersonic, and supersonic ruptures and mach cone formation. *J. Appl. Mech.* 87 (6), 061004.
- Golubović, L., Lubensky, T., 1989. Nonlinear elasticity of amorphous solids. *Phys. Rev. Lett.* 63 (10), 1082.
- Grasinger, M., Dayal, K., 2021. Architected elastomer networks for optimal electromechanical response. *J. Mech. Phys. Solids* 146, 104171.
- Grasinger, M., Mozaffari, K., Sharma, P., 2021. Flexoelectricity in soft elastomers and the molecular mechanisms underpinning the design and emergence of giant flexoelectricity. *Proc. Natl. Acad. Sci.* 118 (21), e2102477118.
- Greco, F., Codony, D., Mohammadi, H., Fernandez-Mendez, S., Arias, I., 2024. Topology optimization of flexoelectric metamaterials with apparent piezoelectricity. *J. Mech. Phys. Solids* 183, 105477.
- Guin, T., Hinton, H.E., Burgeson, E., Bowland, C.C., Kearney, L.T., Li, Y., Ivanov, I., Nguyen, N.A., Naskar, A.K., 2020. Tunable electromechanical liquid crystal elastomer actuators. *Adv. Intell. Syst.* 2 (7), 2000022.
- Gurtin, M.E., Fried, E., Anand, L., 2010. *The Mechanics and Thermodynamics of Continua*. Cambridge University Press.
- Harden, J., Chambers, M., Verduzco, R., Luchette, P., Gleeson, J.T., Sprunt, S., Jákli, A., 2010. Giant flexoelectricity in bent-core nematic liquid crystal elastomers. *Appl. Phys. Lett.* 96 (10), 102907.
- Harden, J., Mbanga, B., Éber, N., Fodor-Csorba, K., Sprunt, S., Gleeson, J.T., Jakli, A., 2006. Giant flexoelectricity of bent-core nematic liquid crystals. *Phys. Rev. Lett.* 97 (15), 157802.
- He, Q., Wang, Z., Wang, Y., Minori, A., Tolley, M.T., Cai, S., 2019. Electrically controlled liquid crystal elastomer-based soft tubular actuator with multimodal actuation. *Sci. Adv.* 5 (10), eaax5746.
- Helfrich, W., 1974. Inherent bounds to the elasticity and flexoelectricity of liquid crystals. *Mol. Cryst. Liq. Cryst.* 26 (1–2), 1–5.
- Herbert, K.M., Fowler, H.E., McCracken, J.M., Schlafmann, K.R., Koch, J.A., White, T.J., 2021. Synthesis and alignment of liquid crystalline elastomers. *Nat. Rev. Mater.* 1–16.
- Hogan, P., Tajbakhsh, A., Terentjev, E., 2002. UV manipulation of order and macroscopic shape in nematic elastomers. *Phys. Rev. E* 65 (4), 041720.
- Hrozhyk, U., Serak, S., Tabiryan, N., White, T.J., Bunning, T.J., 2009. Bidirectional photoresponse of surface pretreated azobenzene liquid crystal polymer networks. *Opt. Express* 17 (2), 716–722.
- Ilnytskyi, J.M., Saphiannikova, M., Neher, D., Allen, M.P., 2012. Modelling elasticity and memory effects in liquid crystalline elastomers by molecular dynamics simulations. *Soft Matter* 8 (43), 11123–11134.
- Iseki, S., 2019. Liquid crystalline elastomer precursor and liquid crystalline elastomer. *US Patent App.* 16/070, 555.
- Jiang, X., Huang, W., Zhang, S., 2013. Flexoelectric nano-generator: Materials, structures and devices. *Nano Energy* 2 (6), 1079–1092.
- Jiang, Y., Yan, D., Wang, J., Shao, L.-H., Sharma, P., 2023. The giant flexoelectric effect in a luffa plant-based sponge for green devices and energy harvesters. *Proc. Natl. Acad. Sci.* 120 (40), e2311755120.
- Jin, L., Yan, Y., Huo, Y., 2010. A gradient model of light-induced bending in photochromic liquid crystal elastomer and its nonlinear behaviors. *Int. J. Non-Linear Mech.* 45 (4), 370–381.
- Kaiser, A., Winkler, M., Krause, S., Finkelmann, H., Schmidt, A.M., 2009. Magnetoactive liquid crystal elastomer nanocomposites. *J. Mater. Chem.* 19 (4), 538–543.
- Khandagale, P., Garcia-Cervera, C., Debotton, G., Breitzman, T., Majidi, C., Dayal, K., 2024. Statistical field theory of polarizable polymer chains with nonlocal dipolar interactions. *Phys. Rev. E* 109 (4), 044501.
- Kim, D.-H., Lu, N., Huang, Y., Rogers, J.A., 2012. Materials for stretchable electronics in bioinspired and biointegrated devices. *MRS Bull.* 37 (3), 226–235.
- Kim, Y., Yuk, H., Zhao, R., Chester, S.A., Zhao, X., 2018. Printing ferromagnetic domains for untethered fast-transforming soft materials. *Nature* 558 (7709), 274–279.
- Krichen, S., Liu, L., Sharma, P., 2019. Liquid inclusions in soft materials: Capillary effect, mechanical stiffening and enhanced electromechanical response. *J. Mech. Phys. Solids* 127, 332–357.
- Krichen, S., Sharma, P., 2016. Flexoelectricity: a perspective on an unusual electromechanical coupling. *J. Appl. Mech.* 83 (3), 030801.
- Kumar, K., Knie, C., Bléger, D., Peletier, M.A., Friedrich, H., Hecht, S., Broer, D.J., Debye, M.G., Schenning, A.P., 2016. A chaotic self-oscillating sunlight-driven polymer actuator. *Nat. Commun.* 7 (1), 1–8.
- Kumar, P., Marinov, Y., Hinov, H., Hiremath, U.S., Yelamagad, C., Krishnamurthy, K., Petrov, A., 2009. Converse flexoelectric effect in bent-core nematic liquid crystals. *J. Phys. Chem. B* 113 (27), 9168–9174.
- Kundler, I., Finkelmann, H., 1995. Strain-induced director reorientation in nematic liquid single crystal elastomers. *Macromol. Rapid Commun.* 16 (9), 679–686.
- Küpfer, J., Finkelmann, H., 1991. Nematic liquid single crystal elastomers. *Die Makromolekulare Chemie, Rapid Communications* 12 (12), 717–726.
- Küpper, J., Finkelmann, H., 1994. Liquid crystal elastomers: Influence of the orientational distribution of the crosslinks on the phase behaviour and reorientation processes. *Macromol. Chem. Phys.* 195 (4), 1353–1367.
- Lee, V., Bhattacharya, K., 2022. Universal deformations of ideal liquid crystal elastomers. *arXiv preprint arXiv:2210.17372*.
- Leigh, D.C., 1968. *Nonlinear Continuum Mechanics: an Introduction to the Continuum Physics and Mathematical Theory of the Nonlinear Mechanical Behavior of Materials*. McGraw-Hill.
- Leslie, F.M., 1966. Some constitutive equations for anisotropic fluids. *Quart. J. Mech. Appl. Math.* 19 (3), 357–370.
- Leslie, F.M., 1968. Some constitutive equations for liquid crystals. *Arch. Ration. Mech. Anal.* 28 (4), 265–283.

- Leslie, F.M., 1979. Theory of flow phenomena in liquid crystals. In: *Advances in Liquid Crystals*. vol. 4, Elsevier, pp. 1–81.
- Leslie, F.M., 1992. Continuum theory for nematic liquid crystals. *Contin. Mech. Thermodyn.* 4 (3), 167–175.
- Li, C., Liu, Y., Huang, X., Jiang, H., 2012. Direct sun-driven artificial heliotropism for solar energy harvesting based on a photo-thermomechanical liquid-crystal elastomer nanocomposite. *Adv. Funct. Mater.* 22 (24), 5166–5174.
- Lin, Y., Jin, L., Huo, Y., 2012. Quasi-soft opto-mechanical behavior of photochromic liquid crystal elastomer: Linearized stress–strain relations and finite element simulations. *Int. J. Solids Struct.* 49 (18), 2668–2680.
- Liu, L., 2014. An energy formulation of continuum magneto-electro-elasticity with applications. *J. Mech. Phys. Solids* 63, 451–480.
- Liu, Y., Ma, W., Dai, H.-H., 2020. On a consistent finite-strain plate model of nematic liquid crystal elastomers. *J. Mech. Phys. Solids* 145, 104169.
- Liu, Y., Ma, W., Dai, H.-H., 2021. Bending-induced director reorientation of a nematic liquid crystal elastomer bonded to a hyperelastic substrate. *J. Appl. Phys.* 129 (10), 104701.
- Liu, L., Onck, P.R., 2017. Enhanced deformation of azobenzene-modified liquid crystal polymers under dual wavelength exposure: A photophysical model. *Phys. Rev. Lett.* 119 (5), 057801.
- Liu, L., Sharma, P., 2013. Flexoelectricity and thermal fluctuations of lipid bilayer membranes: Renormalization of flexoelectric, dielectric, and elastic properties. *Phys. Rev. E-Stat., Nonlinear, Soft Matter Phys.* 87 (3), 032715.
- Liu, L., Sharma, P., 2018. Emergent electromechanical coupling of electrets and some exact relations—The effective properties of soft materials with embedded external charges and dipoles. *J. Mech. Phys. Solids* 112, 1–24.
- LoGrande, K., Shankar, M.R., Dayal, K., 2023. A dimensionally-reduced nonlinear elasticity model for liquid crystal elastomer strips with transverse curvature. *Soft Matter* 19 (45), 8764–8778.
- Luo, C., Calderer, M.-C., 2012. Numerical study of liquid crystal elastomers by a mixed finite element method. *European J. Appl. Math.* 23 (1), 121–154.
- Luo, C., Chung, C., Yakacki, C.M., Long, K., Yu, K., 2021. Real-time alignment and reorientation of polymer chains in liquid crystal elastomers. *ACS Appl. Mater. Interfaces*.
- Mao, S., Purohit, P.K., 2015. Defects in flexoelectric solids. *J. Mech. Phys. Solids* 84, 95–115.
- Mathew, A., Kulkarni, Y., 2023. An electro-chemo-mechanical theory with flexoelectricity: Application to ionic conductivity of soft solid electrolytes. *J. Appl. Mech.* 91 (4).
- Mathur, A., Sharma, P., Cammarata, R., 2005. Negative surface energy—clearing up confusion. *Nature Mater.* 4 (3), 186.
- Mbanga, B.L., Ye, F., Selinger, J.V., Selinger, R.L., 2010. Modeling elastic instabilities in nematic elastomers. *Phys. Rev. E* 82 (5), 051701.
- Menzel, A., 2008. *Nonlinear Macroscopic Description of Liquid Crystalline Elastomers in External Fields* (Ph.D. thesis).
- Menzel, A.M., Brand, H.R., 2007. Cholesteric elastomers in external mechanical and electric fields. *Phys. Rev. E* 75 (1), 011707.
- Menzel, A., Brand, H., 2008. Instabilities in nematic elastomers in external electric and magnetic fields. *Eur. Phys. J. E* 26 (3), 235–249.
- Menzel, A.M., Pleiner, H., Brand, H.R., 2009. Response of prestretched nematic elastomers to external fields. *Eur. Phys. J. E* 30 (4), 371–377.
- Meyer, R.B., 1969. Piezoelectric effects in liquid crystals. *Phys. Rev. Lett.* 22 (18), 918.
- Mihai, L.A., Goriely, A., 2020. A plate theory for nematic liquid crystalline solids. *J. Mech. Phys. Solids* 144, 104101.
- Mihai, L.A., Goriely, A., 2021. Instabilities in liquid crystal elastomers. *MRS Bull.* 46 (9), 784–794.
- Mistry, D., Morgan, P.B., Clamp, J.H., Gleeson, H.F., 2018. New insights into the nature of semi-soft elasticity and “mechanical-Fréedericksz transitions” in liquid crystal elastomers. *Soft Matter* 14 (8), 1301–1310.
- Modes, C., Warner, M., Van Oosten, C., Corbett, D., 2010. Anisotropic response of glassy splay-bend and twist nematic cantilevers to light and heat. *Phys. Rev. E* 82 (4), 041111.
- Mozaffari, K., Ahmadoor, F., Deng, Q., Sharma, P., 2023. A minimal physics-based model for musical perception. *Proc. Natl. Acad. Sci.* 120 (5), e2216146120.
- Müller, O., Brand, H., 2005. Undulation versus Fredericks instability in nematic elastomers in an external electric field. *Eur. Phys. J. E* 17 (1), 53–62.
- Nguyen, T.D., Mao, S., Yeh, Y.-W., Purohit, P.K., McAlpine, M.C., 2013. Nanoscale flexoelectricity. *Adv. Mater.* 25 (7), 946–974.
- Ohm, C., Brehmer, M., Zentel, R., 2010. Liquid crystalline elastomers as actuators and sensors. *Adv. Mater.* 22 (31), 3366–3387.
- Pampolini, G., Triantafyllidis, N., 2018. Continuum electromechanical theory for nematic continua with application to Fredericksz instability. *J. Elasticity* 132 (2), 219–242.
- Pang, X., Lv, J.-a., Zhu, C., Qin, L., Yu, Y., 2019. Photodeformable azobenzene-containing liquid crystal polymers and soft actuators. *Adv. Mater.* 31 (52), 1904224.
- Pence, T.J., 2006. Soft elastic bending response of a nematic elastomer described by a microstructurally relaxed free energy. *Contin. Mech. Thermodyn.* 18 (5), 281–304.
- Prost, J., Marcerou, J., 1977. On the microscopic interpretation of flexoelectricity. *J. Physique* 38 (3), 315–324.
- Rahmati, A.H., Jia, R., Tan, K., Zhao, X., Deng, Q., Liu, L., Sharma, P., 2023. Theory of hard magnetic soft materials to create magnetoelectricity. *J. Mech. Phys. Solids* 171, 105136.
- Rahmati, A.H., Yang, S., Bauer, S., Sharma, P., 2019. Nonlinear bending deformation of soft electrets and prospects for engineering flexoelectricity and transverse (d 31) piezoelectricity. *Soft Matter* 15 (1), 127–148.
- Rajapaksha, C.P., Gunathilaka, M., Narute, S., Albehajjan, H., Piedrahita, C., Paudel, P., Feng, C., Lüssem, B., Kyu, T., Jáklí, A., 2021. Flexo-ionic effect of ionic liquid crystal elastomers. *Molecules* 26 (14), 4234.
- Rivlin, R., 1949. Large elastic deformations of isotropic materials. V. The problem of flexure. *Proc. R. Soc. Lond. Ser. A. Math. Phys. Sci.* 195 (1043), 463–473.
- Roach, D.J., Yuan, C., Kuang, X., Li, V.C.-F., Blake, P., Romero, M.L., Hammel, I., Yu, K., Qi, H.J., 2019. Long liquid crystal elastomer fibers with large reversible actuation strains for smart textiles and artificial muscles. *ACS Appl. Mater. Interfaces* 11 (21), 19514–19521.
- Shang, Y., Wang, J., Ikeda, T., Jiang, L., 2019. Bio-inspired liquid crystal actuator materials. *J. Mater. Chem. C* 7 (12), 3413–3428.
- Sharma, N.D., Maranganti, R., Sharma, P., 2007. On the possibility of piezoelectric nanocomposites without using piezoelectric materials. *J. Mech. Phys. Solids* 55 (11), 2328–2350.
- Stewart, I.W., 2019. *The Static and Dynamic Continuum Theory of Liquid Crystals: A Mathematical Introduction*. Crc Press.
- Style, R.W., Boltyskiy, R., Allen, B., Jensen, K.E., Foote, H.P., Wettlaufer, J.S., Dufresne, E.R., 2015a. Stiffening solids with liquid inclusions. *Nat. Phys.* 11 (1), 82–87.
- Style, R.W., Wettlaufer, J.S., Dufresne, E.R., 2015b. Surface tension and the mechanics of liquid inclusions in compliant solids. *Soft Matter* 11 (4), 672–679.
- Takezoe, H., Takanishi, Y., 2006. Bent-core liquid crystals: their mysterious and attractive world. *Japanese J. Appl. Phys.* 45 (2R), 597.
- Teixeira, P., Warner, M., 1999. Dynamics of soft and semisoft nematic elastomers. *Phys. Rev. E* 60 (1), 603.
- Terentjev, E., Warner, M., Bladon, P., 1994. Orientation of nematic elastomers and gels by electric fields. *J. Phys. II* 4 (4), 667–676.
- Terentjev, E., Warner, M., Meyer, R., Yamamoto, J., 1999. Electromechanical Fredericks effects in nematic gels. *Phys. Rev. E* 60 (2), 1872.
- Thomsen, D.L., Keller, P., Naciri, J., Pink, R., Jeon, H., Shenoy, D., Ratna, B.R., 2001. Liquid crystal elastomers with mechanical properties of a muscle. *Macromolecules* 34 (17), 5868–5875.
- Torbati, M., Mozaffari, K., Liu, L., Sharma, P., 2022. Coupling of mechanical deformation and electromagnetic fields in biological cells. *Rev. Modern Phys.* 94 (2), 025003.
- Turiv, T., Krieger, J., Babakhanova, G., Yu, H., Shiyonovskii, S.V., Wei, Q.-H., Kim, M.-H., Lavrentovich, O.D., 2020. Topology control of human fibroblast cells monolayer by liquid crystal elastomer. *Sci. Adv.* 6 (20), eaaz6485.

- Ube, T., Ikeda, T., 2014. Photomobile polymer materials with crosslinked liquid-crystalline structures: molecular design, fabrication, and functions. *Angew. Chem., Int. Ed. Engl.* 53 (39), 10290–10299.
- Ube, T., Ikeda, T., 2019. Photomobile polymer materials with complex 3D deformation, continuous motions, self-regulation, and enhanced processability. *Adv. Opt. Mater.* 7 (16), 1900380.
- Ula, S.W., Traugutt, N.A., Volpe, R.H., Patel, R.R., Yu, K., Yakacki, C.M., 2018. Liquid crystal elastomers: an introduction and review of emerging technologies. *Liquid Cryst. Rev.* 6 (1), 78–107.
- Urayama, K., 2007. Selected issues in liquid crystal elastomers and gels. *Macromolecules* 40 (7), 2277–2288.
- Urayama, K., Honda, S., Takigawa, T., 2006. Deformation coupled to director rotation in swollen nematic elastomers under electric fields. *Macromolecules* 39 (5), 1943–1949.
- Urayama, K., Kohmon, E., Kojima, M., Takigawa, T., 2009. Polydomain- monodomain transition of randomly disordered nematic elastomers with different cross-linking histories. *Macromolecules* 42 (12), 4084–4089.
- Van Oosten, C., Harris, K., Bastiaansen, C., Broer, D., 2007. Glassy photomechanical liquid-crystal network actuators for microscale devices. *Eur. Phys. J. E* 23 (3), 329–336.
- Verwey, G., Warner, M., Terentjev, E., 1996. Elastic instability and stripe domains in liquid crystalline elastomers. *J. Phys. II* 6 (9), 1273–1290.
- Wang, Z., Guo, Y., Cai, S., Yang, J., 2022. Three-dimensional printing of liquid crystal elastomers and their applications. *ACS Appl. Polym. Mater.* 4 (5), 3153–3168.
- Wang, Z., He, Q., Wang, Y., Cai, S., 2019a. Programmable actuation of liquid crystal elastomers via “living” exchange reaction. *Soft Matter* 15 (13), 2811–2816.
- Wang, Y., He, Q., Wang, Z., Zhang, S., Li, C., Wang, Z., Park, Y.-L., Cai, S., 2023. Liquid crystal elastomer based dexterous artificial motor unit. *Adv. Mater.* 35 (17), 2211283.
- Wang, B., Yang, S., Sharma, P., 2019b. Flexoelectricity as a universal mechanism for energy harvesting from crumpling of thin sheets. *Phys. Rev. B* 100 (3), 035438.
- Warner, M., 1999. New elastic behaviour arising from the unusual constitutive relation of nematic solids. *J. Mech. Phys. Solids* 47 (6), 1355–1377.
- Warner, M., Bladon, P., Terentjev, E., 1994. “Soft elasticity”—deformation without resistance in liquid crystal elastomers. *J. Phys. II* 4 (1), 93–102.
- Warner, M., Mahadevan, L., 2004. Photoinduced deformations of beams, plates, and films. *Phys. Rev. Lett.* 92 (13), 134302.
- Warner, M., Modes, C.D., Corbett, D., 2010. Curvature in nematic elastica responding to light and heat. *Proc. R. Soc. A: Math. Phys. Eng. Sci.* 466 (2122), 2975–2989.
- Warner, M., Terentjev, E.M., 2007. *Liquid Crystal Elastomers*. vol. 120, Oxford University Press.
- Weigert, F., 1919. Über einen neuen effekt der strahlung in lichtempfindlichen schichten. *Verh. Dtsch. Phys. Ges.* 21, 479–491.
- White, T.J., Serak, S.V., Tabiryan, N.V., Vaia, R.A., Bunning, T.J., 2009. Polarization-controlled, photodriven bending in monodomain liquid crystal elastomer cantilevers. *J. Mater. Chem.* 19 (8), 1080–1085.
- Xiang, Y., Jing, H.-Z., Zhang, Z.-D., Ye, W.-J., Xu, M.-Y., Wang, E., Salamon, P., Éber, N., Buka, Á., 2017. Tunable optical grating based on the flexoelectric effect in a bent-core nematic liquid crystal. *Phys. Rev. Appl.* 7 (6), 064032.
- Xu, Y., Huo, Y., 2021. Continuum modeling of the nonlinear electro-opto-mechanical coupling and solid Fréedericksz transition in dielectric liquid crystal elastomers. *Int. J. Solids Struct.* 219, 198–212.
- Xu, Y., Zhang, Y., Huo, Y., 2020. Electric-field induced deformation and bending in nematic elastomer strips with orientation gradient. *Int. J. Solids Struct.* 202, 243–259.
- Xu, Y., Zhang, Y., Huo, Y., 2022. Electromechanical deformation of dielectric nematic elastomers accompanied by the rotation of mesogens. *Int. J. Mech. Sci.* 107061.
- Yan, D., Wang, J., Xiang, J., Xing, Y., Shao, L.-H., 2023. A flexoelectricity-enabled ultrahigh piezoelectric effect of a polymeric composite foam as a strain-gradient electric generator. *Sci. Adv.* 9 (2), eadc8845.
- Yang, S., Sharma, P., 2023. A tutorial on the stability and bifurcation analysis of the electromechanical behaviour of soft materials. *Appl. Mech. Rev.* 75 (4), 044801.
- Yang, S., Zhao, X., Sharma, P., 2017. Avoiding the pull-in instability of a dielectric elastomer film and the potential for increased actuation and energy harvesting. *Soft Matter* 13 (26), 4552–4558.
- You, Y., Xu, C., Ding, S., Huo, Y., 2012. Coupled effects of director orientations and boundary conditions on light induced bending of monodomain nematic liquid crystalline polymer plates. *Smart Mater. Struct.* 21 (12), 125012.
- Yu, H., Ikeda, T., 2011. Photocontrollable liquid-crystalline actuators. *Adv. Mater.* 23 (19), 2149–2180.
- Yuan, C., Roach, D.J., Dunn, C.K., Mu, Q., Kuang, X., Yakacki, C.M., Wang, T., Yu, K., Qi, H.J., 2017. 3D printed reversible shape changing soft actuators assisted by liquid crystal elastomers. *Soft Matter* 13 (33), 5558–5568.
- Yudin, P.V., Tagantsev, A.K., 2013. Fundamentals of flexoelectricity in solids. *Nanotechnology* 24 (43), 432001.
- Yusuf, Y., Huh, J.-H., Cladis, P., Brand, H.R., Finkelmann, H., Kai, S., 2005. Low-voltage-driven electromechanical effects of swollen liquid-crystal elastomers. *Phys. Rev. E* 71 (6), 061702.
- Zentel, R., 1986. Shape variation of cross-linked liquid-crystalline polymers by electric fields. *Liq. Cryst.* 1 (6), 589–592.
- Zhang, Y., Huo, Y., 2018. First order shear strain beam theory for spontaneous bending of liquid crystal polymer strips. *Int. J. Solids Struct.* 136, 168–185.
- Zhang, Y., Xuan, C., Jiang, Y., Huo, Y., 2019. Continuum mechanical modeling of liquid crystal elastomers as dissipative ordered solids. *J. Mech. Phys. Solids* 126, 285–303.
- Zhao, X., Suo, Z., 2010. Theory of dielectric elastomers capable of giant deformation of actuation. *Phys. Rev. Lett.* 104 (17), 178302.
- Zhou, H., Bhattacharya, K., 2021. Accelerated computational micromechanics and its application to polydomain liquid crystal elastomers. *J. Mech. Phys. Solids* 153, 104470.
- Zubko, P., Catalan, G., Tagantsev, A.K., 2013. Flexoelectric effect in solids. *Annu. Rev. Mater. Res.* 43 (1), 387–421.